

COLD WORKING EFFECTS ON MECHANICAL PROPERTIES IN SHEET
METAL JOINING FOR AUTOMOTIVE APPLICATIONS

By

DAVID MATTHEW BLAKE

A thesis submitted in partial fulfillment of
the requirements for the degree of
Master of Science in Mechanical Engineering

WASHINGTON STATE UNIVERSITY
School of Engineering and Computer Science

DECEMBER 2006

To the Faculty of Washington State University:

The members of the Committee appointed to examine the thesis of
DAVID BLAKE find it satisfactory and recommend that it be accepted.

Chair

ACKNOWLEDGMENT

I would like to thank Dr. Dave Kim for his encouragement and guidance over the last two years. His energy gave me perseverance to complete the tasks for this thesis. Thanks to, Dr. Taeksun Nam a critical asset to solving FEA problems as well as accepting to serve on the thesis committee; Lynelle Detrick and Dr. Linda Chen for willingly accepting to help me with my thesis and serve on the committee; StressWave members Eric Easterbrook and Michael Landy were very helpful for supplying the machines, tools and time for cold working the samples; Jake Adams and Chris Rinehart of Freightliner LLC gave guidance to the problems they foresee with cold working in SPR; professor Byeong-Soo Lim and Seung-Jin Ryu at Sungkyunkwan University in Korea for helping with fatigue testing the RSWs; Ray Spitsen who trained me on several machines and Chad Swanson who helped set up many of the testing procedures.

COLD WORKING EFFECTS ON MECHANICAL PROPERTIES IN SHEET

METAL JOINING FOR AUTOMOTIVE APPLICATIONS

Abstract

by David Matthew Blake, M.S.
Washington State University
December 2006

Chair: Dae-Wook (Dave) Kim

With increasing demands from government agencies and consumers to increase fuel economy, automotive industries are having to research and produce lighter vehicles yet maintain safety and durability. Sheet metal is often the focal point for improvement, with the joints being a critical aspect, for automotive applications. RSW (resistance spot welding) is a fusion based joint where a high electrical and thermal energy creates localized melting of sheet metal creating a weld nugget. SPR (self-piercing rivet) is a mechanical joint where a rivet is driven in to the sheet metal with an opposing die causing interlocking between the sheets. In a typical vehicle there are 2000-5000 RSW and in some class 8 trucks there are approximately 1600 SPR joints making these two joining techniques the most common used single point fasteners. Residual stresses are created during the RSW process in both steel and aluminum and are often the cause for failure. A recently developed cold working process for improving the mechanical properties for drilled holes has been applied to RSWs. This process has proven an increase in fatigue strengths for adequately sized steel RSW but this research studies the

post-weld cold working effect on small sized RSWs. This research also develops the optimum cold working parameters for Al RSW. Metallography, microhardness, tensile-shear strength, fatigue strength, and FEA tool LS-DYNA are all used to study cold working on RSWs. In SPR it is unknown what the effect of stamped aluminum sheet metal has on the process force and mechanical properties of the joint. To accomplish the study of cold worked sheets used for SPR, the following analyses were examined: process force, tensile-shear strength, fatigue strength and metallography.

It was found for inadequate sized steel RSWs the cold working process does not improve fatigue life. For Al RSWs the fatigue life can be improved by up to 80 times with the correct cold working parameters. The cold working parameters used on the sheet metal prior to the SPR process resulted in an increase of the riveting process force and no effect on mechanical properties of the joint.

TABLE OF CONTENTS

	PAGE
ACKNOWLEDGEMENTS	iii
ABSTRACT	iv
LIST OF TABLES	x
LIST OF FIGURES	xi
CHAPTER 1: INTRODUCTION	1
1.1 SHEET METAL JOINING	3
1.2 RESISTANCE SPOT WELDING	3
1.3 SELF-PIERCING RIVETS	4
1.4 INTRODUCTION OF CHAPTERS	5
CHAPTER 2: LITERATURE SURVEY	6
2.1 SHEET METAL JOINING PROCESSES	6
2.2 RESISTANCE SPOT WELD PROCESS	9
2.2.1 PROCESS	9
2.2.2 RESIDUAL STRESSES	13
2.2.3 MECHANICAL PROPERTIES	17
2.3 SELF-PIERCING RIVETS	21
2.3.1 PROCESS	21
2.3.2 MECHANICAL PROPERTIES	23
2.4 COLD WORKING ON SHEET METAL JOINTS	28
2.4.1 COLD HOLE EXPANSION METHOD	28
2.4.2 STRESSWAVE TM PROCESS	30

2.4.3 STRESSWAVE PROCESS ON RSW.....	32
CHAPTER 3: OBJECTIVES.....	33
3.1 RSW.....	33
3.2 SPR.....	34
CHAPTER 4: EXPERIMENTAL PROCEDURES.....	36
4.1 MATERIALS.....	36
4.1.1 STEEL RSW.....	36
4.1.2 AL RSW.....	37
4.1.3 SPR.....	37
4.2 SAMPLE FABRICATION.....	39
4.2.1 RSW.....	39
4.2.1.1 STEEL.....	39
4.2.1.2 AL.....	41
4.2.2 SPR.....	42
4.3 COLD WORKING.....	44
4.3.1 RSW.....	44
4.3.2 SPR.....	47
4.4 METALLOGRAPHY.....	47
4.5 MECHANICAL PROPERTY TESTING.....	48
4.5.1 MICROHARDNESS TESTING.....	48
4.5.2 TENSILE-SHEAR TESTING.....	48
4.5.3 FATIGUE TESTING.....	49
4.5.4 X-RAY DIFFRACTION.....	50

CHAPTER 5: RESULTS AND DISCUSSION.....	52
5.1 STEEL RSW	52
5.1.1 METALLOGRAPHY	52
5.1.2 MICROHARDNESS	53
5.1.3 TENSILE-SHEAR TESTING	54
5.1.4 FATIGUE TESTING.....	55
5.1.5 X-RAY DIFFRACTION	64
5.1.6 NUMERICAL ANALYSIS.....	66
5.2 ALUMINUM RSW	74
5.2.1 METALLOGRAPHY	74
5.2.2 MICROHARDNESS	75
5.2.3 TENSILE-SHEAR TESTING	77
5.2.4 FATIGUE TESTING.....	77
5.2.5 NUMERICAL ANALYSIS.....	79
5.3. SPR RESULTS AND DISCUSSION.....	84
5.3.1 MATERIAL SELECTION	84
5.3.1.1 PROCESS FORCE	84
5.3.1.2 METALLOGRAPHY	88
5.3.1.3 TENSILE-SHEAR TESTING	89
5.3.2 COLD WORKED SPR.....	91
5.3.2.1 PROCESS FORCE	91

5.3.2.2 TENSILE-SHEAR TESTING	92
5.3.2.3 FATIGUE TESTING.....	93
5.3.2.4 METALLOGRAPHY	94
CHAPTER 6: CONCLUSIONS	96
6.1 RSW.....	96
6.1.1 STEEL.....	96
6.1.2 ALUMINUM	97
6.2 SPR	99
CHAPTER 7: FUTURE WORK	101
BIBLIOGRAPHY.....	102
APPENDIX	108

LIST OF TABLES

TABLE 2.1. MECHANICAL PROPERTIES OF STEEL AND ALUMINUM RSW.....	17
TABLE 4.1 CHEMICAL COMPOSITIONS OF COLD ROLLED 1008 STEEL (WT%).	36
TABLE 4.2 MECHANICAL PROPERTIES OF COLD ROLLED 1008 STEEL.....	36
TABLE 4.4. MECHANICAL PROPERTIES OF AL 5052.....	37
TABLE 4.5. SPR MATERIAL TYPES AND THICKNESSES.....	38
TABLE 4.6. CHEMICAL COMPOSITIONS OF SPR WORKPIECE MATERIALS (WT%).....	38
TABLE 4.7. MECHANICAL PROPERTIES OF MATERIAL USED FOR SPR.....	38
TABLE 4.8. 1008 STEEL RSW PARAMETERS.....	40
TABLE 4.9. AL SPOT WELDING PROCESS PARAMETERS.....	42
TABLE 4.10. PARAMETERS FOR STEEL RSW.....	46
TABLE 4.11 PARAMETERS FOR AL RSW.....	46
TABLE 5.1. CIRCUMFERENTIAL RESIDUAL STRESS IN MPA.....	65
TABLE 5.2. AL 5052 PROCESS FORCES.....	92

LIST OF FIGURES

FIGURE 1.1 CRACKING IN SHEET METAL JOINTS.	2
FIGURE 1.2. FATIGUE TESTING PROCEDURES.	2
FIGURE 2.1. VARIATION OF RIVETS.....	8
FIGURE 2.2. CROSS-SECTIONAL VIEW OF FSR IN WORKPIECE.....	8
FIGURE 2.3. RSW CROSS-SECTION SCHEMATIC.	9
FIGURE 2.4. SCHEMATIC OF RSW PROCESS.....	10
FIGURE 2.5. AL RSW CROSS SECTION.....	13
FIGURE 2.6. RESIDUAL STRESS DISTRIBUTION OF AL RSW.....	15
FIGURE 2.7. SCHEMATIC OF RSW CROSS SECTION.....	16
FIGURE 2.8. SPR JOINT.....	21
FIGURE 2.9. SPR PROCESS.....	22
FIGURE 2.10. FRETTING LOCATION IN AN SPR.	26
FIGURE 2.11. FRETTING SCARS FROM SPR.....	27
FIGURE 2.12. MICRO-CRACKS AND DELAMINATION AT TWO BODY FRETTING.	27
FIGURE 2.13. CROSS SECTION VIEW OF SPLIT SLEEVE AND SPLIT MANDREL PROCESSES.....	29
FIGURE 2.14. FATIGUE EFFECTS OF COLD WORKING PROCESSES.....	30
FIGURE 2.15. STRESSWAVE TECHNOLOGY™.	31
FIGURE 2.16 RESULTS OF STRESSWAVES ON FATIGUE LIFE.....	31
TABLE 4.3. CHEMICAL COMPOSITION OF AL 5052(WT.%).....	37

FIGURE 4.1. GEOMETRY OF RSW SPECIMENS.	39
FIGURE 4.2. X-RAY VIEW OF STEEL RSW.	40
FIGURE 4.3. SPR SYSTEM.	42
FIGURE 4.4. RIVET CROSS-SECTION.	43
FIGURE 4.5. FORCE MONITOR SYSTEM.	43
FIGURE 4.6. GEOMETRY OF SPR SPECIMENS.	43
FIGURE 4.7. SCHEMATIC DIAGRAMS OF THE POST-WELD COLD WORKING PROCESS.	44
FIGURE 4.8. COLD WORKING BEING PERFORMED ON A RSW SAMPLE.	45
FIGURE 4.9. CROSS-SECTIONAL SCHEMATIC OF A TYPICAL INDENTER.	45
FIGURE 4.10. COLD WORKING ON SPR SPECIMENS.	47
FIGURE 4.11. INSTRON TENSILE-SHEAR MACHINE.	49
FIGURE 4.12. INSTRON 1380 FATIGUE TESTER.	50
FIGURE 4.13. RESIDUAL STRESS MEASUREMENT POSITIONS IN X-RAY DIFFRACTION.	51
FIGURE 5.1. MICROSTRUCTURES OF “AS-WELDED” AND COLD WORKED STEEL RSW.	53
FIGURE 5.2. STEEL MICROHARDNESS DISTRIBUTIONS.	54
FIGURE 5.3. MICRO-STRUCTURE OF STEEL RSW.	54
FIGURE 5.4. TENSILE-SHEAR MAX LOAD OF AS-WELDED RSW SAMPLES WITH VARIOUS NUGGET SIZES.	55
FIGURE 5.5. L-N CURVES FOR THE AS-WELDED AND POST-WELD COLD WORKED SAMPLES.	56

FIGURE 5.6. FAILED STEEL RSW FATIGUE SPECIMEN.	57
FIGURE 5.7. NUMBER OF CYCLES TO FAILURE VS. NUGGET SIZES.	59
FIGURE 5.8. SCHEMATICS AND OPTICAL PICTURES OF SPOT-WELD CROSS- SECTIONS ILLUSTRATING VARIOUS FAILURE TYPES.....	61
FIGURE 5.9. FREQUENCY OF FAILURE TYPES FOR COLD WORKED STEEL SAMPLES WITH UNDERSIZED RSWs.	62
FIGURE 5.10. EFFECT OF NUGGET SIZE ON STEEL RSW FAILURE TYPES.	63
FIGURE 5.11. LS-DYNA FINITE ELEMENT NUMERICAL ANALYSIS ON STEEL RSW.....	67
FIGURE 5.12. COMPARISONS BETWEEN XRD AND FEM OF AVERAGE RESIDUAL STRESSES ON STEEL RSW SURFACES.	68
FIGURE 5.13. FEA CONTOUR PLOT OF HOOP STRESS WITH IS 7.1MM AND VARIOUS IPS AND FRINGE LEVELS.	69
FIGURE 5.14. CORRELATION BETWEEN FEA AND EXPERIMENTAL FATIGUE RESULTS FOR 7.1 MM IS.....	70
FIGURE 5.15. FEM HOOP STRESS RESULTS FOR STEEL RSWs WITH COLD WORKING PARAMETERS OF IS 4.6 MM AND IP 850 MPA.	72
FIGURE 5.16. FEM HOOP STRESS RESULTS FOR STEEL RSW WITH COLD WORKING PARAMETERS OF IS 7.1 MM AND IP 850 MPA.	73
FIGURE 5.17. AL RSW MICROSTRUCTURE.....	75
FIGURE 5.18. MICROHARDNESS OF POST COLD WORKED AL RSW.....	76
FIGURE 5.19. L-N CURVE FOR AS-WELDED AL AND POST-WELD COLD WORKED RSW SPECIMENS WITH VARIOUS IP.....	78

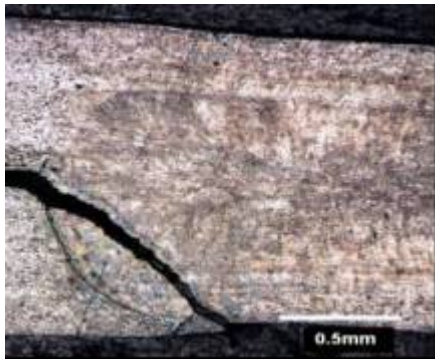
FIGURE 5.20. FEM OF AL RSW WITH 7.1 MM IS.....	79
FIGURE 5.21. FEM OF RESIDUAL STRESS IN THE HOOP DIRECTION WITH FRINGE LEVELS FOR 4.6 MM IS.....	80
FIGURE 5.22. FEM OF RESIDUAL STRESS IN THE HOOP DIRECTION WITH FRINGE LEVELS FOR 7.1 MM IS.....	81
FIGURE 5.23. EFFECT OF INDENTATION PRESSURE (IP) AND SIZE (IS) ON FATIGUE LIFE OF AL RSWs POST-WELD COLD WORKED AT 686 N AND 882 N MAXIMUM LOAD WITH COMPRESSIVE RESIDUAL STRESSES.	83
FIGURE 5.24. SPR C-GUN WITH THROAT SIZE SHOWN.....	85
FIGURE 5.25. SCHEMATIC OF THE STEPS IN THE SPR PROCESS.	85
FIGURE 5.26. TYPICAL SPR INSTALLATION PROCESS FORCE DIAGRAM SHOWING REGIONS I, II.	86
FIGURE 5.27. FORCE CURVES FOR AL SPR.	86
FIGURE 5.28. ULTIMATE FORCES FOR SPR IN AL MATERIALS FOR RESPECTIVE REGIONS.	87
FIGURE 5.29. CROSS SECTIONS OF SPR FOR EACH MATERIAL TYPE AND THICKNESS.....	89
FIGURE 5.30. SPR TENSILE RESULTS FOR AL SHOWING ERROR BARS.....	90
FIGURE 5.31. SPR SAMPLE FAILURE DURING TENSILE-SHEAR TEST.....	90
FIGURE 5.32. SPR PROCESS FORCE FOR AL 5052 CW AND AR WITH RESPECT TO SHEET THICKNESS.....	91
FIGURE 5.33. TENSILE STRENGTH OF CW AND AR SPR AL 5052 SHEET WITH ERROR BARS.....	92

FIGURE 5.34. FATIGUE OF SPR FOR SHEET THICKNESS 1.27 MM.	93
FIGURE 5.35. FATIGUE OF SPR FOR SHEET THICKNESS 1.6 MM.	94
FIGURE 5.36. CRACK INITIATION (SEM).....	95
FIGURE 5.37. SPR FAILURE FROM FRETTING.	95

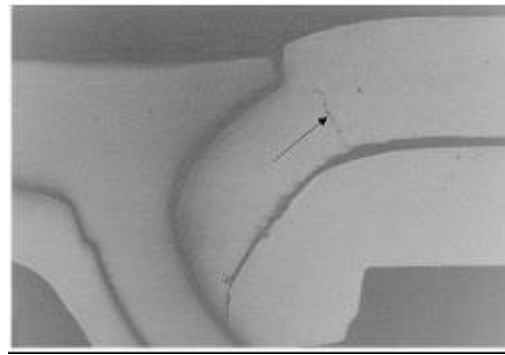
CHAPTER 1:

INTRODUCTION

In today's economy the driving force of the creating a new product is for the marketer to assert to the buyer the reliability and effectiveness of the product at a price the market can bear all the while reducing the cost of manufacturing the product with each new design. This obligation is prevalent in the automotive and aerospace industries which use sheet metal for nearly all of their applications. Sheet metal is defined as the workpiece material with the thickness of $\frac{1}{4}$ inch or less and used for the structural bodies for both automobiles and airplanes. Joining is required to construct the structural elements such as automobile bodies when using steel or aluminum sheet metal. Because of this frequent usage of the joints, the cost of joining process is quite critical. As a result, the quick and inexpensive processes such as resistant spot welding (RSW) and self-pierce rivets (SPR) are widely used in the automotive industries. For example, modern automobiles have 2000-5000 spot weld joints and in a class 8 semi-truck there are approximately 1600 self-piercing rivet joints in their respective bodies [Chao Y., 2003]. Beside the economic standpoint of the joining process, the reliability and durability of the joints are also important. The joining aspect is the most critical with the use of sheet metal because the load applied to the sheet metal is transferred between sheets via the joint. Often, mechanical failures of the sheet metal structures initiated at the joint itself or the holes for the joints. The joints are often the sites for crack origination in sheet metal because they have the highest stress concentration. Figures 1.1 (a) and (b) show fatigue cracks occurring in a RSW and SPR respectively.



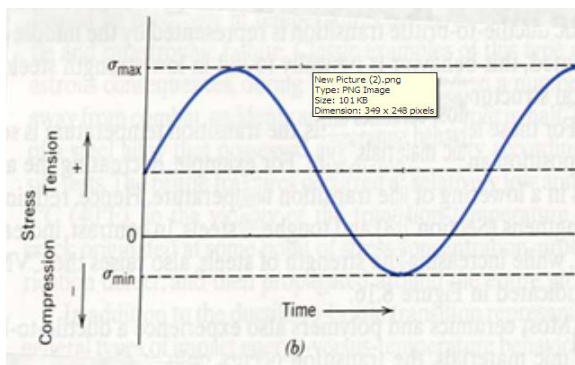
(A.) RSW



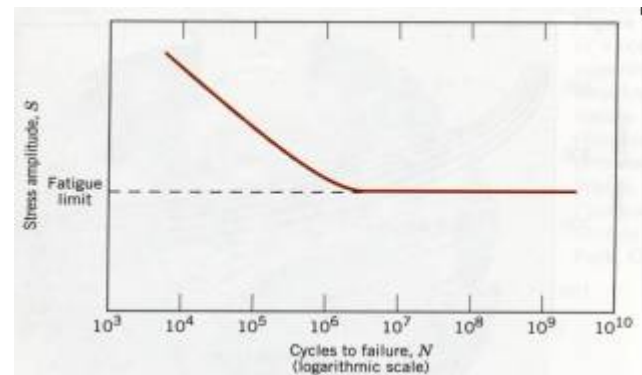
(B.) SPR [FU, M., *ET AL* 2003]

FIGURE 1.1 CRACKING IN SHEET METAL JOINTS.

When an object is subjected to dynamic and cyclic loading the term is called fatigue. Fatigue accounts for 90% of all metallic failures in any application and often fails at a lower stress than its yield strength. Figure 2 (a) show a common cyclic stress plot where the material is under tensile stress then returns to a compressive stress and continues that cycle.



(a) CYCLIC STRESS BEHAVIOR DURING FATIGUE.



(b) FATIGUE S-N CURVE WITH FATIGUE LIMIT.

FIGURE 1.2. FATIGUE TESTING PROCEDURES.

[Callister W., 2007]

The graph in Figure 2 (b) is created by applying several different loads and counting the number of cycles until failure. Fatigue life is the number of cycles needed to generate a

complete failure of the part at a given stress and any stress below the fatigue limit will not cause failure.

1.1 SHEET METAL JOINING

The fatigue life of mechanically fastened structure in sheet metal fundamentally depends on the local state of stress at the fastener and the surface condition (e.g. surface finish, ‘damage’, fretting) of the sheet. The local stress state at the sheet joint is dependent on several factors such as the types of fastener and joint material, joint configuration such as the number of stacked sheets, tolerances, manufacturing methods, and loading magnitudes and sequences. [Urban M., 2003]

1.2 RESISTANCE SPOT WELDING

Resistance spot welding (RSW), or spot-welding, remains the most frequently used sheet metal cohesion process in industry [Li, W., *et al* 2001]. Invented by Elihu Thoson in 1886, RSW has been applied to low carbon steels and aluminum joints. RSW is when a high current is applied through two sheets of metal and the contact surface between the sheets causes a resistance. This electrical resistance creates thermal energy melting the surround metal and ultimately fuses the melted metal from the two sheets together creating a weld [Cho, Y., *et al* 2003 (B)]. The automotive industry prefers to use RSW because it is a quick (approximately 1 second cycle time) and simple operation when compared to conventional riveting processes. RSWs often have problems controlling quality, structural rigidity and durability. Fatigue is a frequent cause of failure for RSW joints in sheet steel and aluminum and are prominent sites for initiation of defects and cracks [Khanna, S., *et al* 2001, Zang, Y., *et al* 2000, Pan N., *et al* 2003, Rajaj, D., 1990]. Even though there is a great amount of

interest in achieving high durability and fatigue resistance for RSW sheets, there are limited publications in regards to developing a process to improve the fatigue strength of RSW low carbon steel joints [Spitsen, R., *et al* 2004].

1.3 SELF-PIERCING RIVETS

The use of lightweight material in the construction of automobiles has found an increasing interest due to vehicle weight reduction which improves fuel economy, drivability, and performance. Aluminum alloys offer considerable potential to reduce the weight of automobile body structures. The selection of an appropriate assembly technology for aluminum is challenging in the design and manufacture of lightweight auto-body structures because of the various material properties when compared to steel. Self-piercing riveting (SPR) first invented in the 1950s but was not until recently it has become one of the promising joining techniques for the automotive applications of aluminum sheets [Cai W., *et al* 2005]. An Audi A8 has 500 RSW and 2600 SPR, 1500 of these SPR have replaced a RSW [Wang B., *et al* 2006]. It is a simple, clean and fast one-step mechanical fastening technique for point joining of sheet material components. Conventional aluminum joining processes such as riveting and resistant spot welding have drawbacks because the need for pre-drilled holes and inconsistent joint quality and durability [Cai W., *et al* 2005]. SPR does not require pre-drilled holes and relies on mechanical interlocking rather than fusion. It can be used with a large combination of materials with different properties, where resistance spot welding is difficult or even impossible. These conditions include heavily zinc-coated, organic coated or pre-painted steels, or combinations of steel to aluminum alloys and some composites to metals. SPR is a cold forming operation where two or more sheets are interlocked together by

a semi-tubular shaped rivet being driven into the sheets with an opposing die causing the rivet to flare out [Sun X., *et al* 2007].

1.4 INTRODUCTION OF CHAPTERS

In chapter 2, sheet metal joining techniques will be described in more detail as to the process involved to produce the joint from previously published literature. Also included is the mechanical properties developed in a joint during and after the joint is installed. The effects of different cold working processes by previous researchers on sheet metal joints to enhance the fatigue life will be discussed

Chapter 3 will give the objective of this research. The view of what the final goal in terms of what will make this a productive and applicable research for today with tomorrow's needs will be covered.

The procedures used in the research for RSW and SPR are exposed in chapter 4. This procedure includes the experimental setup detailing the scope of what was needed to make the research viable. The material used and the experimental approach portion gives the research core of what steps were taken to produce final results.

The results and a discussion will be shown in chapter 5. The first section of this chapter covers the results of each type of test discussed in chapter 4 for steel RSW with the effects of the cold worked process. Next will be Al RSW and lastly SPR are discussed in this chapter.

Chapter 6 will give the final conclusion that can be drawn from the results. Chapter 7 gives future research directions for the joining processes.

CHAPTER 2:

LITERATURE SURVEY

Research on sheet metal joints has intensified over last a few decades to understand the joining processes and investigate their mechanical properties. Most of research work in sheet metal joining can be grouped into two areas: one is to develop and optimize the processes; the other is to test joint properties and improve them. Background information relevant to this research is needed to understand the various sheet metal joining processes and their mechanical properties. Recently introduced sheet metal joining processes will be discussed, then research on the process studies and mechanical property studies on the resistance spot welding (RSW) joints will be developed. Then, some of experimental studies on the self-piercing riveting (SPR) joints will be presented, and finally cold working procedures used in today products.

2.1 SHEET METAL JOINING PROCESSES

Sheet metal joining processes can be categorized in terms of their common principles of operation. The two most popular sheet metal joining processes are fusion welding and mechanical fastening. Fusion welding involves melting together and coalescing materials by means of heat, usually supplied by electrical or other high-energy means. The most representative fusion sheet metal joining process is RSW. Due to its superior characteristics in cost and joint quality, RSW is the most common sheet metal joining process in the automotive and other industries. RSW has its limitations such as instable joint quality, heat affected zone (HAZ), and is more difficult in aluminum joints. A welded joint is permanent

while a threaded fastener can be removed. Mechanical fastening processes typically involve traditional methods, using a wide variety of fasteners, bolts, nuts, screws, and rivets. Riveting is the most common method for permanent or semi-permanent mechanical joining. However it has disadvantages including multi-step process and the need of expensive pre-hole drilling. Research on sheet metal joining process development has been conducted in the direction of improving from RSW by riveting processes and introducing alternative processes to replace them.

The choice of a useful joining technology is a key aspect in designing cold-formed structures using sheet metal [Lorenzo G., *et al* 2004]. In fusion sheet metal joining processes, laser beam spot welding has been introduced and offers a unique combination of high speed, precision and low heat distortion, compared with the conventional RSW process. This combination of advantages is especially attractive for the automotive industry. However, there is still a need of optimizing the laser spot welding process and investigating the joint quality and durability [Yang, Y., *et al* 1999].

In mechanical fastening processes, several different types of rivet joining techniques have been introduced recently and some are shown in Figure 2.1, each of these joining technologies belong to an innovative category because of their structural performance and high-speed assembly.




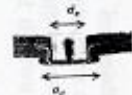
Name	AVDELOK 2611	HEMLOK 2221	FASTRIV FAS11	AVICLINCH
Manufacturer	Avdel Textron	Avdel Textron	Avdel Textron	Avdel Textron
Fastener type	Bi-component blind rivet	Mono-component blind rivet	Self-piercing rivet	Circular press-joint
Material	High-strength low-alloy steel (galvanized 7 μ)	Galvanized high-strength low-alloy steel	High-strength low-alloy steel (galvanized 3 μ)	Sheet material
Diameter (mm)	$d_h = 6.5$	$d_b = 6.5$	$d_b = 4.8$	$d_p = 5.00$ (punch diameter), $d_d = 0.50$ (die diameter)
Nominal shear strength $F_{v,Rn}$ (kN)	14.73	17.00	-	-
Cross-section				

FIGURE 2.1. VARIATION OF RIVETS.

[Lorenzo G., *et al* 2004]

There are new joining technologies still in early development such as Friction Stir Riveting (FSR) researched by R. Stevenson [Stevenson R., *et al* 2005]. FSR uses properties of Friction Stir Welding where local heating caused by friction between the high spinning rivet and sheet metal softens the sheet material allowing penetration of the rivet with little force. A cross sectional view of a rivet entering the workpiece is shown in Figure 2.2. After the rivet enters and the surrounding material cools diffusion bonding occurs thus enhancing the strength. The major benefit of FSR is access is needed from only one side of the workpiece.

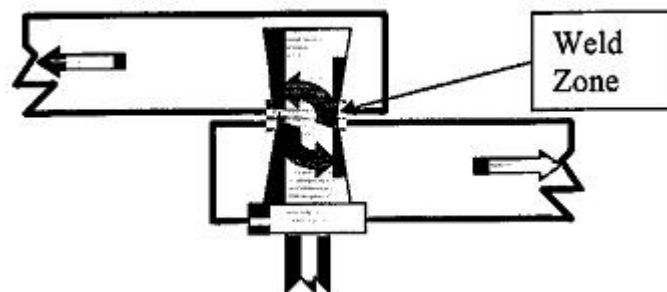


FIGURE 2.2. CROSS-SECTIONAL VIEW OF FSR IN WORKPIECE.

[STEVENSON R., *ET AL* 2005]

RSW and SPR are still the most widely accepted sheet metal joining process in the current automotive industries. RSW and SPR are exceptionally attractive to the auto industry because they provide the greatest strength with the lowest process time.

2.2 RESISTANCE SPOT WELD

2.2.1 PROCESS

Resistance spot welding has been studied heavily for the last 35 years. Previous research has been focused on electrode force, welding current, welding time, electrode shape and surface condition of specimen during the RSW process. Nugget formation and quality has been experimentally and numerically studied. The nugget or weldment is defined as the part of metal from the work piece that has gone through a transformation of heating, melting, fusion and resolidification [Long X., *et al* 2003]. Surrounding the nugget is the heat affect zone (HAZ) which is caused during the RSW process by the heat traveling away from the nugget. A schematic of a RSW cross section is shown in Figure 2.3.



FIGURE 2.3. RSW CROSS-SECTION SCHEMATIC.

Resistance spot welding is a process involving electrical, mechanical, thermal and metallurgical factors [Han, Z., *et al* 1990]. The electrical energy is converted to thermal energy at the tips of two opposing water-cooled copper electrodes. Between the electrode tips

are two sheets of metal to be joined together as shown in Figure 2.4. To create the joint the two electrodes clamp the sheets together under a high force to fashion a direct path for the high electrical current to pass between the electrodes. The two main sources of electrical resistance during the clamping, are the resistivity of the electrode-sheet and the sheet-sheet (also known as the faying surface shown in Figure 2.7) interfaces. The electrical resistance creates the high thermal energy melting the sheet at the sheet-sheet interface to form the weldment.

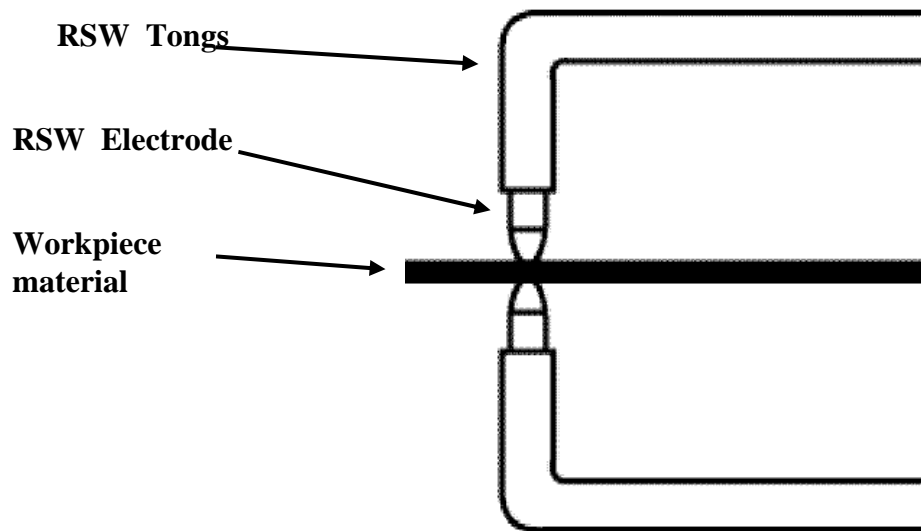


FIGURE 2.4. SCHEMATIC OF RSW PROCESS.

[SPITSEN, R., 2005]

Several material properties influence the weld nugget including melting temperature, specific heat, density, resistivity, thermal conductivity, thermal expansion coefficient, and temperature dependent yield strength. The thermal energy is governed by the equation:

$$E = I^2 R t_h,$$

where E is thermal energy, I is current, R is resistance and t_h is heating time. Because of the nature of the equation the weld current and time have a considerable affect on the thermal

energy which in turns governs the size of the weld. The weld quality, which is also known nugget size, is also influence by the electrode force because the larger the electrode force the larger the contact surface for the current to pass through creating a larger melting zone.

RSW of steel alloys has been studied for more than five decades. The scope of the studies are very wide and include optimization of the process, improvement of RSW quality, automatization of the process, and application to automotive structures. S. Darwish [Darwish S., *et al* 1999] investigated the influence of RSW parameters (welding current, welding time, electrode force and sheet thickness) on the RSW strength using a statistical approach. The most optimal parameters for weld strength in a sheet thickness range (0.5-2.5 mm) are welding time being a minimum of 75 ms, a minimum electrode force of 756.56 N and the maximum welding current of 19.364 kA. Recent trend in steel RSW research is to apply RSW to high-strength steels. Z. Han [Han, Z., *et al* 1990] investigated the weld development in high-strength cold-rolled steel sheets. High-strength steels are judged against low-carbon steels because low-carbon steels are the standard in the RSW process in determining acceptable weld schedules. High-strength steels have a high electrical resistivity thus require lower currents to reduce expulsion but also reduces the weld quality leading to a narrow welding schedule (welding current, time and holding cycle). It was found the welding current and time are the most sensitive parameters to control expulsion. The holding cycles influence the extent of cracking outside the nugget during solidification. It was also found the stresses in the weld are highest at the edges of the electrode and lowest at the center of the weld.

Aluminum RSW sometimes replaces steel RSW because aluminum is lighter than steel. Aluminum though requires a much higher energy level than steel because aluminum is a poor conductor thus requiring more current to create a fusion zone. Y. Cho [Cho, Y., *et al*

2003 (A)] compared the RSW of steel to aluminum under two possible abnormal conditions, angular misalignment (poor fit-up) and wear of the electrodes. These two conditions are the most repetitive problems seen by weld engineers in the industry. It was found the electrode size has a greater effect on the weld quality than the electrode misalignment samples. The electrode size also had a greater influence in steel than in aluminum, the total variance of the weld quality in steel due to electrode size was 80 %. Aluminum was influenced the greatest by poor fit-up conditions with a variation of 65 % on the weld quality. Weld quality can be increased by 13.5 % in steel and 49 % in aluminum when the abnormal process conditions are removed. This suggests that steel is a more robust material for the RSW process than aluminum.

In an analysis of Al RSW X. Sun [Sun X., *et al* 2000] studied the effect of electrode pressure on electrical contact resistivities. Since Al has a higher thermal conductivity, lower melting temperature and lower yield strength than steel, the distortion and spacing between sheets is much more severe on the weld quality than with steel RSW. A lower electrode clamping force produced a larger nugget but at the same time the force is needed to prevent expulsion. A higher current creates more heat thus larger melting area resulting in a bigger nugget. The current density increases as the electrode clamping force decreases while electrical conductivity at the faying surface decreases. All of these factors ultimately produced a larger nugget.

Expulsion during the welding process was researched by J. Senkara [Senkara, J., *et al* 2004]. The cause of expulsion is the ejection of liquid metal during the heating phase of RSW. It occurs frequently in Al RSW because of the use of higher current over a short period of time. This loss of molten metal causes voids in the weldment, which can be seen in Figure

2.5. There are two different locations of expulsion: electrode/workpiece interface and at the faying surface. The interface of the electrode and workpiece has no effect on weld quality only the poor surface quality and increase of electrode wear. The faying surface interface does have an adverse effect on weld performance [Zhang, H., 1999].



FIGURE 2.5. AL RSW CROSS SECTION.

There is little information available on cracking in Al alloy RSW, although J. Senkara [Senkara J., *et al* 2000] studied the phenomenon for cracking in the HAZ and healing during the RSW process. Thermal stresses are formed in Al RSW similar to steel RSW from the heating and cooling process. Crack appearance and orientation were repeatable leading the author to conclude they formed at elevated temperatures during the liquid metal phase. It was concluded the cracks could be filled with liquid metal from the nugget by leaving the current on for a longer period of time. Shown in Figure 2.5 is an Al RSW cross-section showing the nugget and porosity of the weld-zone.

2.2.2 RESIDUAL STRESSES

Residual stresses created during RSW have always kept the interests of researchers because they affect the mechanical properties in the joints. Residual stresses are defined as self-equilibrating stresses existing in materials under uniform temperature conditions without external loading.

S. Khanna [Khanna, S., *et al* 2001] studied the residual stress measurement in RSW. Residual stresses can occur when engineering components are subjected to elastic-plastic loading, machining, welding, forming, heat-treating, or coatings. There are three classes a residual stress can fall into: macroscopic (extends over several grains), micro stress (covers one or part of a grain) and the third covers several atomic distances in one grain. Tensile residual stresses accelerate crack development while compressive residual stresses hinder crack growth [Webster, G., *et al* 2001]. High tensile residual stresses are a major contribution to crack initiation and propagation in RSW. To determine the macro residual stresses in S. Khanna's research they used an optical technique of high sensitivity moiré interferometry. It was found the stresses at the center of the weld were in the range of 250-300 MPa and decreased towards the edge in the range of 40-100 MPa, all in tension.

X. Long [Long X., *et al* 2003] did a numerical study on residual stresses in a spot welding joint. After the intensive local heating during the RSW process, temperature gradients are formed by the non-uniform rapid cooling. Heterogeneous deformations are induced by the temperature gradients and phase changes in the solidifying metal, which results in the development of internal residual stresses. It was found that during the heating cycle as the temperature rises rapidly the expansion of the liquid metal in the weld zone is restricted by the surrounding base metal causing compressive residual stresses inside the weld zone. The surface metal has a higher cooling rate because of its contact with the water cooled electrodes than the hot liquid metal during the hold time. The surface metal is restricted to shrink by the surrounding liquid metal thus causing tensile residual stress at the outside of the weld zone. As the weld zone cools it begins to shrink but is restricted by the surrounding cooler base metal causing tensile stress to dominate the joint. Shown in Figure 2.6 is the

stress distribution for an Al RSW joint in the σ_{11} , σ_{22} and σ_{33} directions. Of interest is the σ_{33} direction also known as hoop stress because it is considered to be the best indicator of all the stresses at a give point.

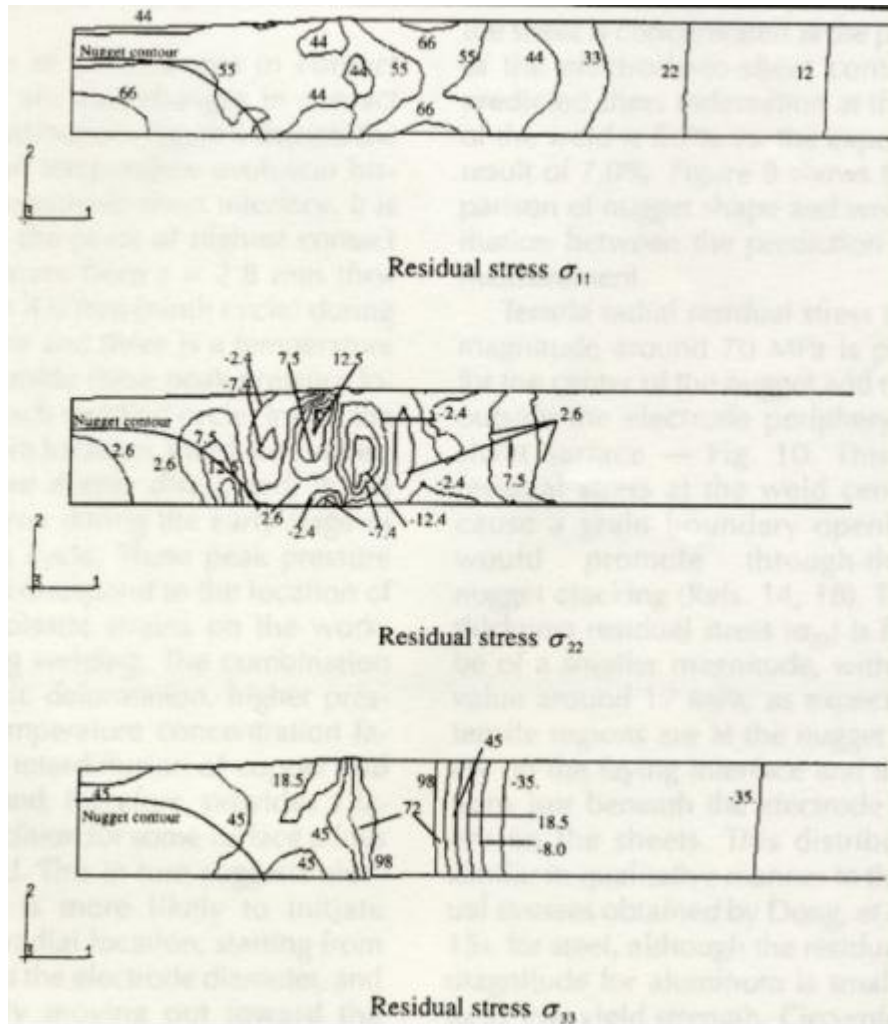


FIGURE 2.6. RESIDUAL STRESS DISTRIBUTION OF AL RSW.
[SUN, X., ET AL 2000]

The fatigue strength of spot welded joints can be assessed on the basis of the local stress state at the weld spot edge [Radaj D., 1989]. D. Radaj examined the notch stress of a spot-welded joint. The notch root (also referred to as notch) is the slit surface at the weld spot edge as shown in Figure 2.7. It was concluded the notch stress can be used to optimize the

design of the RSW as an alternative to fatigue testing because the notch is often the location for crack development. This correlates with the high hoop stress concentration with a value of 95 MPa at the notch region shown in Figure 2.6.

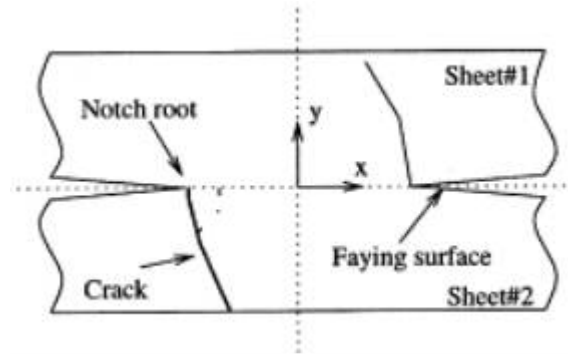


FIGURE 2.7. SCHEMATIC OF RSW CROSS SECTION.
[PAN N. 2003]

Compressive residual stress has a beneficial effect on fatigue life, crack propagation and stress corrosion of materials whereas tensile residual stress reduces their performance [Khanna S., *et al* 2001]. S. Khanna investigated the effect residual stresses in RSW have on fatigue life and found that during fatigue testing the tensile stress at the center of the weld decreased while at the edge was an increase in tensile stress. This correlates with findings of most cracks originating from the edge of the weld (or within the HAZ). The increase in tensile residual stress in this region is a major cause for the joint fracture. Even though the residual stress is significantly below the yield stress the combination of it and the external load is detrimental.

2.2.3 MECHANICAL PROPERTIES

Mechanical properties such as tensile and fatigue strengths have been researched in RSW joints to study their reliability and durability. Research on the mechanical properties of a RSW has been done by F. Haggag [Haggag F., *et al* 1992] on both steel and aluminum. In Table 2.1 the σ_y (yield strength), K (strength proportionality constant) and σ_{UTS} (Engineering Ultimate Strength = $\frac{Kn^n}{(1+n)}$ where n= Strain-hardening-exponent) are shown. In mild steel the mechanical properties increase when moving from the base material to the weld nugget. In aluminum the nugget properties were lower than the base material. Both of these findings are consistent the type of alloy and microstructure of the material. From this table it is shown that the increase in weld size has a direct relationship to the mechanical properties.

	σ_y (MPa)	K (MPa)	σ_{UTS} (MPa)
1020 Mild Steel Small RSW			
Base Material	223	540.1	359
HAZ	345	829.1	553
Weld Nugget	421	1007.4	673
1020 Mild Steel Large RSW			
Base Material	254	613.4	408
HAZ	281	684.7	456
Weld Nugget	353	826.8	554
2219 Aluminum			
Base Material	253	634.3	417
HAZ	184	432.3	289
Weld Nugget	191	44.0	298

TABLE 2.1. MECHANICAL PROPERTIES OF STEEL AND ALUMINUM RSW.

Y. Lee [Lee, Y., *et al* 1998] developed a Design of Experiments (DOE) to determine the ultimate strength of RSW based on three design factors: coupon width, coupon height and

weld nugget diameter. Monotonic tensile-shear loads were applied until they overcame the load capacity of the weld. It was found the coupon width and nugget diameter were the only significant factors with nugget diameter having a 70% influence on the ultimate strength.

Researchers N. Pan and S. Sheppard [Pan, N., *et al* 2003] studied the stress intensity factors in RSW joints. Previous to their work it was assumed the stress intensity factors were based on initial cracks at the notch causing failure through the nugget. However it was found fatigue cracks propagate through the thickness of the sheets rather than through the nugget as shown in Figure 2.7. There are several local maxima and high gradients of tensile stresses and one of these is located at the faying surface. This shows that the residual stress distribution does not decrease strictly outside the nugget but resides in the HAZ [Henrysson H., *et al* 1999].

S. Sheppard [Sheppard S., *et al* 1992] developed a FEA (finite element analysis) model of fatigue crack initiation and growth by examining the stress state that is dependant on the applied load during fatigue. It was found crack initiation and early growth at 1×10^6 cycles is estimated to occur at approximately 26% of the tensile-shear load. At this point the crack length is approximately 0.25 mm, this length is approximately across 10 grains in the HAZ with an average grain length of 20 μm . Thus all crack initiation and propagation were found in the HAZ near the weld notch.

H. Kang [Kang H., *et al* 2000] discussed the effects of combined tension and shear load on the fatigue life of welds. There is a transition value developed by A. Rupp [Rupp A., *et al* 1995] between the sheet thickness and the weld nugget diameter that effects the mode failure of a RSW. When the nugget diameter is $\geq 3.5\sqrt{t}$, where t is the sheet metal thickness,

the crack propagated through the HAZ but when the diameter is less than the transition value the weld fails by the crack traveling through the weld.

For RSW in automotive components it is important to understand their fatigue behavior under variable-amplitude load fluctuations [EL-Sayed M., *et al* 1996]. M. El-Sayed developed a FEA to help predict the relationship between the nugget maximum and the sheet metal thickness to the fatigue life. They concluded that a small increase in load level or small decrease in sheet thickness would significantly reduce the fatigue life. This correlates with findings in industry where sheet metals are being replaced by lighter gage (same as sheet thickness) or higher strength sheets, and when no other RSW design modifications are considered this is detrimental to the fatigue strength.

An evaluation of different automotive sheet steels was investigated with respect to fatigue life of an RSW by M. Gentilcore [Gentilcore M., 2004]. The materials used in this research ranged from mild to advanced high strength dual phase and TRIP (Transformation Induced Plasticity) steels. For the mild steels with yield and tensile strengths ranging 40 MPa there was no impact on the fatigue life of the weld when comparing the different specimens. On formed mild steel samples, where the material strength increased, there was a slight increase on the fatigue resistance. For the advanced and TRIP steels as the tensile and yield strengths increase the base material fatigue resistance increases also. After the spot-weld process the fatigue resistance for these high strength materials was similar to the mild steels. Results concluded design adjustments need to be made in the RSW process to optimize the effectiveness of advanced steels.

P. Thornton [Thornton P., *et al* 1996] researched on Al RSW fatigue mechanics and they concluded the fatigue performance depends primarily on the nugget diameter. Even

though the military and aerospace consider porosity, crack expulsion as weld defects this research showed they do not lead to lower weld strengths. Similar results were found by A. Gean [Gean A., *et al* 1999] who studied both static and fatigue behavior of Al RSW. Porosity up to 40% of the nugget diameter (6.3 mm) affected neither static nor fatigue strengths. Increasing the weld diameter from 4.2-7.2 mm significantly increased the static performance but in fatigue there was only a small enhancement for high-load/low-endurance and no effect for low-load/high-endurance. The most influential parameter on fatigue strength was the electrode force, with an increase from 4 kN to 6.5 kN the fatigue load increase 15% for 10^6 cycles. Lowering the electrode force by the same magnitude decreased the fatigue load by 15%. The deep surface indentation caused by the high force of the electrode enhanced the fatigue strength. All of the RSW process parameter changes have a limited influence on the final mechanical properties of the joint.

2.3 SELF-PIERCING RIVETS

2.3.1 PROCESS

Self-piercing riveting (SPR) is the mechanical fastening process that consists of a rivet being driven into the sheets. Due to the lack of producing consistent high quality spot welds in aluminum because of surface oxidation and high conductivity, SPR provides an alternative for sheet metal joining [Cai W., *et al* 2005]. Figure 2.8 shows the cross section of the SPR joint. The top sheet is referred to as the pierced sheet while the bottom is the locked sheet. The rivet head is the upper horizontal plane of the rivet while the rivet tail is the bottom tubular shape.

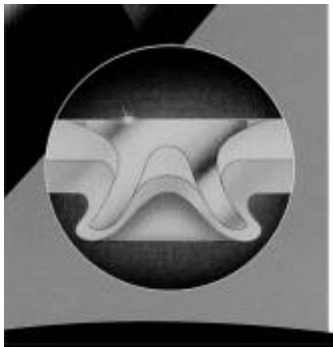


FIGURE 2.8. SPR JOINT.
[FU, M., *et al* 2003]

There are four steps in the SPR process shown in Figure 2.9:

- Clamping: Punch forces rivet against top sheet perpendicularly.
- Penetration: Rivet penetrates top sheet causing plastic strain.
- Expansion/Flaring: Rivet tail flares out to the contour of the opposing die in the locked sheet causing mechanical interlocking.

- Compression: Punch continues to push the rivet into the sheets until a certain force or stroke is reached.

This process takes approximately 1 sec.

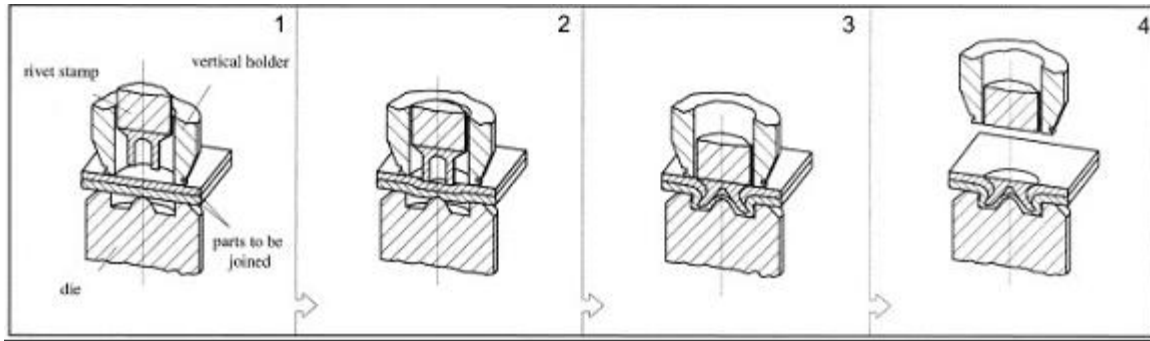


FIGURE 2.9. SPR PROCESS.

[SUN, X., *et al* 2007]

W. Cai researched the dimensional effects SPR assembly does to severe joint distortion. The concern was this joint distortion could transmit the residual stresses throughout the whole structure being joined and cause global distortions. It was found the SPR joint distortion is two to four times greater than a RSW; the distortion in the top and bottom sheets in a RSW is symmetric whereas in an SPR the locked sheet has less distortion than the pierced sheet. Design and process effects on the rivet distortion are: die type, rivet head set-down (how flush the rivet is with the pierced sheet), rivet length and material types. Non-design and non-process parameters that effect SPR distortions are alignment of the sheets with the rivet, variation in gaps between the sheets, the peak rivet force, and the surface condition of the sheet. Global assembly dimensions can be affected in a negative manner by SPR density (number of rivets for given area).

E. Atzeni [Atzeni, E., *et al* 2005] did experimental and numerical investigations on variables that can affect the mechanical characteristics of a SPR joint. Two different failure mechanisms were noticed; the first was pierced sheet failure where the crack in the sheet

propagated perpendicular to the applied load while the second failure mode was rivet pull out. It was found with changing rivet and die shape effects the failure mechanism, which in turn determines the tensile-shear strength. With the correct rivet-die combination there is good sheet overlapping and more complete rivet expansion thus increasing rivet resistance to failure. This correct combination changed the failure mode from material failure to rivet pull out. An ANOVA (Analysis Of VAriance test) was performed on the independent parameters and the conclusion was upper sheet thickness and rivet shape were the most significant variables with die shape being next. This is justified if the pierced sheet is thin the fracture stress is reached before the rivet pulls out. It was also concluded the lower sheet needs to have good deformation characteristics.

Conventional SPR process uses an electric motor or hydraulic cylinder referred as a quasi-static process which forces the rivet into the sheet metal. B. Wang [Wang B., *et al* 2006] introduced an impact method using gunpowder to drive the. From appearance the two methods seem to produce the same joint but looking at the cross-section the amount of deformation and fracture in the sheets are drastically different. This is because of the deformation rates are different between the two processes. Impact SPR reduces internal damages and residual stresses in the sheets around the rivet. In tensile-shear loading and fatigue, impact SPR has higher yield strengths than quasi-static SPR.

2.3.2 MECHANICAL PROPERTIES

SPR creates high residual stress concentrations which degrades the tensile and fatigue strengths of the joint. Because a hole is made in the pierced sheet there is a frictional force between all the contact points of the joint. In cyclic loading these surfaces can move relative

to each other causing contact damage and eventually cracks which lead to failure [Li B., *et al* 2006].

R. Porcaro *et al* [Porcaro R., *et al* 2004] did a numerical study on the mechanical properties of SPR. Failure loads were looked at under shear static loading conditions. For their testing procedure they found all specimens failed in the pierced sheet and the behavior of the rivet was elastic. The tensile strength of the SPR was found to be equal to 50% of its shear strength.

A study of fatigue behaviors of similar and dissimilar materials was performed by X. Sun [Sun X., *et al* 2007]. It was found by doubling the pierced sheet thickness and leaving the locked sheet constant the fatigue strength more than double.

X. Sun also compared RSW mechanical properties to SPR. For a typical 2 mm gage 5182-O SPR joint the fatigue strength is almost 100% greater than its RSW counterpart. A probable reason for this superiority is the different stress concentration between the two processes leads to different failure mechanism under fatigue loading. The critical stress concentration is at the faying surface which in RSW is in tension while in SPR is compression.

M. Fu [Fu M., *et al* 2003] studied the fatigue of SPR in Al 6111 by doing constant and two-level amplitudes as well as affects of rivet setting pressure (RSP and RSF, rivet setting pressure are interchangeable). RSP is the pressure required to press the rivet into the overlapping sheets. The RSP had a direct affect on the static strength of the rivet up to 90 bar, after it reached this point the static strength leveled off. RSP had no influence on fatigue performance. For the two-level amplitudes the SPR was pre-cycled, high load followed by low load or vice versa. When the low load followed the high load there was an increase in

fatigue life, the cause of this may be the cyclic hardening of the Al at the rivet joint. For high loading following low loading there was no increase in fatigue life, it was determined the cyclic hardening is less at lower loads than higher load levels. Sequential fatigue and static tests were performed where the specimen was pre-cycled to a fraction of the fatigue life at a maximum load then tested in tension until failure. It was found that pre-cycling up to 75% of the fatigue life gradually deteriorates the rivet strength and above 90% of the fatigue life the rivet strength decreases drastically.

Fatigue behavior of single and double SPR joints was studied by K. Iyer [Iyer K., *et al* 2005]. Two different sheet thicknesses were used 2 mm and 3mm, the 2 mm sheet joints have a higher fatigue life than the 3 mm sheet joints concluding that the rivet has an optimum sheet thickness. Three different failure modes were noticed from the fatigue testing:

Mode 1: cracking in the pierced sheet (85%)

Mode 2: rivet pullout from the locked sheet (37 %)

Mode 3: cracking of the locked sheet (15%).

More than one failure mode was possible in a single specimen. All crack initiations were found 1-2 mm ahead of the rivet head at the faying surface, along with severe, permanent and localized sheet bending. This bending is the reaction to the moment at the rivet head. Along with the fatigue crack, fretting wear was observed. Fretting wear occurred at the locations shown in Figure 2.10, location A is the rubbing between the two sheets at the faying surface and location B is the rivet shaft and hole in pierced sheet. FEA showed the highest computed tensile stress in the pierced sheet occurs at A, this is the same location the majority of fatigue cracks were observed. With an increase in sheet thickness the amount of fretting increased also while the degree of sheet bending decreased.

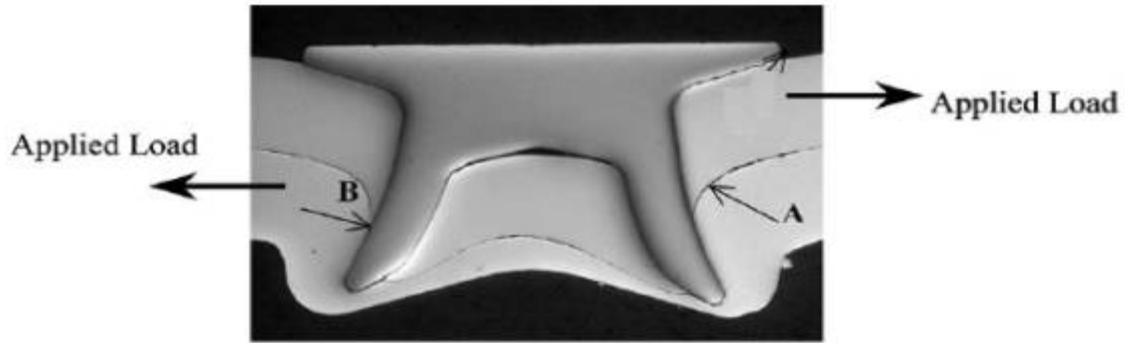


FIGURE 2.10. FRETTING LOCATION IN AN SPR.

[HAN L., *et al* 2004]

Fretting wear can be determined by the FEA equation:

$$F = \mu p \delta$$

F is the measurement of energy expended in frictional microslip, μ is the coefficient of friction, p is contact pressure and δ is the microslip amplitude (amount of relative movement between the two surfaces in question).

Fretting wear was investigated by Y. Chen [Chen Y., *et al* 2003] in Al SPR. They found at a maximum load for the rivet fretting began to occur at location A at approximately 15% of the fatigue life. The size of fretting wear increased as the cycles and load increased. At location B fretting was circumferential around the rivet located 2 mm (sheet thickness) below the rivet head. From EDX (energy dispersive X-ray) analysis there is a high level of aluminum concentration at this fretting scar.

Two types of fretting occurred at location A, two-body and three-body fretting. Two-body fretting is the bright region inside the scar shown in Figure 2.11. Three-body is the black oxidized region containing debris. Debris are created at the high contact stress concentration between the moving surfaces.

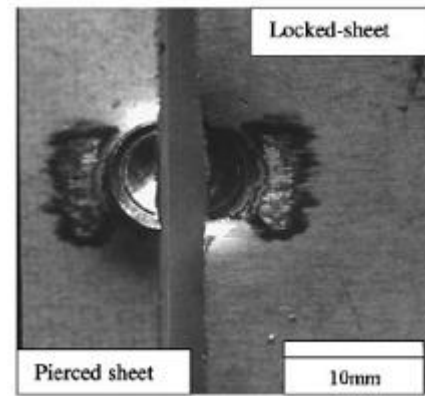


FIGURE 2.11. FRETTING SCARS FROM SPR.

[Chen Y., *et al* 2003]

Shown in Figure 2.12 micro-cracks are causing delamination to occur which become abrasive particles that travel from the two-body fretting zone to the three-body fretting. The microhardness readings show the abrasive particles cause local work hardening on the sheet surface. The micro cracks in two-body fretting can lead to macro cracks resulting in complete failure of the joint.

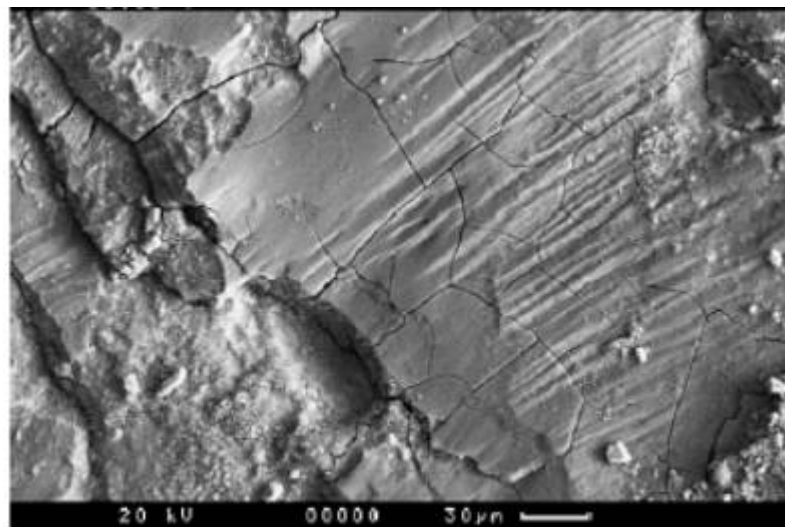


FIGURE 2.12. MICRO-CRACKS AND DELAMINATION AT TWO BODY FRETTING.

[Chen Y., *et al* 2003]

2.4 COLD WORKING ON SHEET METAL JOINTS

Cold working on sheet metal joints is primarily done to increase fatigue life. Almost all joints in an airliner, whether they be sheet metal or metal plates have some extent of cold working performed around the joint during manufacturing.

2.4.1 COLD HOLE EXPANSION METHOD

Residual stresses often reside at fastening/joining locations especially when a hole is present because holes cause stress concentrations and when a load is applied the localized stress becomes magnified. If there is enough knowledge of the stress profile and if there is accessibility to redistribute the unwanted tensile stress, reliable procedures can be made to enhance fatigue performance [Webster G., *et al* 2001]. Cold expansion of fastening holes by mechanically forcing a hole bigger than when it was made is a common technique to improve the fatigue life of the hole. Of the three principal residual stresses, (hoop, transverse and radial), hoop stress distribution at the periphery of the hole can improve fatigue life by a factor of two to ten times by retarding crack initiation or reducing the growth of the crack by the cold working method called split-sleeve [Ozdemir A., *et al* 1999]. A. Ozdemir studied the effects of the split-sleeve process developed by Fatigue Technology Incorporated (FTI). The process involves an oversized tapered mandrel being pulled through the hole with a lubricated sleeve used to prevent contact between the hole and mandrel. Similar to this process is the split mandrel which allows for the mandrel to collapse and then be pulled through the hole. Both of these processes can be seen in Figure 2.13

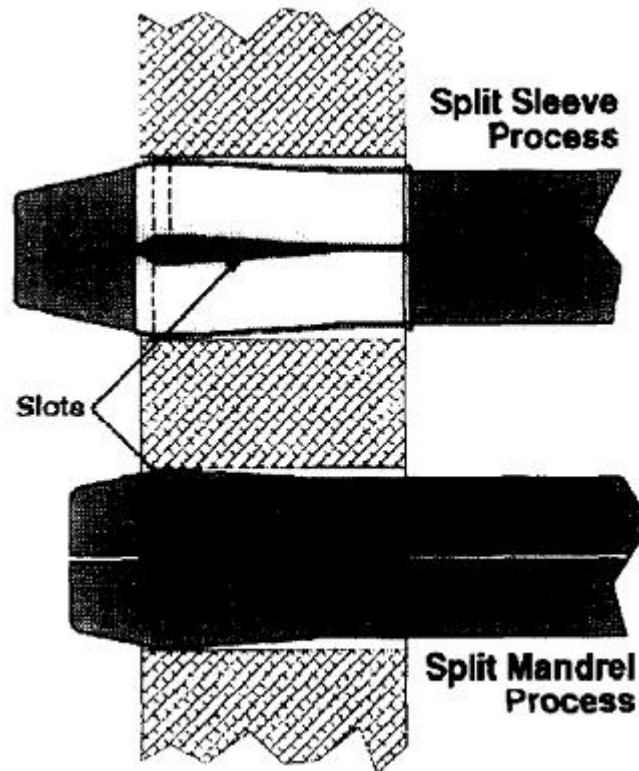


FIGURE 2.13. CROSS SECTION VIEW OF SPLIT SLEEVE AND SPLIT MANDREL PROCESSES.

[LEON A., 1998]

There is local plastic region developed by the yielding material around the hole, after the mandrel is removed the surrounding material, which is still in elastic state, springs back causing compressive tangential residual stress at the hole periphery [Chakherlou T., *et al* 2003]. Shown in Figure 2.14 is the effect this cold working process has on fatigue life with respect to hole size. Both split sleeve and split mandrel processes have significant improvements over non-cold worked material with the split mandrel having the highest improvement. As the hole diameter increases the split sleeve method becomes less effective while the split mandrel method becomes more effective.

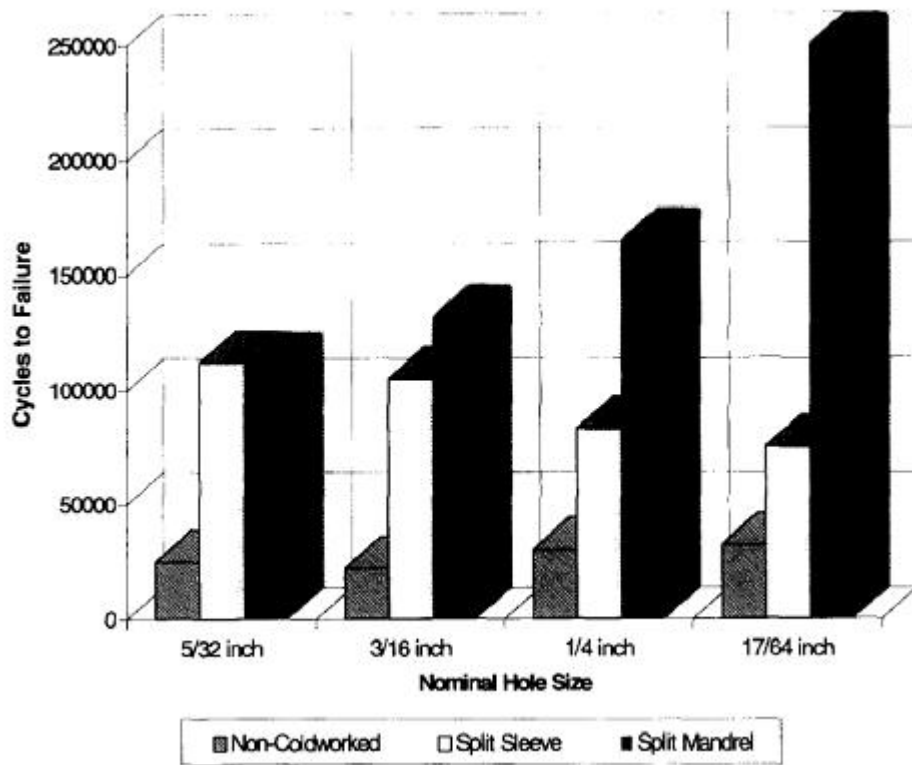


FIGURE 2.14. FATIGUE EFFECTS OF COLD WORKING PROCESSES.
 [LEON A., 1998]

2.4.2 STRESSWAVE™ PROCESS

StressWave™ has invented an alternative method to improve fatigue life of holes. B. Flinn [Flinn, B., *et al* 2005] helped developed this technology to create a compressive residual hoop stress before the hole is drilled. Before drilling a hole the sample is place between two indenters with a determined IS (indenter pressure) IP (indenter size) that make stresswaves into the metal, this forces material to flow plastically away from the indenters leaving a compressive (any negative value shown in the fringe level) residual stress distribution shown in Figure 2.15. Then the hole is drilled where the cold working was performed. As shown

from the LS DYNA model in the figure compressive stresses remain throughout the hole after drilling.

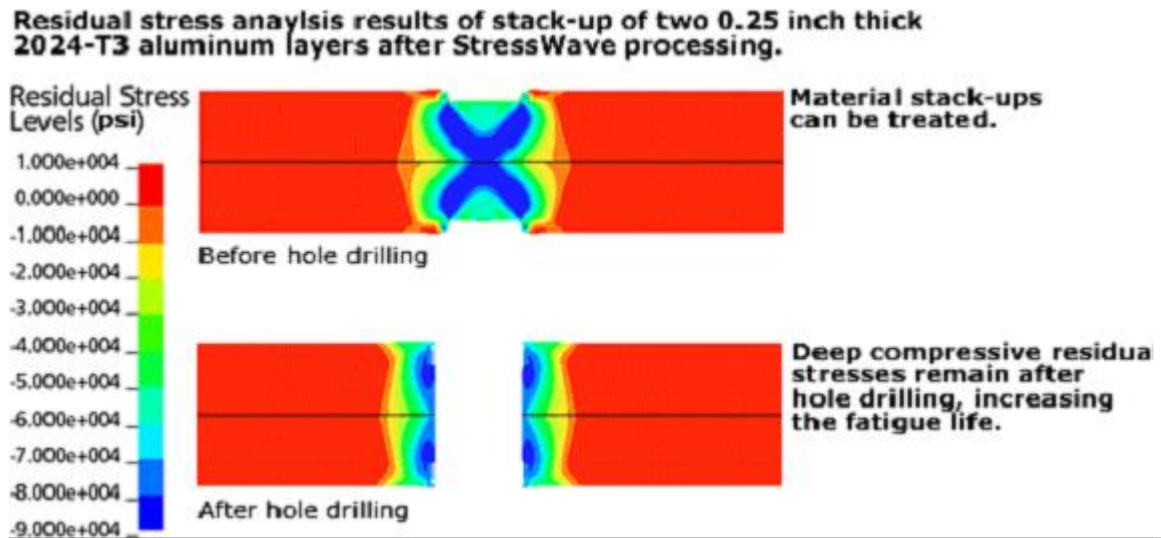


FIGURE 2.15. STRESSWAVE TECHNOLOGY™.
[STRESSWAVE™]

The results of stresswaves being implemented into holes is shown in Figure 2.16. As shown the non-treated samples have a much lower fatigue life than the StressWaved samples for all loads.

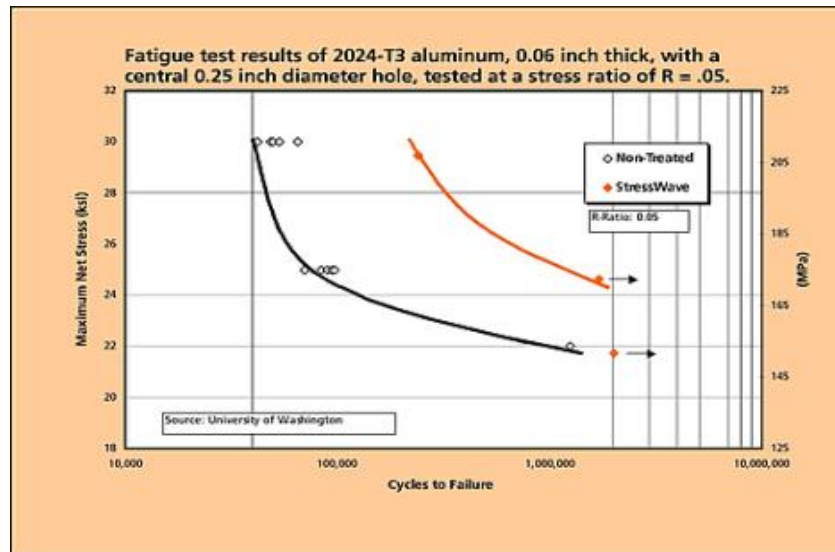


FIGURE 2.16 RESULTS OF STRESSWAVES ON FATIGUE LIFE.
[STRESSWAVE™]

2.4.3 STRESSWAVE PROCESS ON RSW

A DOE (Design of Experiments) has been performed on process parameter (indenter size and pressure) setup and testing procedures for post-weld cold working on RSWs similar to the StressWave procedure by R. Spitsen [Spitsen, R., 2005]. Experimental testing had begun to determine the effectiveness of the post-weld cold working process and optimum parameters for fatigue strength enhancement for both steel and aluminum. Also, a preliminary FEA of the cold working process had been developed for steel specimens. It was found the post-weld cold working process increased the fatigue life of low carbon steel RSWs. The purpose of this cold working is to retard fatigue crack initiation and growth in a RSW thus improving the strength mechanics. From initial research there was a foundation to continue this course for cold working RSW. There though was no conclusion on the post-weld cold working effects on Al RSWs.

CHAPTER 3:

OBJECTIVES

3.1 RSW

Resistance spot welding is a major joining method in today's automotive industry and it is of high importance to have RSW be reliable. Most improvements of RSW have been focused on the process itself such as correct pressure, hold time, weld current and specimen parameters. Because fatigue is the major failing mechanism in RSW process parameters changes can enhance the fatigue life of a RSW but the improvements are very limited. To answer the interest for a method that can significantly improve the fatigue life of a weld the post-weld cold working method similar to the StressWave method has been developed but limited research has been performed.

The objectives for steel RSW are as follows:

- Investigate the effects of weld quality on the mechanical properties of the cold working processed steel RSWs.
 - Examine microstructures and conduct microhardness test.
 - Perform tensile-shear and fatigue test.
 - Observe failure modes in the fatigue failed samples.
- Conduct a numerical simulation using FEM (finite element method) of the cold working process on unacceptable welds.
- Develop FE model of cold working process on acceptable welds to compare their residual stress distributions with the experimental values.

The objectives for Al RSW are as follows:

- Investigate the effect of cold working on mechanical properties of Al RSWs.
 - Examine microstructures and conduct microhardness test.
 - Perform fatigue test.
- Conduct a numerical simulation using FEM (finite element method) of the cold working process on Al RSWs

3.2 SPR

Self-piercing riveting has limited research literature with only a few research institutes actively pursuing SPR research. SPR is a relatively new joining technology used in approximately five automotive manufactures. The airline industry is hesitant in using SPR because of the limited research of SPR capability. Freightliner LLC is one of these industries currently using SPR and involved with their SPR supplier in design of the rivets and dies. From a discussion with a Freightliner representative who was involved with the SPR process it was mentioned that process characteristics and mechanical properties are unknown when SPR is performed in stamped sheet metal.

To study the stamping effects the following are the objectives for the SPR process:

- Determine the optimum material type and thickness for the provided rivets and die.
 - Analyze the RSF (rivet setting force) characteristics.
 - Perform tensile testing.
 - Observe cross sectional geometry of rivet.
- Perform a stamping like process to produce residual stress then SPR

- Analyze the RSF characteristics.
- Perform tensile and fatigue testing.
- Observe the fatigue failed samples to find out failure mechanisms.

CHAPTER 4:

EXPERIMENTAL PROCEDURES

To fully research the objectives several experimental tests were performed to understand the engineering facts of cold working in sheet metal joining.

4.1 MATERIALS

4.1.1 STEEL RSW

1008 steel is readily available and was used for this research to determine the effectiveness of the newly developed post-weld cold working process on steel RSW. Material used was commercially available AISI 1008 0.82 mm thick cold rolled steel sheet since it is widely used in the automotive industry. The chemical composition of the work piece material is given in Table 4.1 and the mechanical properties of the “as received” cold rolled 1008 steel are shown in Table 4.2.

TABLE 4.1. CHEMICAL COMPOSITIONS OF COLD ROLLED 1008 STEEL (WT.%).

% C	% Mn	% P	% S	% Si	% Al
0.034	0.270	0.009	0.008	0.007	0.037

TABLE 4.2. MECHANICAL PROPERTIES OF COLD ROLLED 1008 STEEL.

Elastic Modulus (GPa)	Tensile Strength (MPa)	Yield Strength (MPa)	% Elongation	Hardness (HK)
210	270	163	40	134

4.1.2 AL RSW

The workpiece material for this study was Aluminum 5052 with a sheet thickness of 0.77 mm. Al 5052 was chosen for the material because it is widely used for paneling in the cabs of commercial trucks. The chemical composition of the work piece material is given in Table 4.3. The mechanical properties of the as received Al 5052 are shown in Table 4.4.

TABLE 4.3. CHEMICAL COMPOSITION OF AL 5052(WT.%).

% Fe	% Si	% Cu	%MN	%Mg	% Cr	% Zr	Others	% Al
0.4	0.25	0.1	0.1	2.2-2.8	0.15-0.35	0.1	0.2	95.7-97.7

TABLE 4.4. MECHANICAL PROPERTIES OF AL 5052.

Elastic Modulus (GPa)	Tensile Strength (MPa)	Yield Strength (MPa)	% Elongation	Hardness (HK)
70	193	89	25	80

4.1.3 SPR

Experimental design for SPR took several steps to study the sheet metal stamping effects on the mechanical properties and the process in SPR. The first step was to find the most suitable material for the provided rivet. Table 4.5 gives the materials and the three thicknesses of each aluminum material. These three materials are used in truck cab panels that are joined by the SPR process. The next step was to perform cold working on the sheet metal and its influence on mechanical properties. Tables 4.6 and 4.7 give the material compositions and properties respectively.

TABLE 4.5. SPR MATERIAL TYPES AND THICKNESSES.

Material Type	2024 T3	5052 H32	6061 T6
Thickness (mm)	1.27	1.27	1.27
	1.6	1.6	1.65
	2.03	2.03	2.03

TABLE 4.6. CHEMICAL COMPOSITIONS OF SPR WORKPIECE MATERIALS (WT%).

	Al 2024 T3	Al5052-H32	Al 6061 T6
Al	93.5	97.3	98
Mg	1.2-1.8	2.2-2.8	0.8-1.2
Cr	Max 0.1	0.15-0.35	0.04-0.35
Si	Max 0.5	Max 0.25	0.4-0.8
Mn	0.3-0.9	Max 0.1	Max 0.15
Cu	3.8-4.9	Max 0.1	0.15-0.4
Fe	Max 0.5	Max 0.4	Max 0.7
Ti	Max 0.15	-	Max 0.15
Zn	Max 0.15	Max 0.1	Max 0.25
Other, each	Max 0.05	Max 0.05	Max 0.05
Other, total	Max 0.15	Max 0.15	Max 0.15

TABLE 4.7. MECHANICAL PROPERTIES OF MATERIAL USED FOR SPR.

	Elastic Modulus (GPa)	Tensile Strength (MPa)	Yield Strength (MPa)	% Elongation	Hardness (HK)
Al 2024 T3	73.1	441	290	19	150
Al 5052-H32	70.3	228	193	12	80
Al 6061 T6	68.9	310	276	12	120

4.2 SAMPLE FABRICATION

Sample fabrication details the process for making the specimens used for the research.

4.2.1 RSW

The configuration and dimensions of the RSW specimens used throughout this study are given in Figure 4.1. Metal was cut to dimensions by using a shear then deburred using a grinder. The area of the spot weld was cleaned with Acetone before the RSW process.

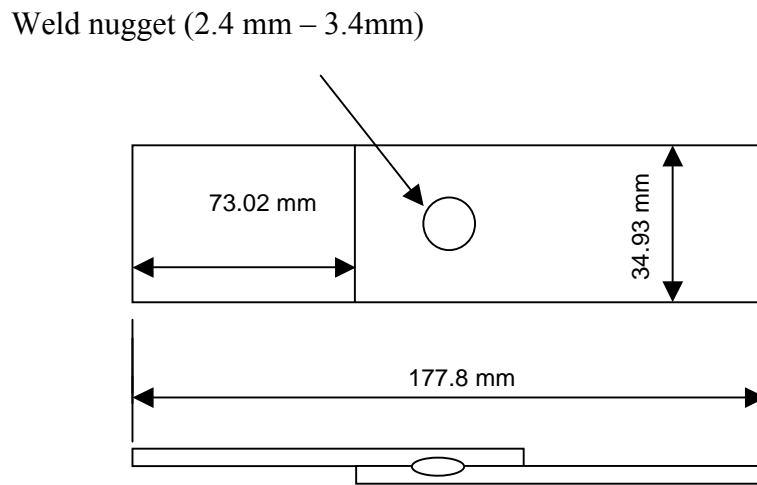


FIGURE 4.1. GEOMETRY OF RSW SPECIMENS.

4.2.1.1 Steel

Welding was conducted using a Miller SSW-2020ATT resistance spot welding machine with a copper based electrode cap. The cap dimensions are 12.11 mm diameter hemispherical dome with a flat tip having a diameter of 5.6 mm. The welding conditions chosen in this series of experiments for the selected steel sheet thickness and grade of material the welding parameters given in Table 4.8 were based on the recommendation of Resistance Welders Manufacturer Association [RWMA, 1981].

TABLE 4.8. 1008 STEEL RSW PARAMETERS

Average Weld Force (kN)	Weld Time (Cycles)	Hold Time (Cycles)	Welding Current (kA)
<1.49	8.5	10	8.1

There were two different groups of RSWs that were post-weld cold worked. The first group included samples with a weld nugget size larger than $4\sqrt{t}$ (3.2 mm) which are considered to be adequately sized and of acceptable quality. The other group included samples with a weld nugget size smaller than $4\sqrt{t}$ (3.2 mm) and were considered to be undersized and of unacceptable quality. While the same welding parameters were used to produce all the unacceptable quality RSW specimens, the nugget diameter varied from 2.4 – 2.9 mm and the average weld nugget diameter was found to be approximately 2.6 mm. Nugget diameters were measured using a Phoenix X-Ray CTM-100 PCMA Inspector prior to fatigue testing. Figure 4.2 shows an X-Ray photo of an acceptable RSW.

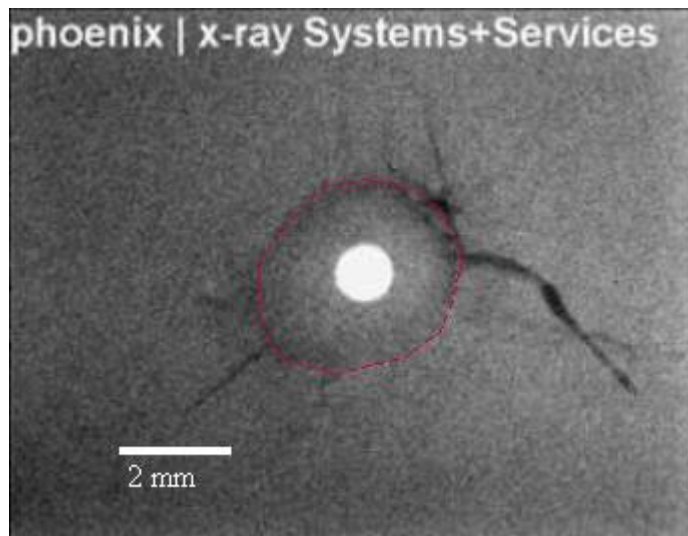


FIGURE 4.2. X-RAY VIEW OF STEEL RSW.
(RED CIRCLE CIRCUMFERENCES SPOT WELD)

After all samples had been through the RSW process, samples were randomly selected for the post weld cold working process.

4.2.1.2 AL

The spot welding was done on a 150 KVA single phase AC pedestal welding machine. The transformer of this machine had seven tap settings used to change the current levels. The electrodes used were male, truncated cone type with a 6.4 mm face diameter. The welding conditions were selected based upon a weld lobe study by R. Spitsen [Spitsen, R. 2005]. The weld lobe study was conducted with electrodes that had been previously conditioned through their use on approximately 20 spot welds. Various welding settings were used to find the cold weld and expulsion boundaries of the weld lobe. Two replicates of each lobe experiment were conducted in order to improve accuracy. For the first set of experiments, the effects of welding current, force and the cycle time were explored. Three force levels - 2.45 kN, 4.22 kN and 5.55 kN were used. Under each force level, three welding times - 4, 6 and 8 cycles, based upon a 60 Hz alternating current power source, were examined. At each force and cycle time combination, the welding current was varied from 8.8 kA to 12.7 kA, and three spot welds were made to search for the good weld settings. All the resistance spot welds made in the experiments were peeled and the button sizes were measured. Based on these experiments, a cycle time of 4 cycles and a force of 2.45 kN was found to yield the best results in terms of button size consistency. In the second set of experiments, three transformer tap settings - 1, 5, and 7 were tested using 4 cycles and 2.45 kN. For each setting, the current was also varied from 8.8 kA to 12.7 kA and three spot welds were made for each setting.

After the lobe study the weld schedule used for making all the fatigue test samples was chosen. This schedule is listed in Table 4.9. The welding current of 9.3kA was used with a transformer tab setting at 5. The welding current profile used had 2 cycles of preheating

followed by 2 cycles of cooling and finally 4 cycles of welding. The average weld button size was 4.5 ± 0.2 mm.

TABLE 4.9. AL SPOT WELDING PROCESS PARAMETERS.

Weld Force (kN)	Weld Time (Cycles)	Hold Time (Cycles)	Welding Current (kA)
2.45	4	10	9.3 with tap at 5

4.2.2 SPR

The SPR system used in the experiment was a Henrob double acting, twin user interlock model PP2212. The SPR system is shown in Figure 4.3.

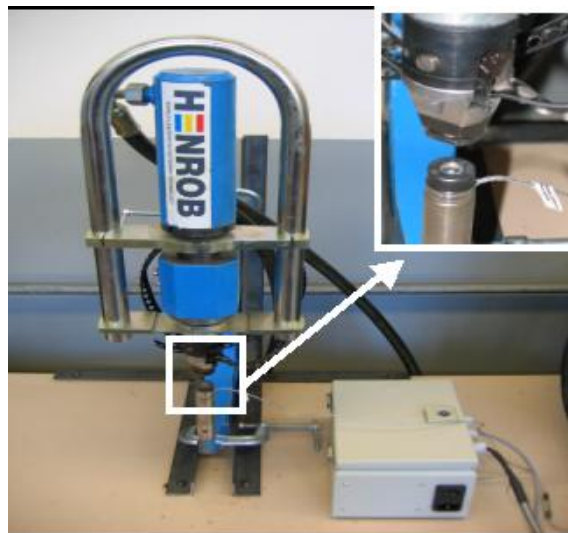


FIGURE 4.3. SPR SYSTEM.

The rivets used were countersunk type, made of low carbon steel (Henrob C50542AZ04/BAQ, Batch #R5071). The diameter of the rivets were 5.3 mm and the length was 5 mm. A cross-sectional view of a rivet is shown in Figure 4.4.



FIGURE 4.4. RIVET CROSS-SECTION.

The SPR system was instrumented with a load cell and a data acquisition system to monitor the force variation during the SPR process. The load cell was placed between the die and base column of the lower arm of the SPR gun. The data collection software recorded the entire RSF (rivet setting force). Figure 4.5 shows a schematic of the force monitoring system used in the study. A program was written using the software MatLab to record and display the RSF readings.

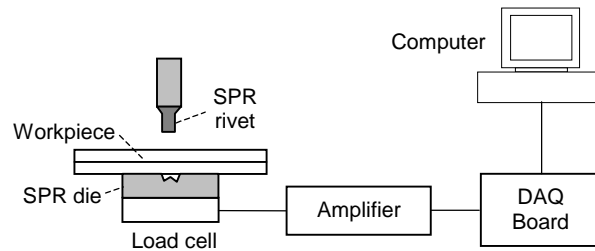


FIGURE 4.5. FORCE MONITOR SYSTEM.

[KIM, D., *ET AL* 2005]

The size of the SPR specimens is similar to the RSW as shown in the schematic in Figure 4.6.

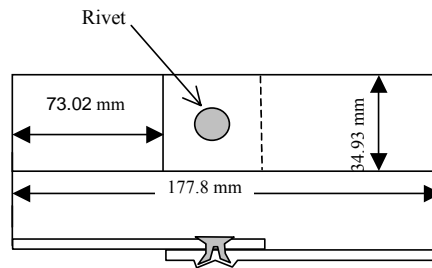


FIGURE 4.6. GEOMETRY OF SPR SPECIMENS.

4.3 COLD WORKING

Cold working is done to induce localized residual stresses on an area of interest. The system used for both RSW and SPR was hydraulic driven machine controlled by a pressure gage. Specially sized indenters were forced into the metal until a predetermined load programmed by a digital controller was reached. After the set load was reached the indenters were held for approximately 2 sec and then allowed to retract.

4.3.1 RSW

The cold working process represents a new approach for improving the fatigue lives of holes and other features in metal structures [Easterbrook, E., *et al* 2001]. Figure 4.7 shows a schematic of the spot weld process and the post-weld cold working process. In a typical production application, the indenters are positioned normally over and concentric to the RSW location as shown in the photographs of Figure 4.8. The RSW structure is locally cold worked as the process imparts beneficial residual compressive stresses.

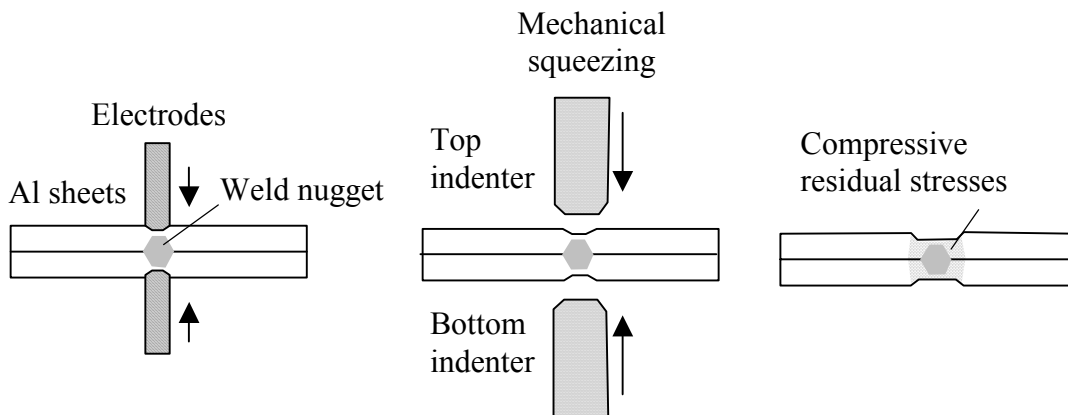


FIGURE 4.7. SCHEMATIC DIAGRAMS OF THE POST-WELD COLD WORKING PROCESS.

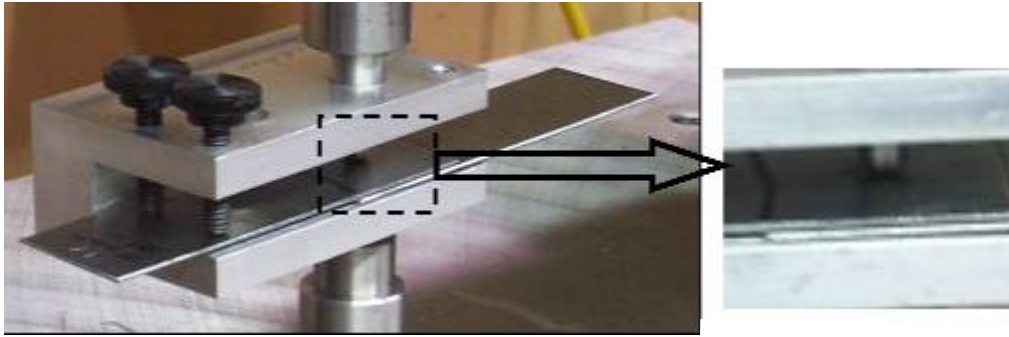


FIGURE 4.8. COLD WORKING BEING PERFORMED ON A RSW SAMPLE.

[SPITSEN, R., 2005]

The post weld cold working parameters, IP (indenter size) and IP (indenter pressure), were chosen based upon the size of the nugget diameter and on the maximum shear stress of the RSW. A schematic of a typical indenter is shown in Figure 4.9.

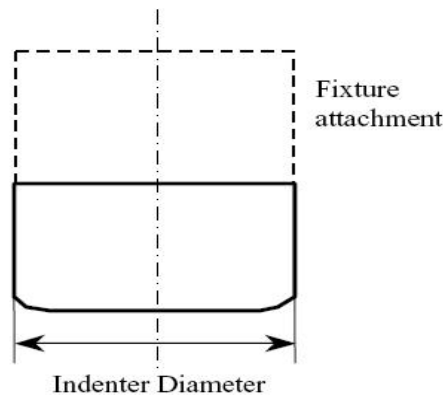


FIGURE 4.9. CROSS-SECTIONAL SCHEMATIC OF A TYPICAL INDENTER.

[SPITSEN, R., 2005]

For steel three different parameters were developed for investigating the cold working process: indenter size (IS), indenter pressure (IP) and nugget diameter (ND). The matrix for these parameters is shown in Table 4.10, each IS and IP were used for both acceptable and non-acceptable welds. For the acceptable 1008 steel RSW previous research had been done

but was not complete. To acquire unacceptable RSW the electrode force on the RSW machine was reduced. All results were compared against each other and specimens which were non-cold worked (as received) RSW.

TABLE 4.10. PARAMETERS FOR STEEL RSW.

IS (mm)	IP (MPa)	ND (mm)
4.6	700	2.6-3.2,
7.1	850	3.2-3.5
	1000	

For researching the post-weld cold working effects on aluminum RSW two different parameters were used: IS and IP. Shown in Table 4.11 are the IP used for each IS. As shown there are different ranges of IPs for each IS because any small change in either cold working parameter has a drastic effect on the Al base material around the weld. For IS 4.6 mm and IP larger than 600 MPa there was gross deformation of the base material which is injurious to the weld and the same was true for IS 7.1 mm and IP larger than 450 MPa. All results were compared against each other and non-cold worked RSW.

TABLE 4.11. PARAMETERS FOR AL RSW.

IS (mm)	4.6	7.1
IP (MPa)	300	150
	450	300
	600	450

4.3.2 SPR

Localized cold working was done to replicate a stamped sheet where the SPR joint was to be on the specimen. Figure 4.10 shows how the cold working process was done on the SPR specimens. A steel block was placed below the specimen while the cold working was performed on the face of the specimen so when SPR was performed the mating faying surfaces were flush with each other (no gap in between). Note: cold working was performed before the SPR process requiring both pierced and locked sheet to be cold worked separately. The IS used was 10 mm with IP of 350 MPa.

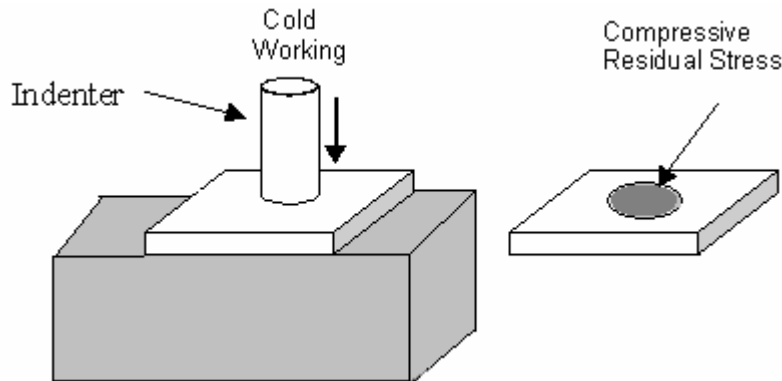


FIGURE 4.10. COLD WORKING ON SPR SPECIMENS.

4.4 METALLOGRAPHY

Randomly selected samples of post weld cold worked and non-cold worked RSW and SPR joints were sectioned using a diamond tip blade. The samples were then mounted in black Bakelite powder using a Leco® PR-15 machine and polished with a Leco® Spetrum System 1000 with a minimum size of 1.22 μm diamond compound polish. Steel RSW were then etched using 5% Nital while for Al RSW the etched was HF. This process was performed to view the cross section of the joints. For RSW joints the weld nugget, heat

affected zone (HAZ), and the base material could be examined and for SPR the joint geometry could be viewed. To visually analyze the RSW microstructures and SPR geometries a Nikon Epiphot 200 optical microscope integrated with a Nikon Digital Camera DXM1200 were used.

4.5 MECHANICAL PROPERTY TESTING

Mechanical properties are important for studying and predicting the behavior of all materials. The mechanical behavior of a material reflects the relationship between its response or deformation to an applied load or force. The most important mechanical properties are hardness, tensile-shear strength and fatigue strength. [Callister, W., 2007]

4.5.1 MICROHARDNESS TESTING

Knoop microhardness measurements were taken on the RSW cross section using the samples mounted in Bakelight. The measuring device used was a Leco DM-400 Hardness Tester with a diamond tip. The exact center of the weld was considered the origin and recording were made approximately every 200 μm (for steel) 300 μm (for Al) in the x and y directions. Three recordings were made at each interval then averaged. Measurements were taken until the percent difference between two consecutive readings was less than 1%. Test force conditions were 300 grams for steel RSW and 100 grams for Al RSW. All forces were applied for a hold time of 20 seconds.

4.5.2 TENSILE-SHEAR TESTING

Tensile-shear testing was conducted to investigate the cold working effects on the joint's strength. All joint samples were subjected to tensile-shear tests on an Instron 4482 machine per ASTM Standard Test Methods of Tension Testing of Metallic Materials (E8). A

constant extension rate of 5.1 mm/min was used with a sampling speed of 10 readings per second for both RSW and SPR. Sheet metal shims were placed in the wedge grips of the Instron to minimize bending of the lap shear specimens. Figure 4.11 shows the Instron machine used for all tensile shear joint testing.

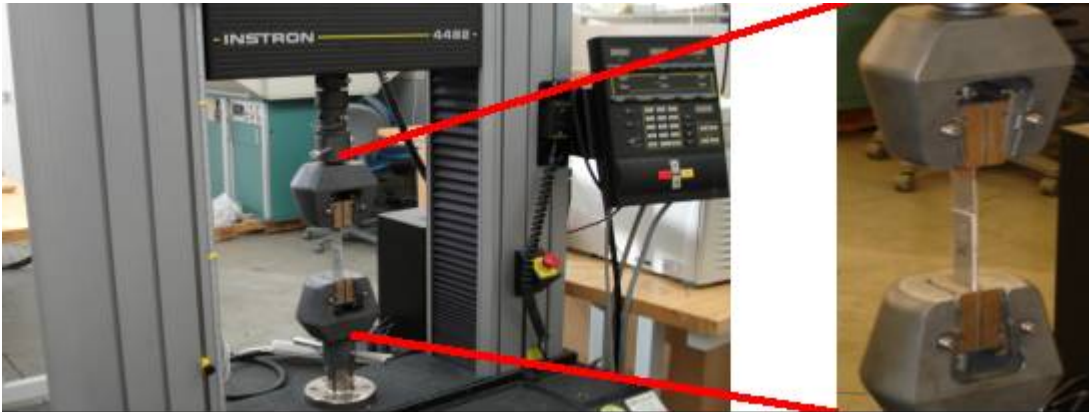


FIGURE 4.11. INSTRON TENSILE-SHEAR MACHINE.

4.5.3 FATIGUE TESTING

Fatigue testing all joint specimens was conducted to evaluate and compare the fatigue performances. The following machines were used for fatigue tests on the specimen joint: steel RSW – Shimazu servo-hydraulic test frame, Al RSW – Shimazdu electrohydraulic test frame and for SPR – Instron 1380 servo-hydraulic test frame (shown in Figure 4.12). All machines were in load control mode with the following conditions: R (load ratio) = 0.1, frequency = 20 Hz, sine wave cyclic loading at room temperature. Different fatigue machines were used based on availability. Shims were placed in the grips to minimize bending stress due to the offset from the lap shear specimen geometry. The number of cycles to failure was determined when a fatigue crack appeared on the outer surface of the specimen. However, because cracks did not appear on the outer surface of the specimen in some conditions, the

number of cycles to failure was determined when the weld joint completely failed. Fatigue test was done on 72 steel RSW joints, 69 Al RSW joints and 34 SPR joints.

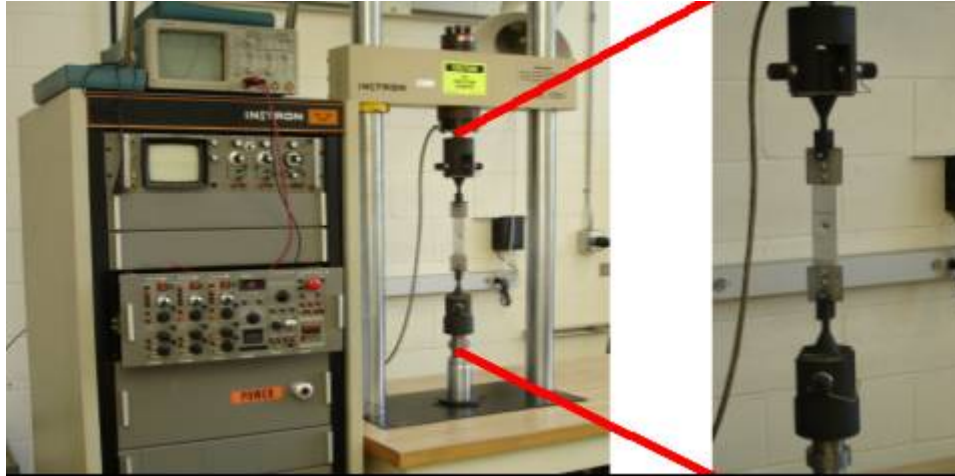


FIGURE 4.12. INSTRON 1380 FATIGUE TESTER.

4.5.4 X-RAY DIFFRACTION

X-Ray diffraction (XRD) was used to measure the residual stress made on the steel RSW surfaces by the standardized technique [ASTM E915-90, 1992]. All the measurement was performed at TEC Materials Testing Laboratory. The magnitude of the circumferential residual stresses were measured on the samples' surfaces. Due to three regions (nugget, HAZ, and base metal) on the spot welds, three positions on the surface were measured. As shown in Figure 4.13 (a) and (b), target position 1, 2, and 3 represented the nugget area, HAZ, and the base metal, respectively. The smallest diameter of the X-ray around the target area is 1 mm.

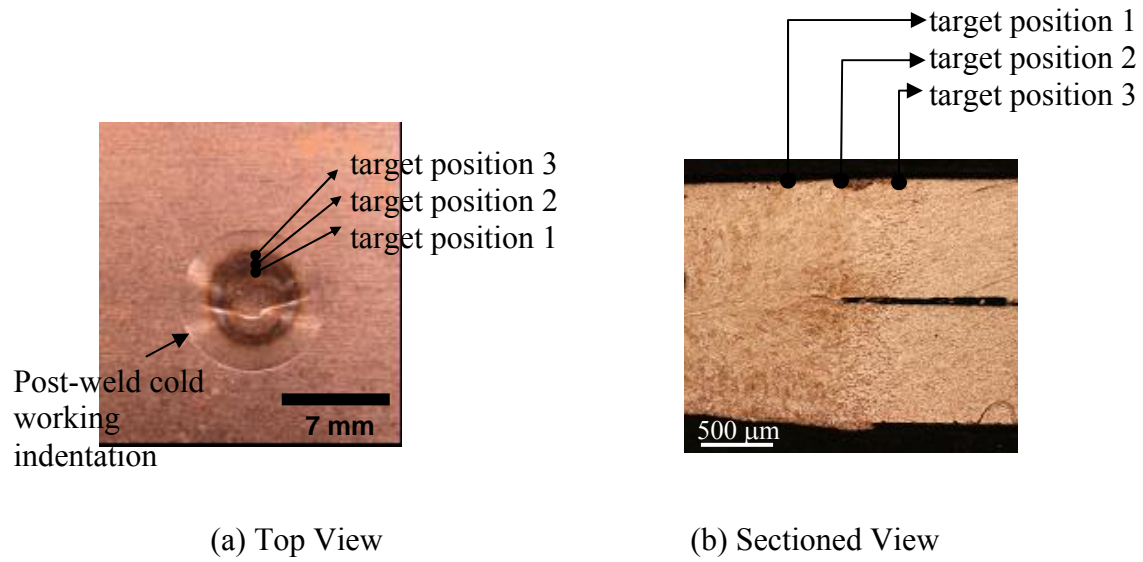


FIGURE 4.13. RESIDUAL STRESS MEASUREMENT POSITIONS IN X-RAY DIFFRACTION.

CHAPTER 5:

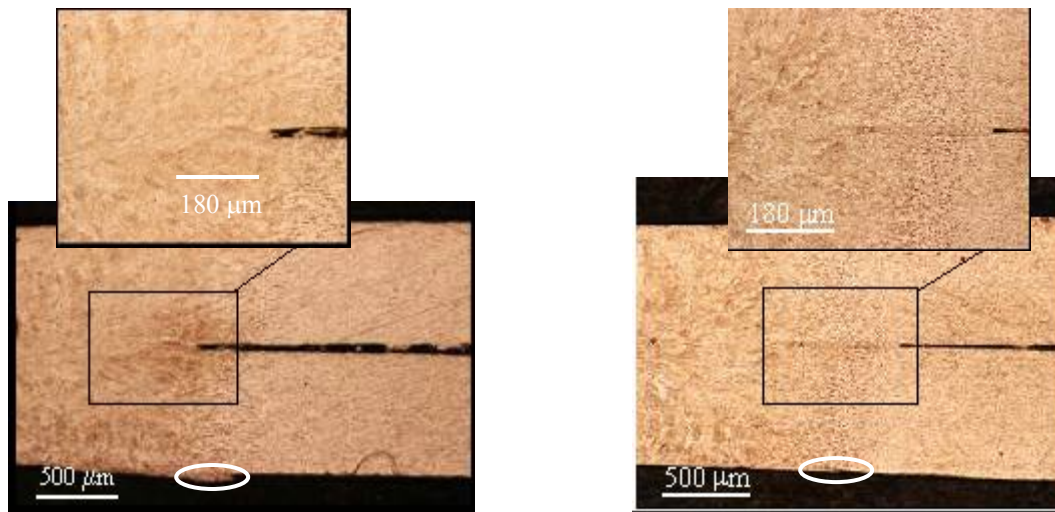
RESULTS AND DISCUSSION

The findings from researching the joint characteristics and properties are shown with explanations and theories. All the results are intriguing and help give insight to the engineering phenomena that occurs during sheet metal joining and cold working. A numerical analysis was used to complement and validate the experimental results in the RSW portion of this research.

5.1 STEEL RSW

5.1.1 METALLOGRAPHY

Metallography in Figure 5.1 shows (a) as-welded (non-cold worked) and (b) cold worked sample. When comparing the two metallographies there are two material deformations of significance. The first, in Fig. 5.1 (a) there is a “bulge” near the center of the bottom sheet highlighted by the white circle but in Figure 5.2 (b) cold working produces a dimple. Depending on the IS the dimple depth ranged from 0.07 mm for 700 MPa IP to 0.1 mm for 1000 MPa IP. The location of the dimple helps approximate how large the range of compressive stress outside the nugget is. The most important difference in the geometries is the change at the faying surface. As shown in the insert of Figure 5.1 (a) there is a large notch radius but in the insert of Figure 5.2 (b) the notch radius has drastically reduce, in some cases eliminated. This decrease of notch radius is important for studying the stress concentration at this region, which will be expounded later.



(a) “AS-WELDED” (ND: 3.2 MM)

(b) POST-WELD COLD WORKED
(IP: 1000 MPA, IS: 4.6 MM)

FIGURE 5.1. MICROSTRUCTURES OF “AS-WELDED” AND COLD WORKED STEEL RSW.

5.1.2 MICROHARDNESS

Microhardness test results for undersized and adequately sized spot welds are shown in Figure 5.2. Both non-cold worked and a cold worked samples are shown for adequately sized nuggets along with undersized non-cold worked sample. As shown the microhardness values in the nugget region have little variance between the post-weld cold worked plot and the as welded plots. [Spitsen R., 2005]. When moving from the nugget region to the HAZ the microhardness gradient is reduced for all specimens. As expected the microhardness for the undersized weld decreased sooner than for the adequate size. The reason the nugget is harder than the HAZ is a result of the increase in the strain-hardening coefficient in the HAZ. When there is a decrease in the volume fraction of martensite the strain-hardening coefficient increases [Tsai, C., *et al* 1992]. This decrease of martensite from the nugget to the HAZ is shown in the cross-sectional view in Figure 5.3 where the grain size decreases in the HAZ.

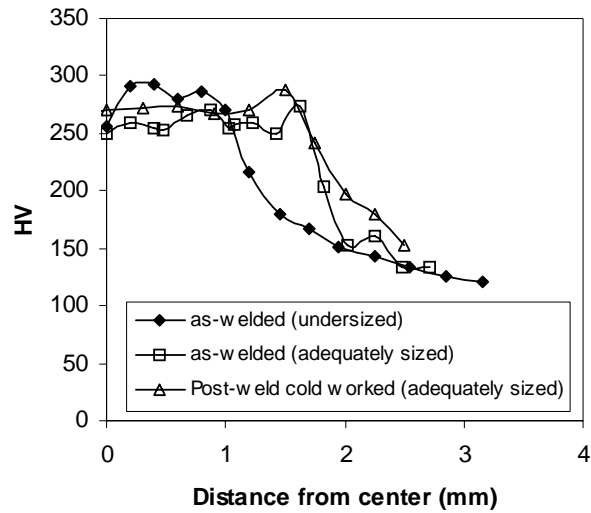


FIGURE 5.2. STEEL MICROHARDNESS DISTRIBUTIONS.
 (POST-WELD COLD WORKING CONDITION: IS=4.6 MM, IP = 1000 MPA)



FIGURE 5.3. MICRO-STRUCTURE OF STEEL RSW.

5.1.3 TENSILE-SHEAR TESTING

Tensile-shear testing was conducted to investigate the effect of nugget diameter on weld strength. Nugget diameter ranges from 2.2 mm to 3.7 mm. Figure 5.4 shows the relationship between weld nugget diameter and the maximum load, which is the most common monitored variable in tensile-shear testing. The sample with 2.35 mm nugget

diameter experienced the maximum tensile-shear load at 1.95 kN whereas the sample with 3.55 mm nugget diameter increased by almost 50% to 3.7kN. The strong influence of nugget diameter on the weld quality was found in tensile-shear test results. The average maximum tensile-shear load with adequately sized RSWs (nugget diameter = 3.2 mm to 3.8 mm) is 3.7kN. The post-weld cold working process did not change tensile-shear properties of adequate sized 1008 steel RSWs [Spitsen, R., 2005].

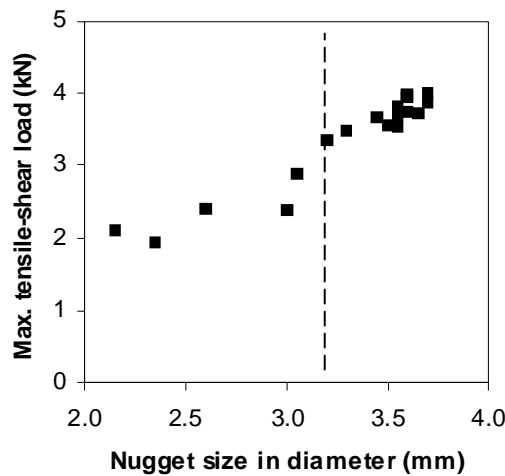


FIGURE 5.4. TENSILE-SHEAR MAX LOAD OF AS-WELDED RSW SAMPLES WITH VARIOUS NUGGET SIZES.

5.1.4 FATIGUE TESTING

Fatigue tests were performed on all possible types of as-welded and cold worked RSW. Figure 5.5 compares the L-N curves between as-welded samples and post-weld cold worked samples for adequately sized RSWs. The post-weld cold worked samples displayed greater fatigue lives as compared to as-welded specimens below a load of 1.6 kN, approximately 35% of maximum tensile-shear load. Above approximately 1.6 kN, the post-weld cold working did not increase fatigue life of acceptable sized RSWs [Spitsen, R., 2005].

The post-weld cold worked samples boasts a fatigue endurance limit approximately by 30% improvement in RSWs. This is due to the fact the compressive residual stresses induced at the faying surface during the post-weld cold working process delay the crack initiation and/or crack propagation. All 1008 steel fatigue tests were concluded when the cyclic loading did not cause detectable cracks after 5 million cycles. Figure 5.6 shows a fatigue crack in a RSW.

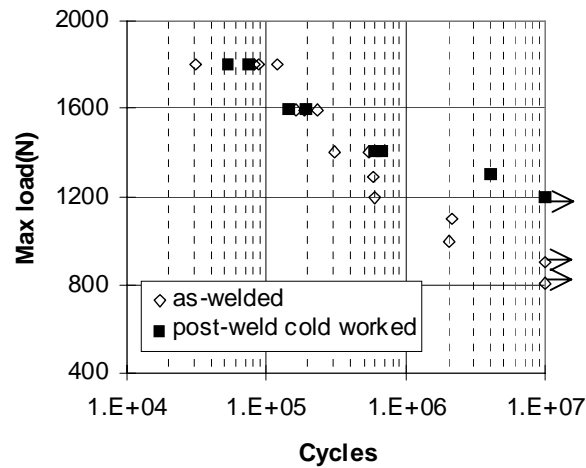


FIGURE 5.5. L-N CURVES FOR THE AS-WELDED AND POST-WELD COLD WORKED SAMPLES.

(RSW NUGGET SIZE = 3.4 MM – 3.9 MM; POST-WELD COLD WORKING CONDITION: IS=7.1MM, IP=700MPA; ARROWS INDICATE THE SAMPLES DID NOT FAIL AT 10^7 CYCLES)

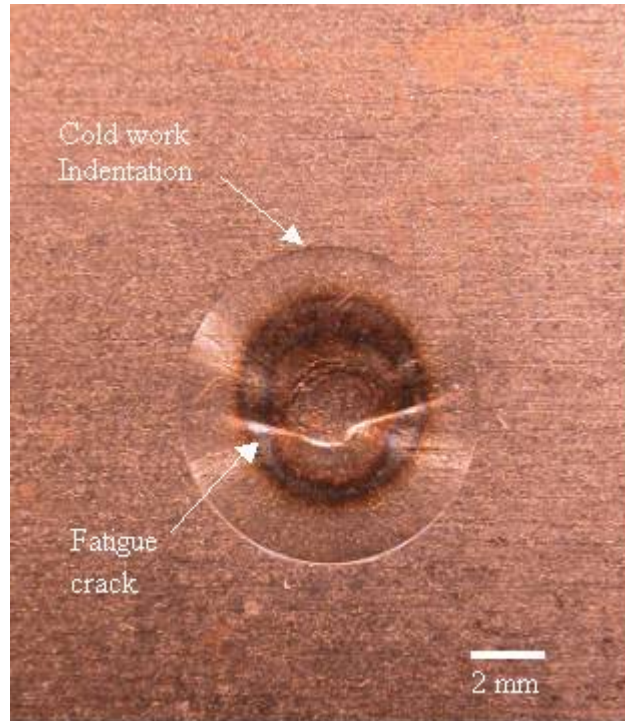
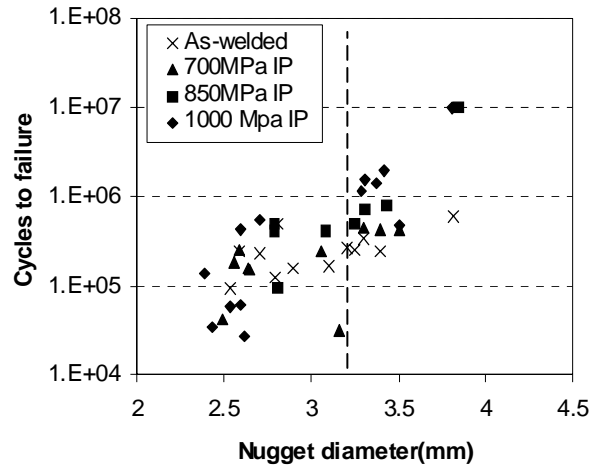


FIGURE 5.6. FAILED STEEL RSW FATIGUE SPECIMEN.

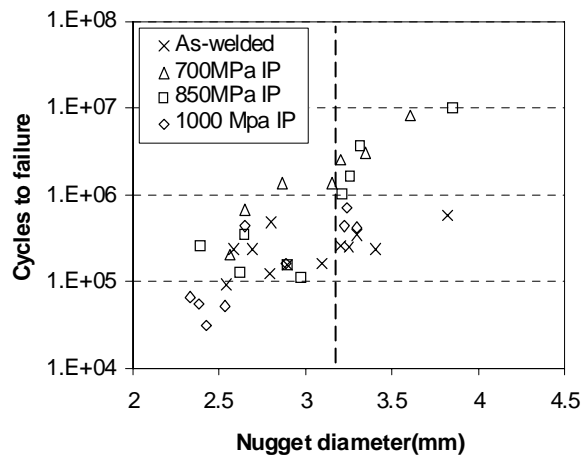
(THE ARROWS INDICATE THE AREA OF COLD-WORK AND RESULTANT FATIGUE CRACK. THE PARAMETERS FOR THE POST-WELD COLD WORK IS 7.1MM IS, 1000 MPA IP.) [SPITSEN, R., *ET AL* 2004]

The fatigue life of RSW with IS of 4.6 mm and 7.1 mm are shown in Figures 5.7 (a) and (b) respectively. These figures compare the fatigue life of both as-welded and post cold worked specimens which included adequately sized and undersized nuggets for each indenter at the maximum fatigue load of 1.2 kN. Data points to the right of the 3.2 mm nugget size are considered to be adequately sized welds while those to the left are undersized welds. The as-welded sample with 2.6 mm nugget diameter experienced the average fatigue life of 150,000 cycles whereas the sample with 3.4 mm nugget diameter experienced 300,000 cycles. As

shown in Figure 5.4, maximum tensile-shear strength increased by 50% for nugget diameters of 2.6 mm to 3.4 mm. It can be explained that increased tensile-shear properties can contribute to an increase in fatigue life of RSWs with increasing nugget diameter. As shown in Figure 5.7 (a), IP 1000 MPa has the highest improvement of fatigue life for the 4.6 mm IS. The post-weld cold worked sample with 2.8 mm nugget diameter experienced the average fatigue life of 300,000 cycles whereas the sample with 3.44 mm nugget diameter experienced 800,000 cycles. Thus fatigue life enhancement by the post-weld cold working process with IS of 4.6 mm is increased by approximately 375%. For IS 7.1 mm the lower the IP the higher the fatigue life, IP 700 MPa shows the greatest improvement as shown in Figure 5.7 (b). There was little to none improvement in the fatigue life for any samples with undersized welds and there was substantial improvement in the fatigue life for all samples with adequately sized welds as a result of post-weld cold working.



(a) IS = 4.6 MM

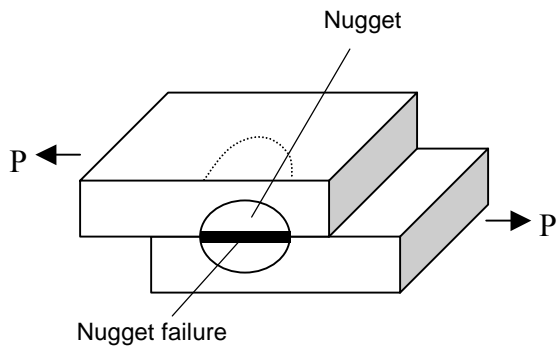


(b) IS= 7.1 MM

FIGURE 5.7. NUMBER OF CYCLES TO FAILURE VS. NUGGET SIZES.
(FATIGUE TEST CONDITION; R=0.1, MAX LOAD APPLIED = 1.2 KN.)

Due to the large temperature induced hardening in the heat affected zone (HAZ) of the spot-welds, fatigue cracks often propagate in the panel thickness direction, instead of in the nugget interfacial direction [Lee, H., *et al* 2005]. It was true that most of the as-welded RSW specimens showed fatigue crack growth in the HAZ. However, three different failure types: A, B and C, as shown in Figure 5.8, occurred during fatigue testing the post weld cold worked

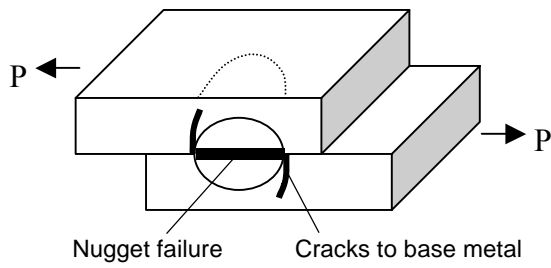
RSW specimens. The type A failure mode is when fatigue crack initiation occurs at the nugget and the subsequent crack propagates through the nugget (Figure 5.8 (a)). In type B failures, the fatigue crack initiation also occurs and propagates through the nugget and there are noticeable cracks into the heat effect zone (HAZ) and base metal surrounding the nugget (Figure 5.8 (b)). Type C failures are ones where fatigue cracks occur and propagate completely within the HAZ and base metal surrounding the nugget (Figure 5.8 (c)). All samples with a nugget size greater than 2.7 mm failed in the HAZ, type C.



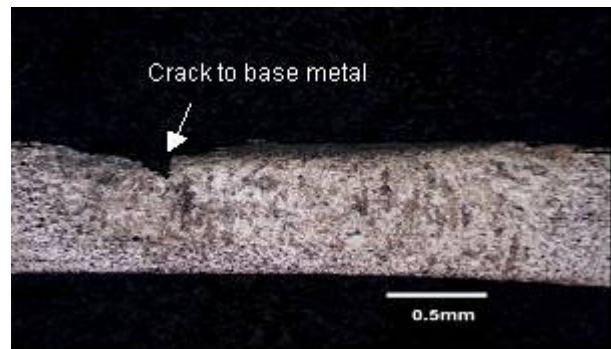
(a) FAILURE TYPE A.



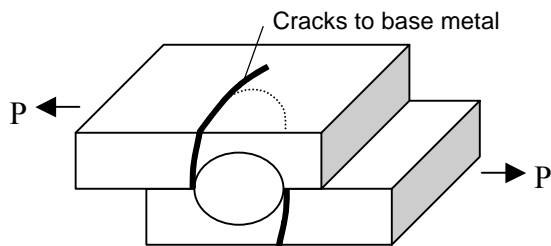
(b) SIDE VIEW OF FAILURE TYPE A (LOWER SHEET ONLY)



(c) FAILURE TYPE B.



(d) SIDE VIEW OF FAILURE TYPE B (LOWER SHEET ONLY)



(e) FAILURE TYPE C.



(f) SIDE VIEW OF FAILURE TYPE C (LEFT SIDE ONLY)

FIGURE 5.8. SCHEMATICS AND OPTICAL PICTURES OF SPOT-WELD CROSS-SECTIONS ILLUSTRATING VARIOUS FAILURE TYPES.

In order to map the failure types for the post-weld cold worked samples with undersized RSWs, 4 to 6 samples were fatigue tested at each condition. In Figure 5.9, it can be observed that the failure modes for as welded samples were type C but for the 4.6 mm IS type A and B failures became dominant at both IPs. For IS 7.1 mm once the IP parameter increases to a value of 1000 MPa, failure type A becomes dominant. Another trend of the 1000 MPa IP parameter is the failure mode type A and B are predominant.

IS (mm)	7.1	type A: 1 type B: 0 type C: 4	type A: 1 type B: 0 type C: 3	type A: 3 type B: 2 type C: 1
	4.6		type A: 3 type B: 1 type C: 1	type A: 2 type B: 3 type C: 1
		0 (as welded)	850	1000
		IP (MPa)		

FIGURE 5.9. FREQUENCY OF FAILURE TYPES FOR COLD WORKED STEEL SAMPLES WITH UNDERSIZED RSWs.

Figure 5.10 shows the effect of the nugget size and failure type on the fatigue life. It shows type C failures generally have higher cycles to failure than either the type A or type B failures for similar sized weld nuggets. Also, for similar sized weld nuggets, an IP treatment of 850 MPa appears to cause significantly higher percentages of type C fatigue failure in welded structures than an IP treatment of 1000 MPa. This indicates that there are some negative effects imparted into the material as a result of the higher-pressure cold working treatment and that there is some optimum indentation pressure at which the fatigue resistance of the RSW structure is maximized. As expected, an undersized weld nugget has a lower number of cycles to failure than do adequately sized weld nuggets. However, it is interesting

to note that both type A failures and type B failures have a similar number of cycles to failure regardless of the size of weld nugget.

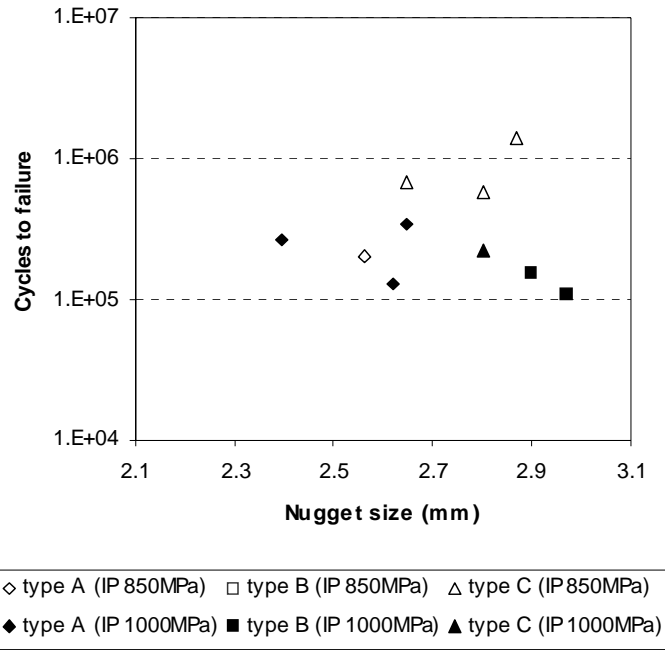


FIGURE 5.10. EFFECT OF NUGGET SIZE ON STEEL RSW FAILURE TYPES.

In fatigue testing, the spot weld boundary is subjected to combined tensile forces, moments, and shear forces [Lee, H., *et al* 2005]. For this reason, both mode I (type C) cracking and mode II (type A) cracking can be encountered in tensile shear spot-weld specimens. Without cold working, fatigue cracks tend to grow along the HAZ in the panel thickness direction (type C) because the fusion zone of low carbon steel specimens is hardened regardless of the nugget size. Therefore, mode I cracking is dominant for as-welded specimens. However, when undersized specimens are post-weld cold worked, mode II cracking becomes more dominant. This reflects the findings of Figure 5.9 in which most of

the nugget interfacial failures (failure types A or B) were found in undersized specimens treated with a 1000 MPa IP parameter.

5.1.5 X-RAY DIFFRACTION

Table 5.1 presents residual stress magnitudes for the three target positions (shown in Figure 4.13) of 4 different samples. As-welded samples have the tensile residual stresses on the surface while all cold worked samples have compressive residual stresses. Residual stresses of the cold worked samples with 7.1 mm IS and 550 MPa IP ranged from -214.1 ± 19.6 MPa to -110.1 ± 25.6 MPa. With 1000 MPa IP, the residual stresses are in the range of -370.8 ± 21.8 MPa to -307.2 ± 18.6 MPa. In order to investigate the residual stresses induced by spot welding, selected samples were heat treated at 650°C for 30 minutes in order to relieving the residual stress after spot welding. Based on X-ray diffraction experiments, higher IP produced higher compressive residual stresses on the surfaces. Once the sample was heat-treated and the welding induced tensile residual stresses were released, post-weld cold working provided almost uniform compressive residual stresses around the surface. It can be concluded there is an interaction between existing residual stress (induced by spot welding) and cold working afterward.

Target area 1 is the closest to the nugget which explains why this has the highest tensile residual stress for the as welded specimen. This location has the greatest difference in heating and cooling during the RSW process (see section 2.2.2). Target area 2 has the highest compressive stress of the only cold worked samples, this can be explained by the shape of the RSW. During cold working the first contact location between the indenter and specimen occurs at target 2 creating the highest deformation (this is the same location as the dimple in Figure 5.1). Target area 3 is the last point of contact between indenter and specimen, resulting

in least deformation thus the lowest compressive stress of the cold worked samples. As expected the greater the IP the higher the compressive stresses.

TABLE 5.1. CIRCUMFERENTIAL RESIDUAL STRESS IN MPA.

Description	Post-weld cold working process parameter		Residual stress data (MPa)		
	IS (mm)	IP (MPa)	Target position 1 (2.0 mm)	Target position 2 (2.5 mm)	Target position 3 (3.0 mm)
As-welded	-	-	365.6±28.8	135.7±15.2	65.7±15.8
Cold worked	7.1	550	-173.3±20.6	-214.1±19.6	-110.1±25.6
Cold worked	7.1	1000	-354.4±26.1	-370.8±21.8	-307.2±18.6
Heat treated and cold worked	7.1	550	-200.1±21.6	-190.9±25.4	-199.8±22.6

5.1.6 NUMERICAL ANALYSIS

A nonlinear quasi-static finite element analysis using axisymmetric modeling procedures was used to quantify the state of residual stress in a typical post-weld treated 1008 cold rolled steel RSW specimen. Using LS-DYNA as the finite element program for the analysis, an implicit 2-D surface-to-surface contact algorithm was used. A ½ model with symmetric boundary conditions was constructed as shown in Figure 5.11. Figure 5.11 (a) shows the acceptable weld size with top and bottom IS of 7.1 mm and in Figure 5.11 (b) an unacceptable weld with IS of 4.6 mm is shown. An axisymmetric solid - volume weighted formulation was used for the shell elements with each element having a thickness (Z-dimension) of 0.1 mm. It should be noted for these ½ models it is constructed of a fused or nugget zone, three segmented heat affected zones (HAZ) and a base material zone shown by the different colors in the figures. Each HAZ and base material was given different material properties in order to obtain a more accurate representation of the actual property variance. All of the modeled dissimilar zones were based upon a piecewise linear plasticity constitutive formulation devised using an isotropic hardening rule. The assigned material properties specifically Yield Strength and Tensile Strength were found by the following equations [Zhou et al 2003]:

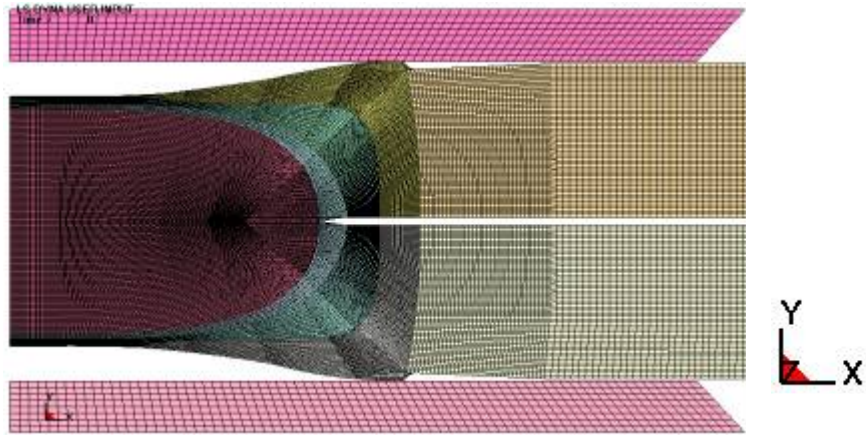
$$\sigma_{\text{uts}} = \sigma_0 + k_1 * H_v$$

$$\sigma_y = k_1 * H_v$$

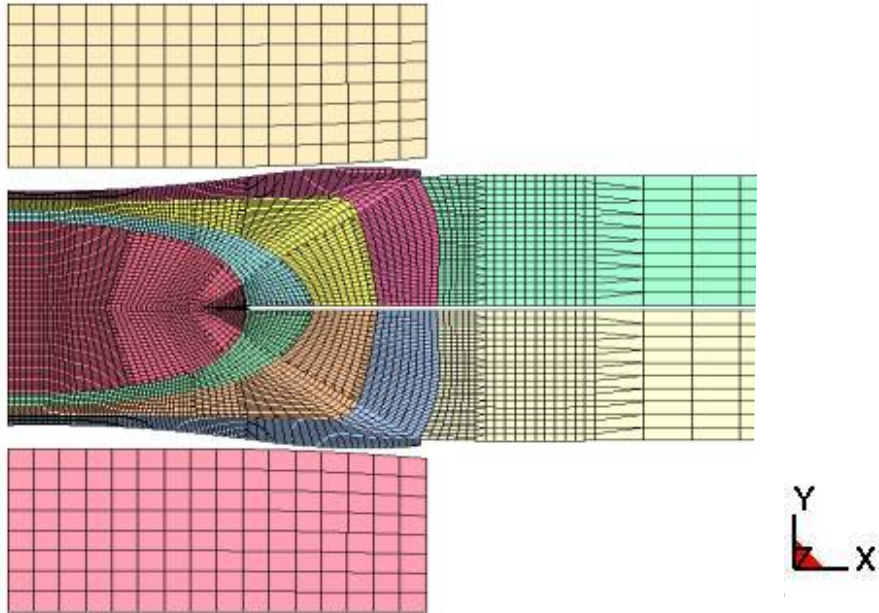
$$e = k_2 / H_v$$

where σ_{uts} , σ_y , σ_0 , e , H_v , k_1 , and k_2 are the ultimate strength in MPa, yield strength in MPa, a constant in MPa, ductility (elongation) in %, Vickers hardness, and unitless proportional constants, respectively. Microhardness data from Figure 5.2 was used in this FEA.

An implicit time marching scheme and solver was used for stress relaxation and material springback. In this model eight-node quadratic quadrilateral elements with six-node quadratic triangular elements were used. All shell elements had 6 degrees of freedom. The FEM contained approximately 55,000 rectangular and triangular elements and 64,000 nodes.



(a) ACCEPTABLE SIZE RSW WITH 7.1 MM INDENTERS.



(b) UNACCEPTABLE SIZE RSW WITH 4.6 MM INDENTERS.

FIGURE 5.11. LS-DYNA FINITE ELEMENT NUMERICAL ANALYSIS ON STEEL RSW.

After the simulated cold working where the indenters were applied to the nugget and released the resulting FEM of the post-weld cold worked RSW is shown in Figure 5.12. Shown in the figure is the residual hoop stress with a fringe level range of -600 MPa (compressive stress) to 400 MPa (tensile stress). In Figure 5.13 (a), the hoop stresses are shown for the FEM with the three circles showing the approximate target areas of the X-ray diffraction. Because the target area was approximately 1 mm in diameter, the stresses were averaged over the whole area to obtain a single numerical value. As presented in Figure 5.12, the FEM estimation of residual stresses on the post-weld cold worked RSW complements the corresponding X-ray diffraction residual stress measurements.

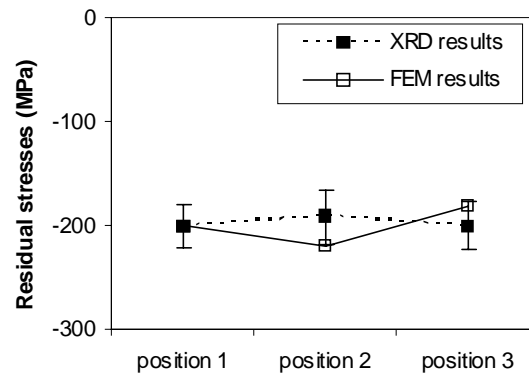


FIGURE 5.12. COMPARISONS BETWEEN XRD AND FEM OF AVERAGE RESIDUAL STRESSES ON STEEL RSW SURFACES.

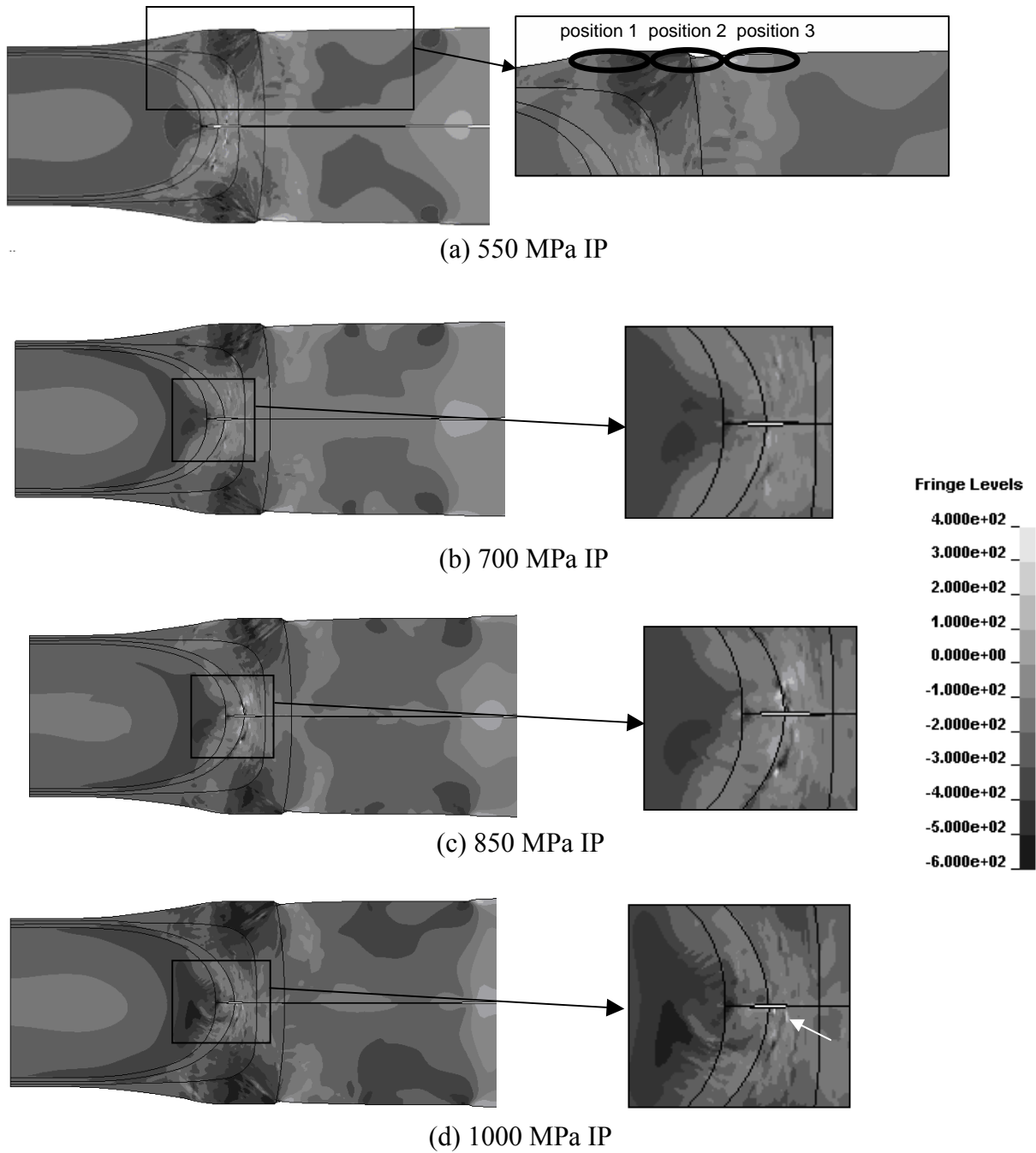


FIGURE 5.13. FEA CONTOUR PLOT OF HOOP STRESS WITH IS 7.1MM AND VARIOUS IPS AND FRINGE LEVELS.

From Figure 5.13 (b, c, d) the boxes on the half models are obtruded to show the faying surface where crack initiation occurs the most. For the 1000 MPa IP visually there is

more compressive residual stresses (darker regions) than 700 MPa IP and 850 MPa IP. The white arrow of on Fig. 5.13 (d) (1000 MPa IP and 7.1 mm IS) indicates higher tensile residual stress zone (average of +230 MPa) than the other two IPs. It can be predicted from FEM results in Figure 5.14 for the 1000 MPa IP the maximum tensile stress is higher than the other two IPs is why the 1000 MPa IP has a lower fatigue life. Even though the average stress for 1000 MPa IP is lower and compressive stress is much greater than the other IPs, the location of the high tensile stress is directly at the critical zone of crack initiation. When comparing contour plots of 700 MPa IP to 850 MPa IP, the 850 MPa IP has more area of tensile (white in color) regions than the 700 MPa IP, but when the average stress is computed over the whole area there is very little difference. This concurs with the experimental data which is shown in Figure 5.14 where the difference of fatigue life between 700 MPa IP and 850 MPa IP is insignificant. In conclusion, the FEA results match very well with the experimental fatigue results which show improved fatigue life of post-weld cold worked RSWs.

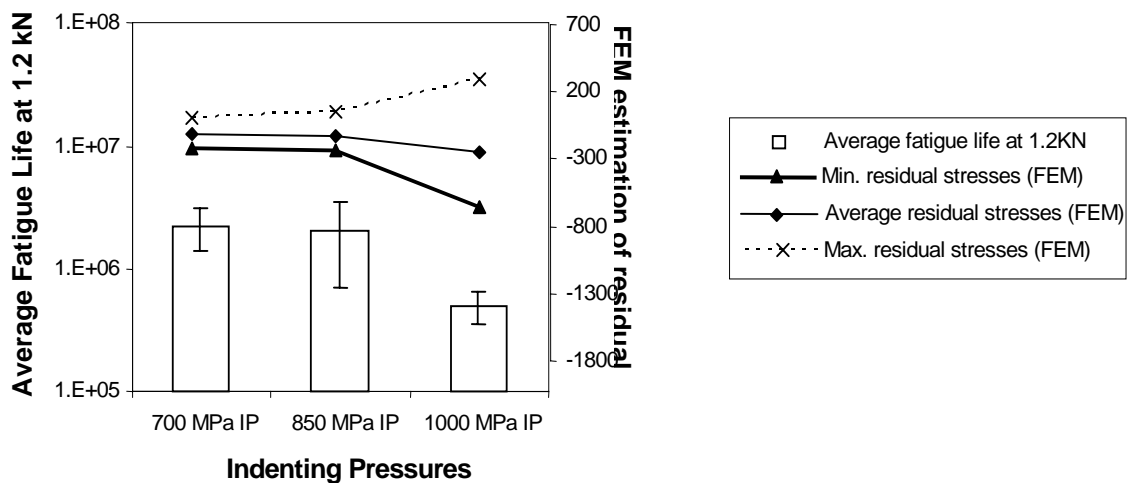
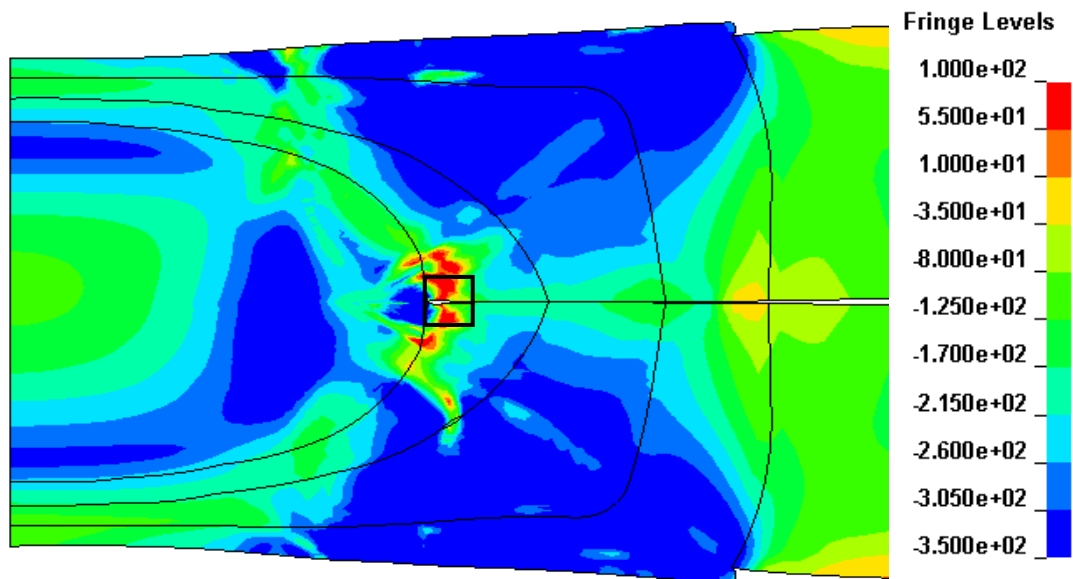


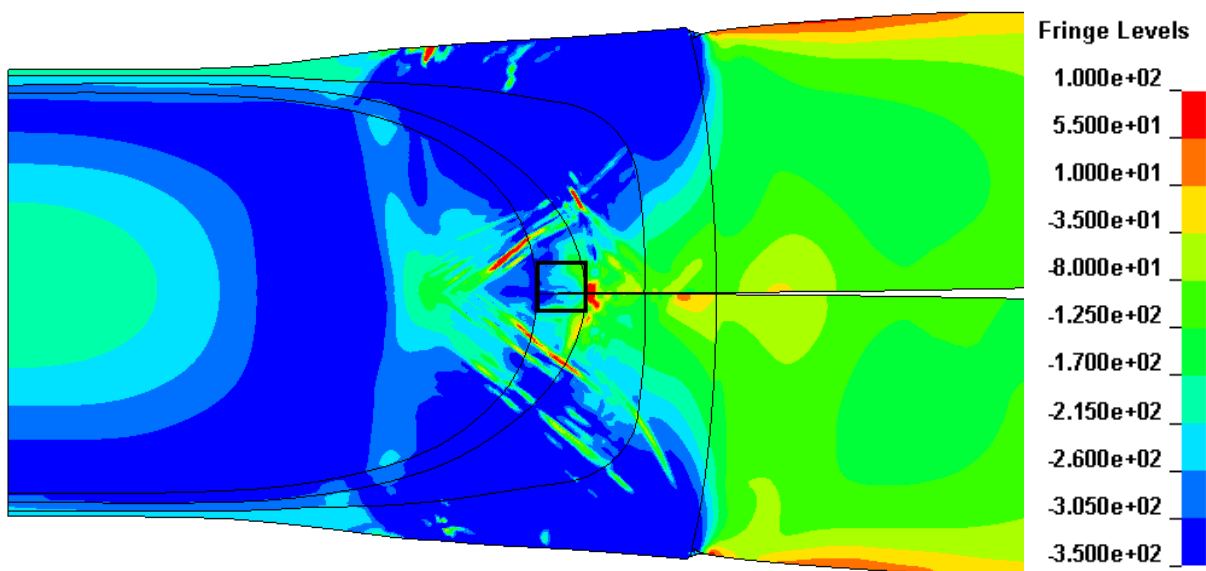
FIGURE 5.14. CORRELATION BETWEEN FEA AND EXPERIMENTAL FATIGUE RESULTS FOR 7.1 MM IS.

In Figures 5.15 and 5.16 there are much higher tensile (red regions) stresses at the notch location (notch region is highlighted by box) for both small nugget diameters (ND) when compared to the acceptable weld nugget diameters. These higher tensile stresses in the small nugget diameter correlate directly with the fatigue life results where smaller nuggets had shorter life that was shown in Figure 5.7. The stress contours from FEM results explain why the fatigue life of undersized spot-welds shows little to no improvement or even detrimental effects when cold worked.

In Figure 5.15 (b), the post-weld cold working process with IS 4.6 mm and IP 850 MPa induced an average of 250 MPa compressive residual stresses in a hoop direction at the notch region. The similar results are found with IP 700 MPa and 1000 MPa. However, undersized spot welds did not have sufficiently deep compressive residual stresses in the notch region, as shown in Figure 5.15 (a) and 5.16 (a). Instead they contain tensile residual stresses. The notch condition of a specimen has an overriding negative effect on its fatigue strength because it is often the location for fatigue crack initiation [Radaj, D., 1990]. For the adequate sized welds the first area of contact between the specimen and indenter took place closer in the vertical direction with the notch region whereas as for undersized RSW the initial point of contact was farther into the HAZ and base material. When the indenters force the upper and lower sheets together compressive stresses are developed at the point of contact between the sheets and trap the tensile stresses at the notch region. These tensile residual stresses of the undersized post-weld cold worked RSW samples showed detrimental effects to fatigue life. The FEM also supports increased fatigue life of adequately sized RSWs by post-weld cold working.



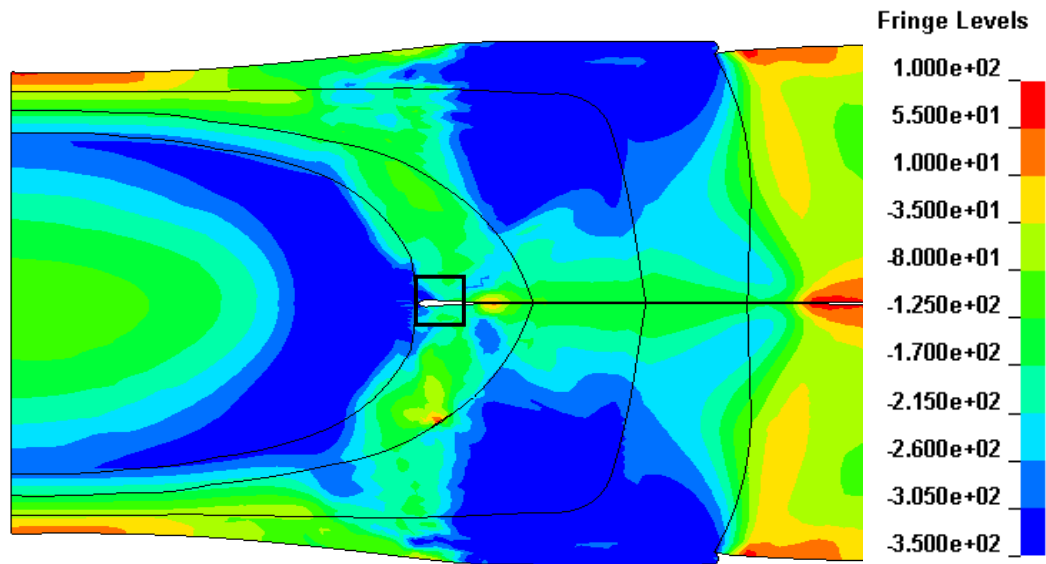
(a) UNDERSIZED (ND=2.6 MM)



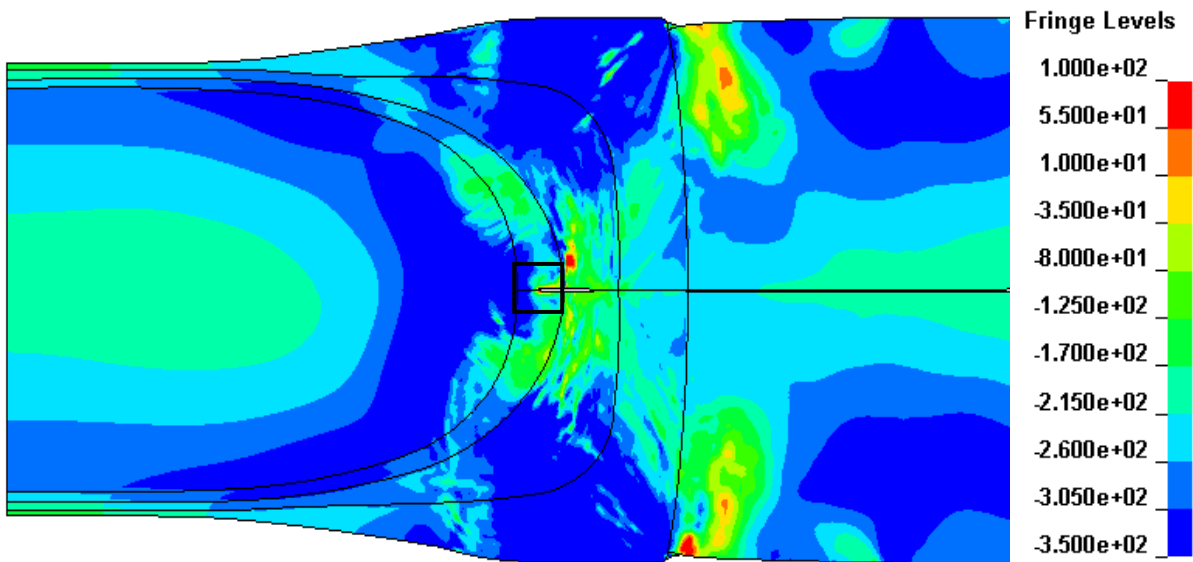
(b) ADEQUATELY SIZED (ND=3.4MM)

FIGURE 5.15. FEM HOOP STRESS RESULTS FOR STEEL RSWS WITH COLD WORKING PARAMETERS OF IS 4.6 MM AND IP 850 MPA.

(FRINGE LEVELS UNITS OF MPA).



(a) UNDERSIZED (ND=2.6 MM)



(b) ADEQUATELY SIZED (ND=3.4MM)

FIGURE 5.16. FEM HOOP STRESS RESULTS FOR STEEL RSW WITH COLD WORKING PARAMETERS OF IS 7.1 MM AND IP 850 MPA.

(FRINGE LEVELS UNITS OF MPA).

5.2 ALUMINUM RSW

5.2.1 METALLOGRAPHY

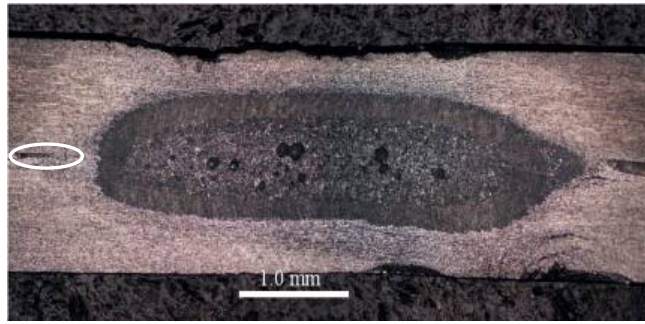
Microstructures of an as-welded specimen and two post-weld cold worked specimens with 4.6 mm IS, 450 MPa IP and 7.1mm IS, 300 MPa IP are shown in Figures 5.17 (a) , (b), and (c) respectively. The nugget can be seen clearly along with voids contained in the nugget region. As shown in Figure 5.17 (b) and (c) the nugget is non-uniform because of the volatile conditions of Al during spot welding. Particularly of interest in these figures is the difference in the faying surface notch radii highlighted by the white circles. The as-welded specimen in Figure 5.17 (a) has a relatively large notch radius whereas the post-weld cold worked specimen in Figure 5.17 (b) has a much smaller radius. Therefore, the cold working process causes the radius of the notch at the intersection of the faying surface and fused zone to decrease significantly.



(a) AS-WELDED [KIM ET AL 2005]



(b) POST-WELD COLD WORKED (4.6 MM IS, 450 MPA IP)



(C) POST-WELD COLD WORKED (7.1MM IS, 300 MPA IP)
FIGURE 5.17. AL RSW MICROSTRUCTURE.

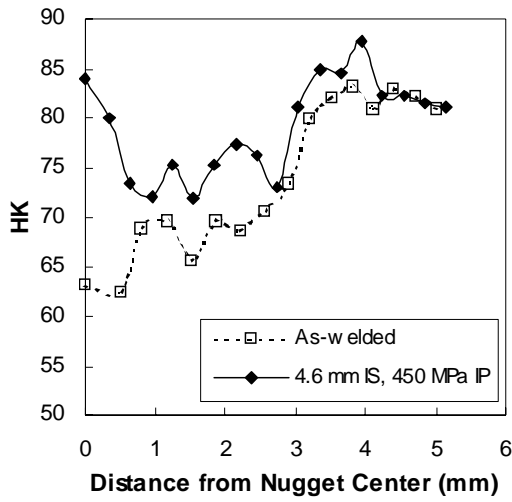
5.2.2 MICROHARDNESS

Microhardness test results are shown in Figure 5.18. Microhardness in the nugget area is generally lower than that in the base metal area. Fusion zones in Al RSW have much larger grains due to welding as shown in Figure 5.17. The effect of post-weld cold working parameters on the microhardness profiles of as-welded and post-weld cold worked samples for varying indenter sizes and pressures was investigated.

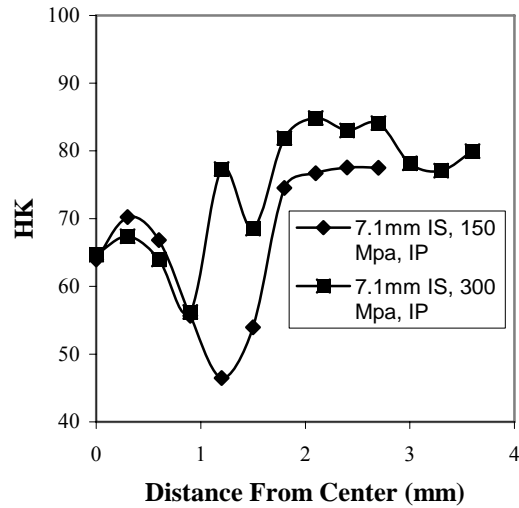
It is shown in Figure 5.18 (a) cold working increases the microhardness. For the 4.6 mm IS a 20% increase in hardness was found in the cold worked area by the 450 MPa IP and with the 300 MPa IP, it increased by 10% when compared to the base material.

Figure 5.18 (b) shows that an increase in IP directly causes a greater increase in the microhardness, since the 300 MPa IP specimen showed a higher hardness than the 150 MPa specimen. Hardness in the cold worked area by 300 MPa IP was measured approximately 10% higher than that of the non-cold worked area. This increase is an indication of the strain hardening that takes place during the cold work process, translating to an increased strength in the Al RSW.

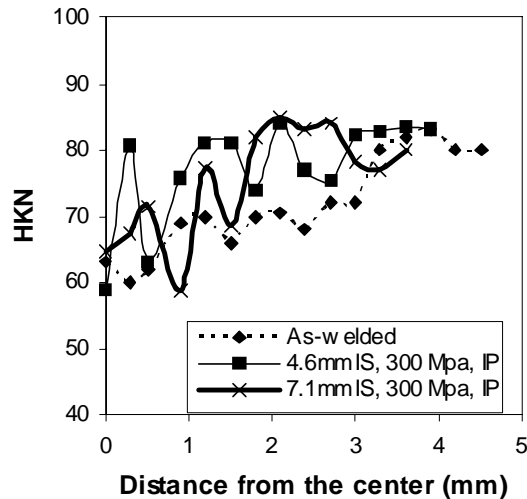
In Figure 5.18 (c), the increased microhardness for the 7.1 mm IS extends farther into the base material whereas the 4.6 mm indentation diameter experiences only a local hardness increase near the center of the nugget. All plots in Figure 5.18 plots show significant randomness to the hardness profile which is a result of the voids in the nugget.



(A) EFFECT OF COLD WORKING



(b) EFFECT OF IP



(c) EFFECT OF IS

FIGURE 5.18. MICROHARDNESS OF POST COLD WORKED AL RSW.

5.2.4 TENSILE-SHEAR TESTING

R. Spitsen determined from ANOVA research on aluminum RSW that the nugget diameter has a much stronger influence on weld strength than the post-weld cold working parameters IS and IP. Therefore, while the post-weld cold working process does slightly increase the tensile strength of Al RSW, the nugget size is the most important contributor of the tensile strength of the RSW. [Spitsen, R., 2005] In view of these findings tensile testing is not a dynamic aspect for determining the mechanical properties of cold worked Al RSWs.

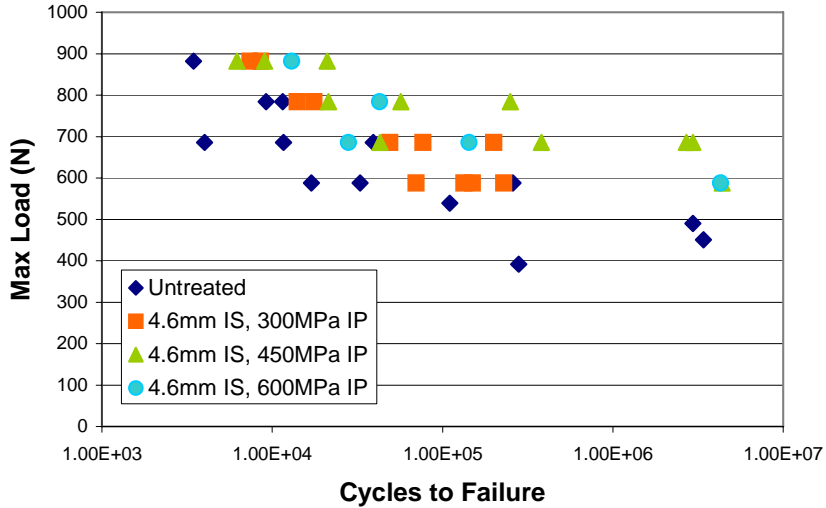
5.2.4 FATIGUE TESTING

The L-N curves of as-welded specimens and post-weld cold worked specimens with varying IP (300MPa, 450MPa and 600MPa) at 4.6 mm IS are shown in Figure 5.19 (a). For all 4.6 mm IS cold worked samples the fatigue life increased over the as welded samples. The higher fatigue loads during the fatigue testing show very little improvement of the cold working process over the as welded specimens; when the load decreases the enhancement between the different IPs over as welded specimens increases immensely. Specimens with 450 MPa IP shows the highest fatigue life of 2.9×10^6 cycles at a load of 686 N which is approximately 70 times greater than the as welded specimens.

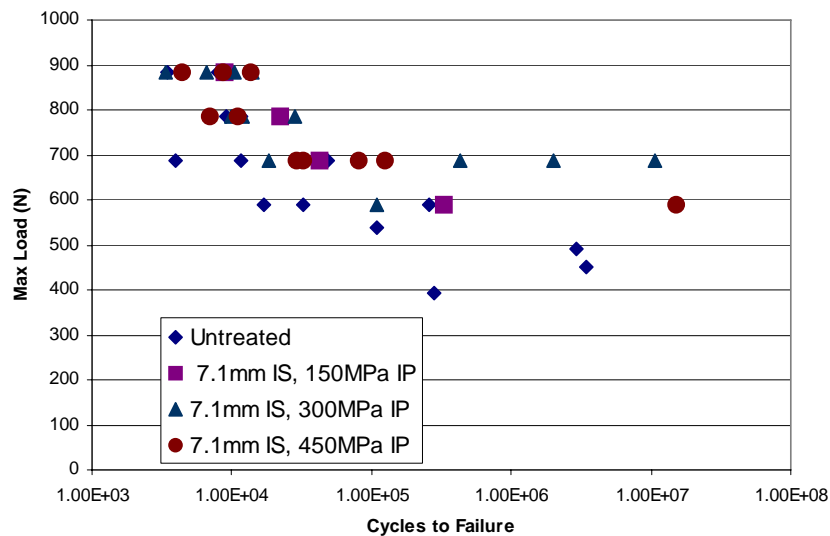
Figure 5.19 (b) shows the L-N curves of as-welded specimens and post-weld cold worked specimens with varying IP (150MPa, 300MPa and 450MPa) at 7.1 mm IS. At this IS all pressure parameters had a higher fatigue life over the as welded group. As with the 4.6 mm IS the largest change in fatigue life occurs at the lower loads. The load of 686 N shows an increase of fatigue life for 300 MPa IP to be approximately 80 times better when compared to the as welded specimens. The superior fatigue resistance of the post-cold worked specimens is due to the compressive residual stresses induced during the post-weld cold

working process, which delays the crack initiation and/or crack propagation at the faying surface.

Comparing figure 5.19 (a) and (b) shows the optimum parameters of the cold working process at lower fatigue loads with respect to fatigue life of the Al RSW are 300 MPa IP with 7.1mm IS. At higher fatigue loads there is no conclusive optimal parameter.



(a) 4.6 MM IS



(b) 7.1 MM IS

FIGURE 5.19. L-N CURVE FOR AS-WELDED AL AND POST-WELD COLD WORKED RSW SPECIMENS WITH VARIOUS IP.

5.2.5 NUMERICAL ANALYSIS

A similar FEA was performed on Al as was on steel (see section 5.1.5) except with different material properties and different nugget, HAZ and base material geometries. The Al FEM is shown in Figure 5.20 with the 7.1 mm IS, the cross sectional view of a ½ model RSW is shown with the weld nugget being the fully enveloped zone surrounded by the HAZ and the base material to the right. This model contains approximately 21700 nodes and 2000 elements.

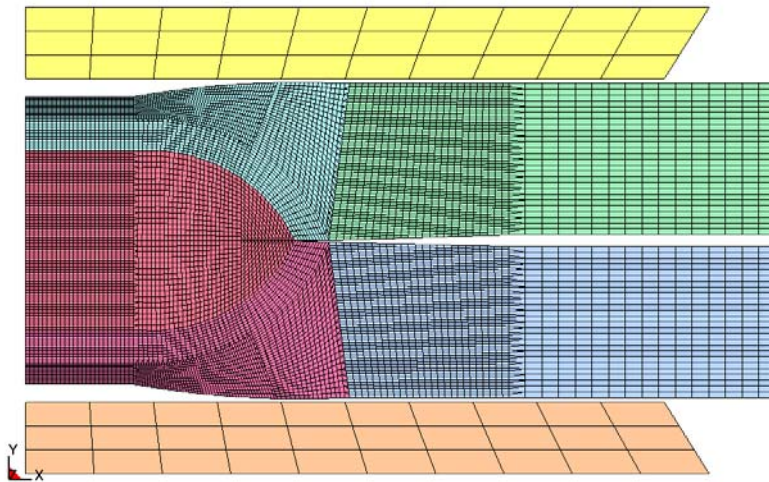
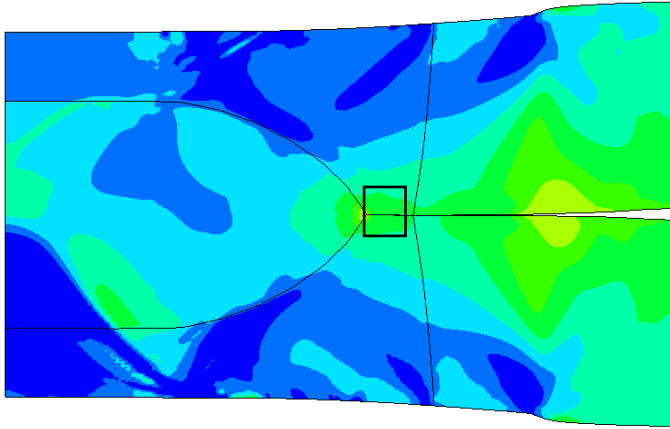
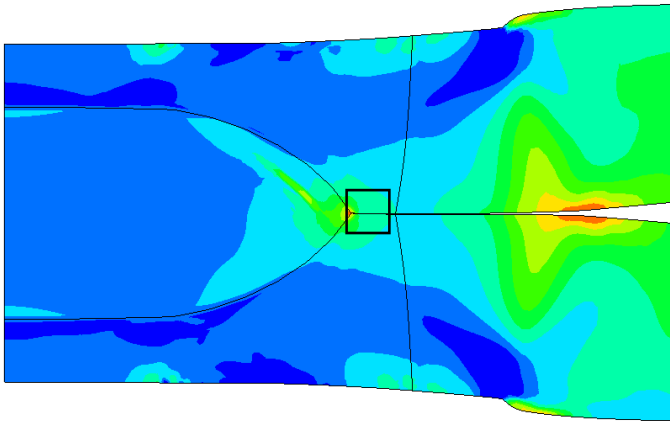


FIGURE 5.20. FEM OF AL RSW WITH 7.1 MM IS.

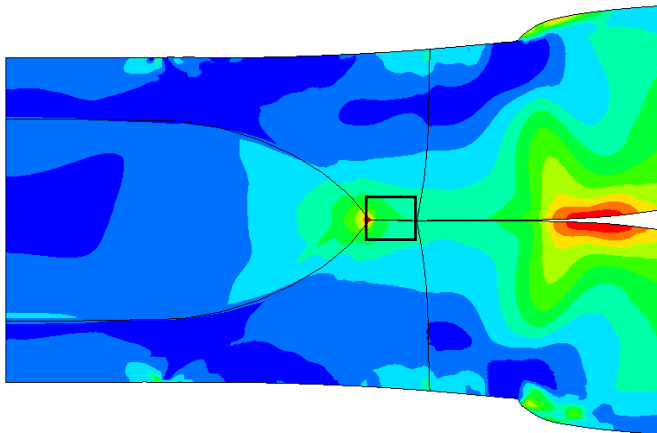
From FEM the area of interest is at the faying surface, which is defined at the interface of the weld notch root and HAZ. The faying is where crack initiation often originates outlined by the black boxes in Figures 5.21, 5.22 where the residual stress was analyzed by taking an average of the stresses. Figure 5.21 shows the greener contours are less compressive stresses than the bluer contours. For the 4.6 mm IS in Figure 5.21, (b) has the darkest region in around the faying surface, which is the 450 MPa IP. Between all the contours in Figures 5.21 and 5.22, the darkest faying surface region is the 7.1 mm IS and 300 MPa IP (Figure 5.22 (b)).



(a) 300 MPA IP



(b) 450 MPA IP

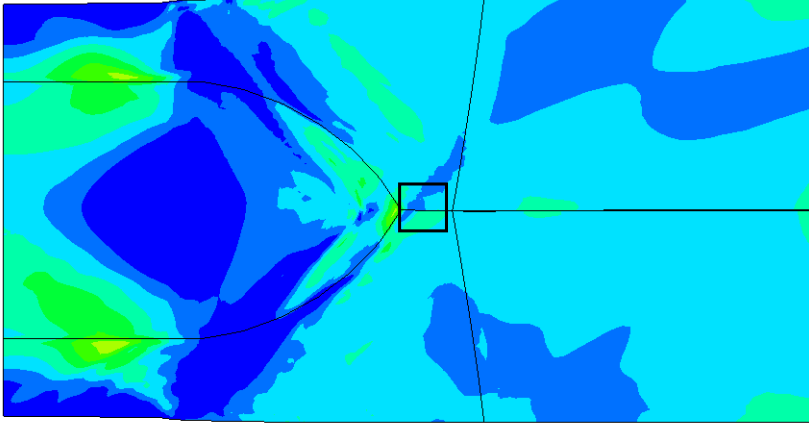


(c) 600 MPA IP

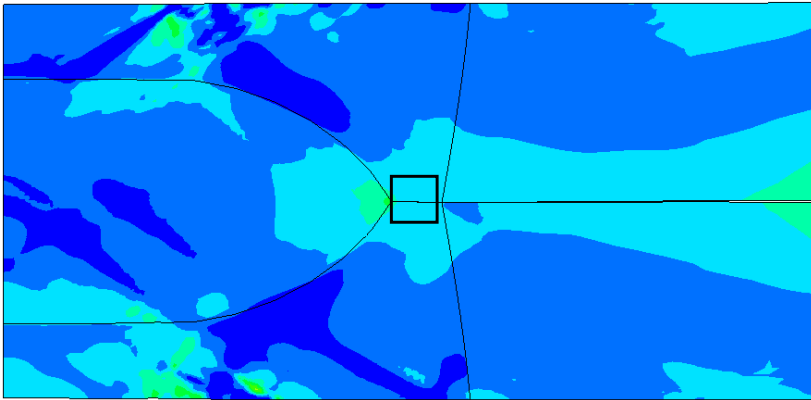
Fringe Levels



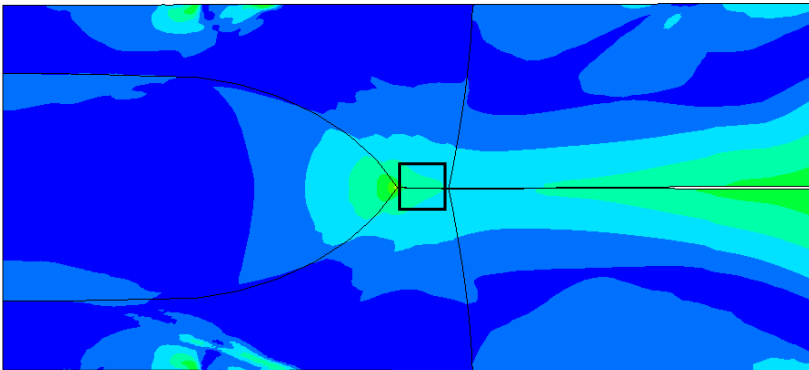
FIGURE 5.21. FEM OF RESIDUAL STRESS IN THE HOOP DIRECTION WITH FRINGE LEVELS FOR 4.6 MM IS.



(a) 150 MPA IP



(b) 300 MPA IP



(c) 450 MPA IP

Fringe Levels

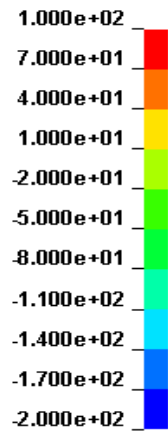
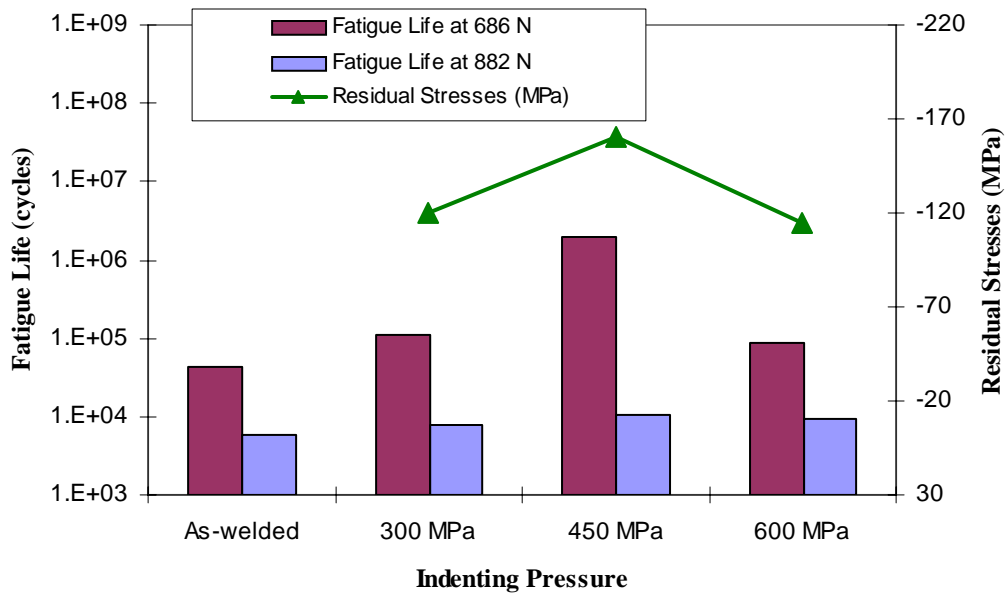
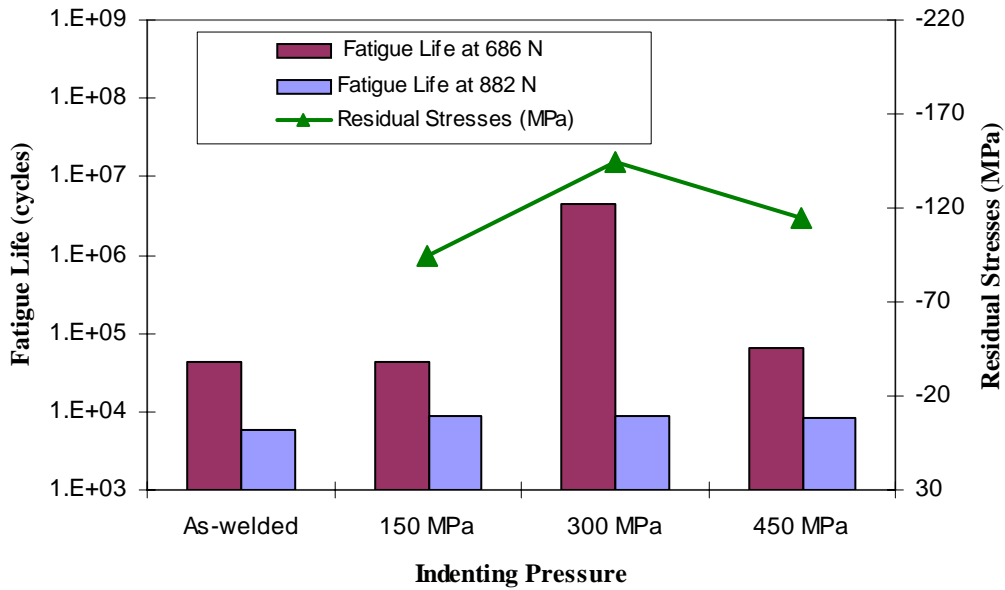


FIGURE 5.22. FEM OF RESIDUAL STRESS IN THE HOOP DIRECTION WITH FRINGE LEVELS FOR 7.1 MM IS.

Figure 5.23 graphs the fatigue life and the compressive residual stress in the hoop direction of each parameter. The trend of the average residual stress of the target area from FEM follows closely the trend of the fatigue life. In Figure 5.23 (a) for 4.6 mm IS the optimum pressure for both fatigue life and residual stress is 450 MPa IP and in Figure 5.23 (b) with 7.1 mm IS the pressure is 300 MPa. As IP increases or decreases for both ISs from the optimum conditions so does the fatigue life and residual stress. The values for fatigue life and stresses are similar in magnitude for the optimum pressures of each IS. The 4.6 mm IS is similar to the size of the RSW nugget, thus to induce a compressive stress at the target area outside the nugget a higher pressure is required than for a 7.1 mm IS. This explains why a higher pressure is necessary for a smaller IS to reach the same fatigue life and compressive stress values compared to a larger IS. Lower pressures do not create enough compressive residual stresses at the faying surface thus do not improve the fatigue life significantly when compared to the as-welded samples. The reason for inadequate results for higher pressures of both IS maybe due to defects caused by gross plastic deformation.



(a) 4.6 MM IS



(b) 7.1 MM IS

FIGURE 5.23. EFFECT OF INDENTATION PRESSURE (IP) AND SIZE (IS) ON FATIGUE LIFE OF AL RWS POST-WELD COLD WORKED AT 686 N AND 882 N MAXIMUM LOAD WITH COMPRESSIVE RESIDUAL STRESSES.

5.3 SPR

Initial research was performed to determine the optimal material type and thickness for the provided rivet. After this was accomplished cold working was done on the chosen materials with RSF (rivet setting force), tensile test and fatigue test to study the effects of cold working.

5.3.1 MATERIAL SELECTION

Each rivet and die combination is designed for specific material types and thicknesses. With the provided rivet and die used in this research the material type and thickness were unknown. To determine the optimum material the following test were performed: RSF (rivet setting force), metallography, and tensile-shear.

5.3.1.1 PROCESS FORCE

The SPR process requires a substantially high RSF to drive the rivet into the workpiece. This results in large, cumbersome riveting guns with limited accessibility to complex sheet metal assemblies that demand assembly robots with much larger load carrying capacities. Figure 5.24 shows a typical C-gun type SPR machine with the throat size shown by the variable 'b'. A higher RSF requires a smaller throat size, thus limiting the C-gun's capability to reach tight locations. To join 1.0 mm thick (5000 or 6000 series aluminum), sheets, the required RSF is approximately 20 kN while for thickness range 2.0-3.0 mm, the required RSF may be up to 40 kN. As a result, an SPR gun has to be built much bulkier and heavier. [Kim, D., *et al*, 2006]

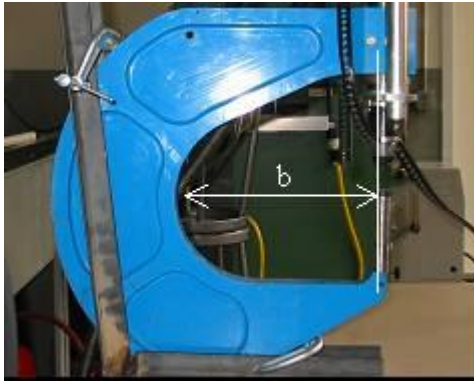


FIGURE 5.24. SPR C-GUN WITH THROAT SIZE SHOWN.

[KIM, D., *ET AL* 2006]

Of the four steps during the SPR process shown in Figure 5.25 steps two and three are of significance when considering process force. The step when the rivet pierces through the first layer of sheet metal and penetrates into the second layer is defined as Region I. When the rivet penetrates into the second layer, deforms, and spreads outwards to form the sealed joint is defined as Region II. Once the rivet starts to penetrate the second layer, the force goes up drastically. As expected in Figure 5.26 the maximum force occurred during the deformation of the steel rivet for a typical SPR installation. At the end of region II the press retracts and the force decreases back to zero.

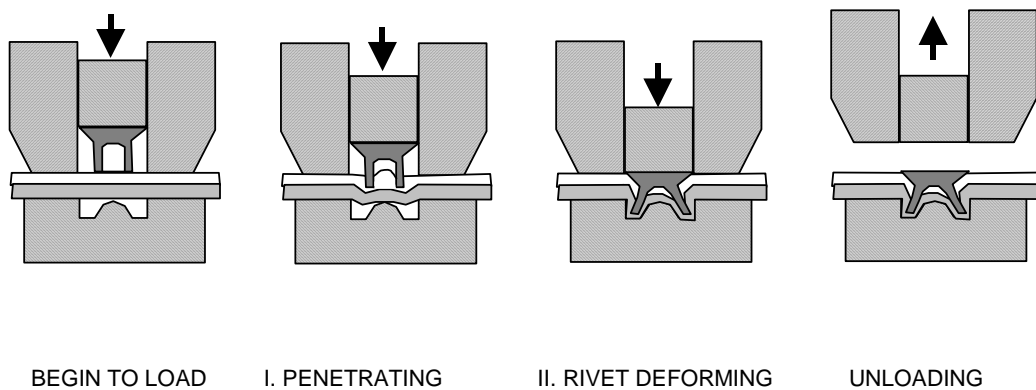


FIGURE 5.25. SCHEMATIC OF THE STEPS IN THE SPR PROCESS.

[KIM, D., *ET AL* 2006]

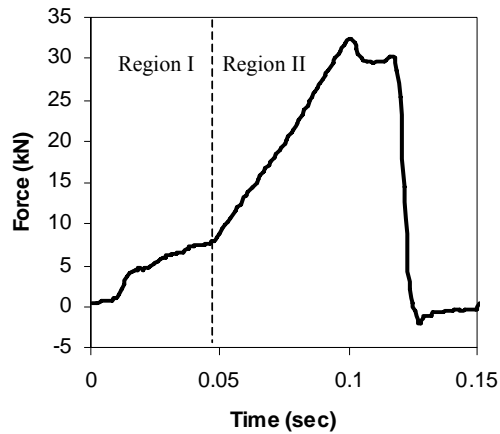
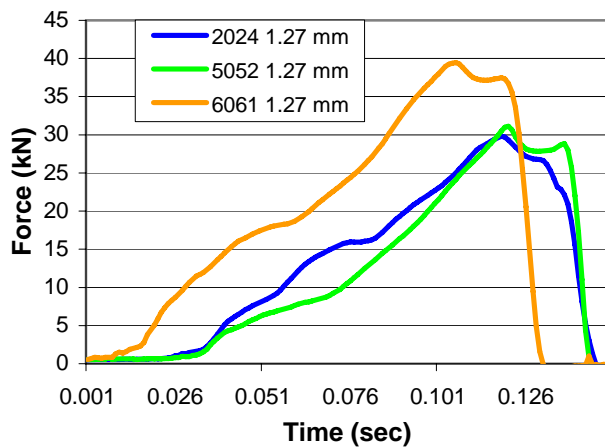
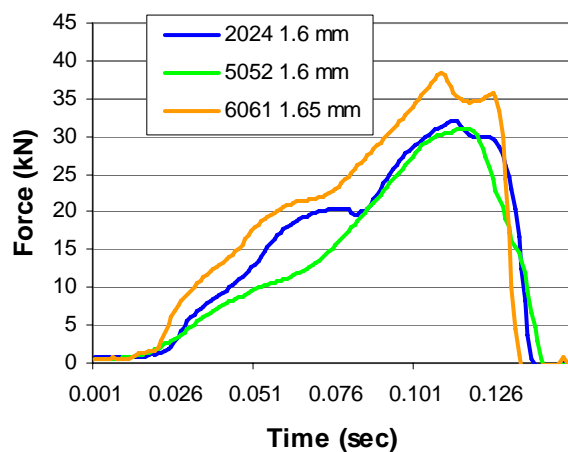


FIGURE 5.26. TYPICAL SPR INSTALLATION PROCESS FORCE DIAGRAM SHOWING REGIONS I, II.

Two sets of RSF curves are shown in Figure 5.27 for each material type. For the 1.27 mm thickness (Figure 5.27 (a)) during region I Al 5052 shows the lowest penetration force while Al 2024 and Al 5052 have similar force magnitudes. For region II Al 6061 required the highest rivet deformation force. This trend followed for the 1.6 mm samples shown in Figure 5.27 (b).



(a) 1.27 MM



(b) 1.6 MM

FIGURE 5.27. FORCE CURVES FOR AL SPR.

Figure 5.28 gives the ultimate riveting force during each region for all material and thickness types. In region I Al 2024 and Al 6063 forces in each respective thickness are similar, whereas Al 5052 was approximately 50% less for each respective thickness when compared to the other two materials. In region II Al 2024 and Al 5052 all forces were similar to each other but Al 6063 shows a higher force requirement in this region.

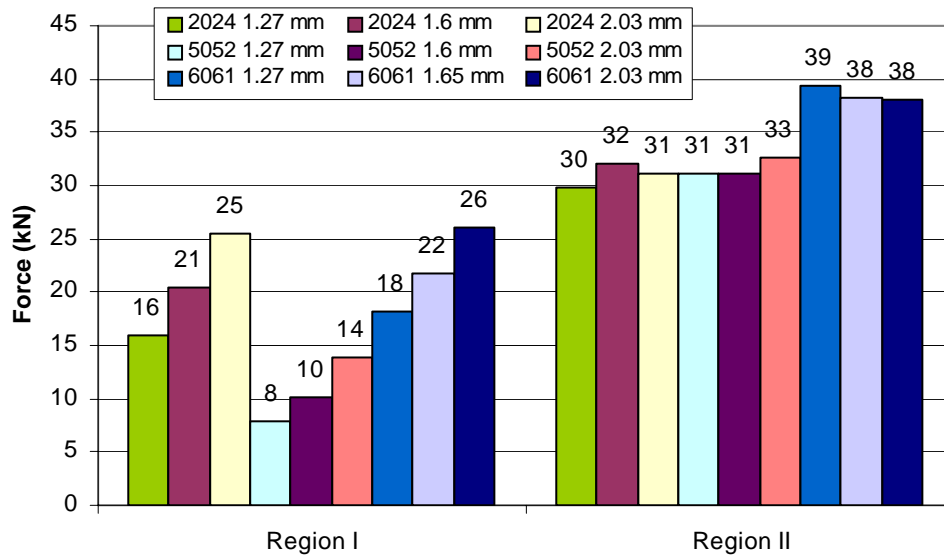


FIGURE 5.28. ULTIMATE FORCES FOR SPR IN AL MATERIALS FOR RESPECTIVE REGIONS.

For all materials in region I as the thickness increased the penetrating force increased. The reason for this is the aluminum deformation and penetration force is proportional to the product of the shear strength of the sheet metal and the cross-sectional area being sheared. The operation force, F , thus can be express as

$$F = C(\sigma_{flow})(t)(L)$$

where C is a constant, σ_{flow} is the flow stress of the sheet metal, t is the penetration depth, and L is the total length of the sheared edge. So it is expected for thicker materials, which have a

larger L , to have a greater force. The flow stress of a material is a direct relationship to yield strength, this is the reason why Al 2024 and Al 6061 have higher region I force than Al 5052. From section 4.3.1 the yield strength of Al 2024 and Al 6061 are similar to each other but both are greater than Al 5052.

5.3.1.2 METALLOGRAPHY

Cross sectional SPR views are shown in a matrix in Figure 5.29 of all Al materials and respective thicknesses. A good SPR is when there is little to no voids around the rivet and the rivet head is flush with the pierced sheet. The purpose for having no voids near the rivet is to reduce fretting during fatigue loading, the greater the void the larger the microslip between surfaces leading to greater fretting. For each thickness of Al 2024 there is a significant amount of shear preventing the material to form to the rivet shape and also causing non-uniform cross-sectional views. Al 5052 shows the best formation with the 1.6 mm and 2.03 mm thickness specimens having the least gaps. Similar to Al 2024, Al 6063 does not allow the material to form to the rivet shape resulting in significant voids.

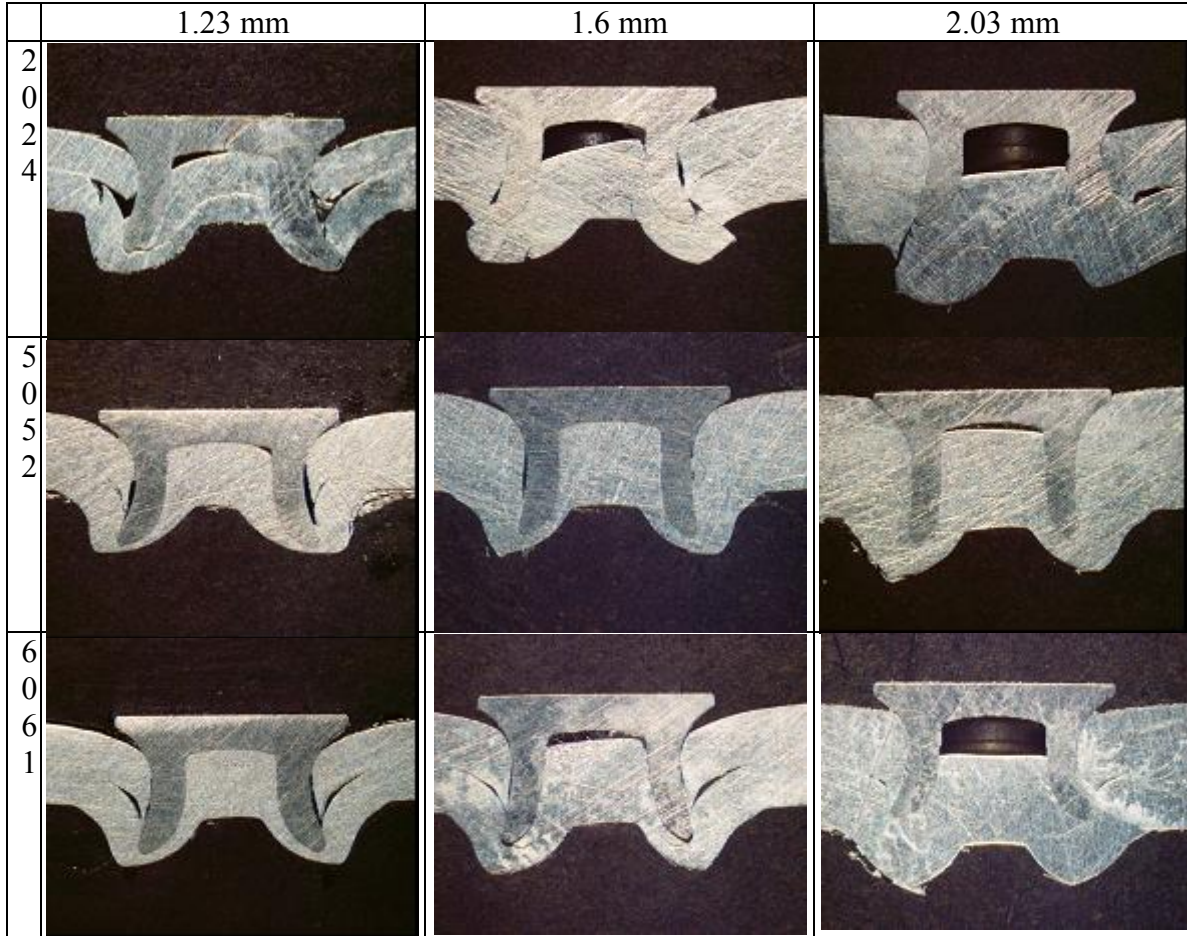


FIGURE 5.29. CROSS SECTIONS OF SPR FOR EACH MATERIAL TYPE AND THICKNESS.

(NOTE: Al 6061 has a thickness of 1.651 mm instead of 1.6 mm shown in the matrix.)

5.3.1.3 TENSILE-SHEAR TESTING

The ultimate tensile properties are shown in Figure 5.30 for all Al types and thicknesses. The material type with the greatest strength was Al 2024 with thickness 1.6 mm. All specimens failed by the rivet deforming the pierced sheet allowing pulling out of locked sheet known as Mode 2 failure shown in Figure 5.31. As expected the material with the highest yield strength would have the highest tensile-shear strength because of the deformation required for failure in the pierced sheet. For some 2.03 mm specimens the rivet

never interlocked in to the bottom sheet, resulting in failure at low loads while others did interlock, this shown by the large error bars. The 1.27 mm and 1.6 mm thick specimens had consistent strengths for each respective material type and thickness.

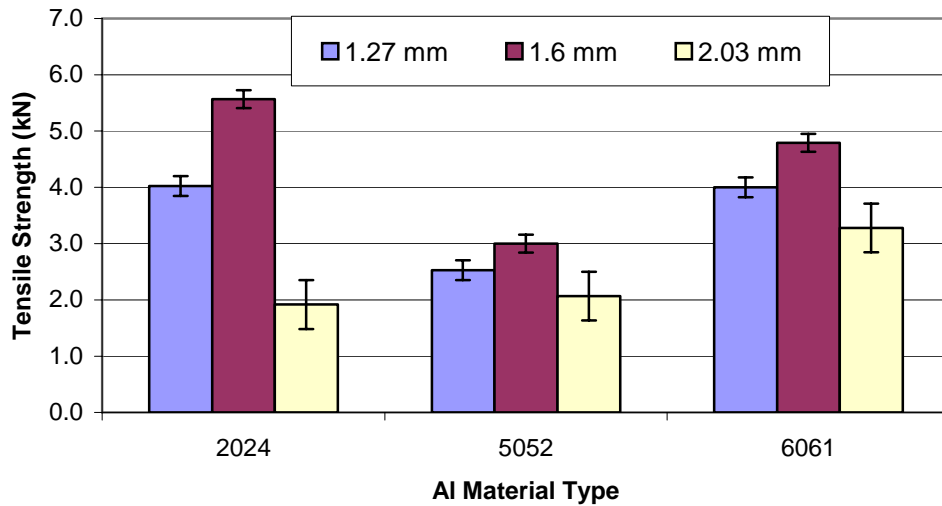


FIGURE 5.30. SPR TENSILE RESULTS FOR AL SHOWING ERROR BARS.

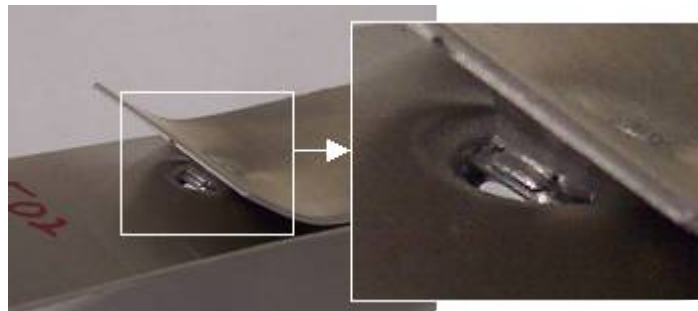


FIGURE 5.31. SPR SAMPLE FAILURE DURING TENSILE-SHEAR TEST.

The material type chosen to perform the cold working on was Al 5052 with sheet thicknesses of 1.27 mm and 1.6 mm. These were chosen based off of the overall RSF, metallography and tensile results. They were also chosen because of the pliability of the material for the cold working procedures to be affective due to the limitations of cold working equipment.

5.3.2 COLD WORKED SPR

Cold working was performed on the Al 5052 with sheet thicknesses of 1.27 mm and 1.6 mm according to section 4.3.2.

5.3.2.1 PROCESS FORCE

The effects of cold worked (CW) and as-received (AR) Al 5052 on the RSF are shown in Figure 5.32 (a) 1.27 mm sheet thickness and (b) 1.6 mm sheet thickness. For both thicknesses the RSF for cold worked is higher than as-received in each region.

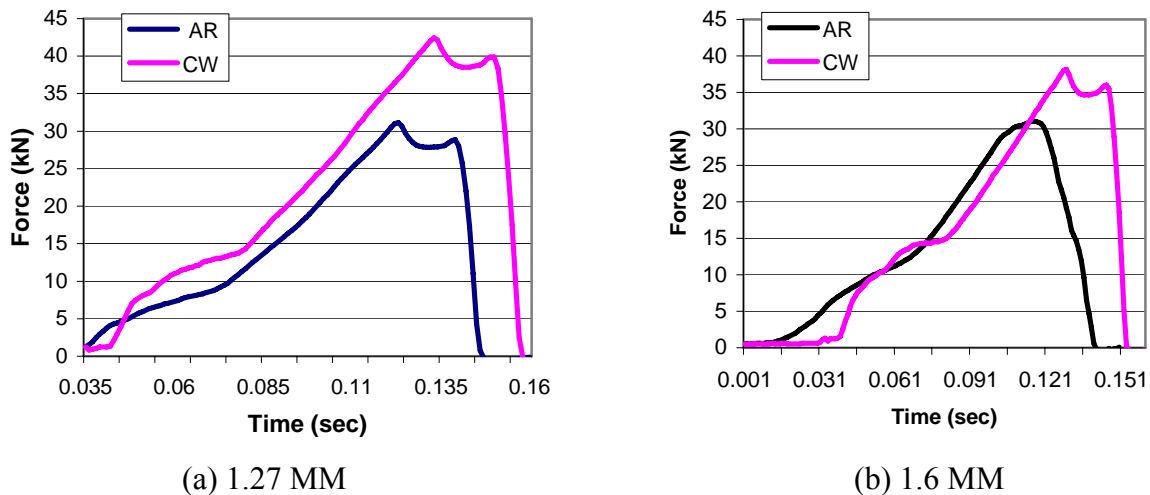


FIGURE 5.32. SPR PROCESS FORCE FOR AL 5052 CW AND AR WITH RESPECT TO SHEET THICKNESS.

Table 5.2 gives the numerical values for the process force. The forces in region I and region II for sheet thickness 1.27 mm increased by 57 % and 36% respectively for cold worked over as received samples. For 1.6 mm sheet thickness the increase of RSF in region I was 45% and in region II 23% for cold worked over as received. With the same load being applied to both material thicknesses during cold working implies the thinner material will have greater strain hardening. This strain hardening increases the flow stress ultimately

resulting in greater RSF. This gives reason for the 1.27 mm material having a greater change in RSF over the 1.6 mm thickness. This higher operational force ultimately requires a larger C-gun for the riveting process.

TABLE 5.2. AL 5052 PROCESS FORCES.

Sheet Thickness	1.27 mm AR		1.27 mm CW	
	Region I	Region II	Region I	Region II
Average Force (kN)	7.79	31.14	12.22	42.44
STDV	0.01	0.05	0.02	0.01

Sheet Thickness	1.6 mm AR		1.6 mm CW	
	Region I	Region II	Region I	Region II
Average Force (kN)	10.21	31.04	14.77	38.14
STDV	0.01	0.14	0.02	0.13

5.3.2.2 TENSILE-SHEAR TESTING

Figure 5.33 shows the tensile results for cold worked and as received Al 5052 SPR specimens. As shown with the error bars there is limited difference in the tensile strengths between as received and cold worked rivets. The main theory for this is because during the rivet process the induced stress during plastic deformation has an overriding effect of the residual stress implemented during the cold working process.

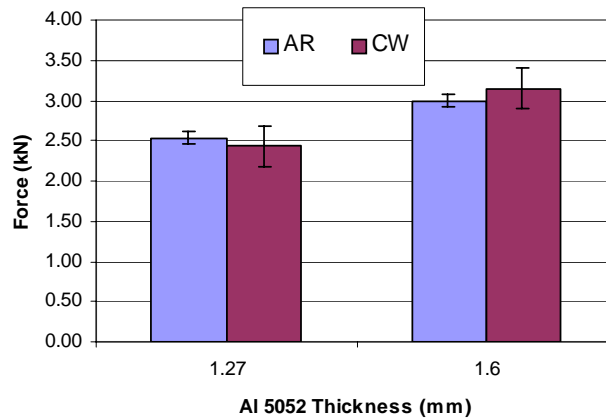


FIGURE 5.33. TENSILE STRENGTH OF CW AND AR SPR AL 5052 SHEET WITH ERROR BARS.

5.3.2.3 FATIGUE TESTING

The fatigue comparison between CW and AR for sheet thickness 1.23 mm is shown in Figure 5.34. The cold working appears to have no effect on the fatigue life of a SPR. The arrow on the cold worked 1.3 kN load specimen indicates there was no failure after approximately 5 million cycles. All high loads failed by Mode 1 (pierced sheet crack) while some lower loads failed by Mode 3 (locked sheet crack).

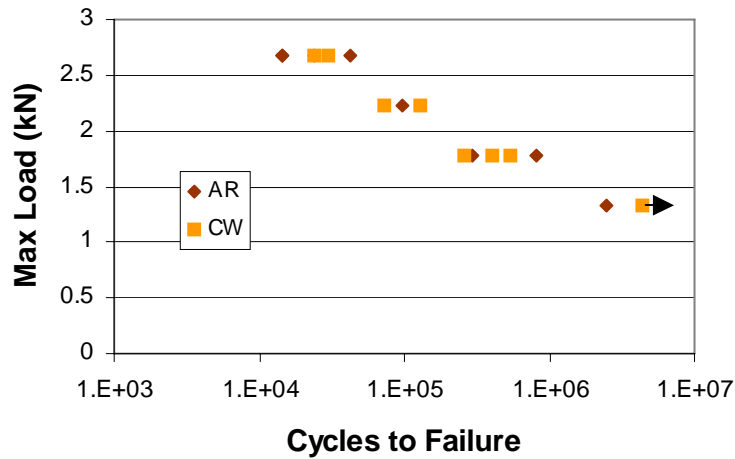


FIGURE 5.34. FATIGUE OF SPR FOR SHEET THICKNESS 1.27 MM.

For SPR in sheet thickness of 1.6 mm the fatigue life is shown in Figure 5.35. There is no conclusive effect of CW on the SPR fatigue life in 1.6 mm Al 5052. One theory for this trend of CW having no effect on fatigue life follows closely with the monotonic tensile shear results in that the residual stresses created during cold working are annulled during the SPR process. Residual stresses from the SPR process are the only stresses influencing fatigue. As with 1.27 mm specimens the 1.6 mm specimens failed at higher loads by Mode 1 while some lower loads failed by Mode 2.

When comparing Figures 5.34 and 5.35 the thicker sheet had greater strength. For a load of 2.2 kN the average life for 1.23 mm was 100,000 cycles whereas for 1.6 mm had a life of 500,000 cycles. This is because all specimens failed in the base material which for a thicker sheet there is a greater cross sectional area lowering the stress concentration when compared to a thinner sheet with the same loading.

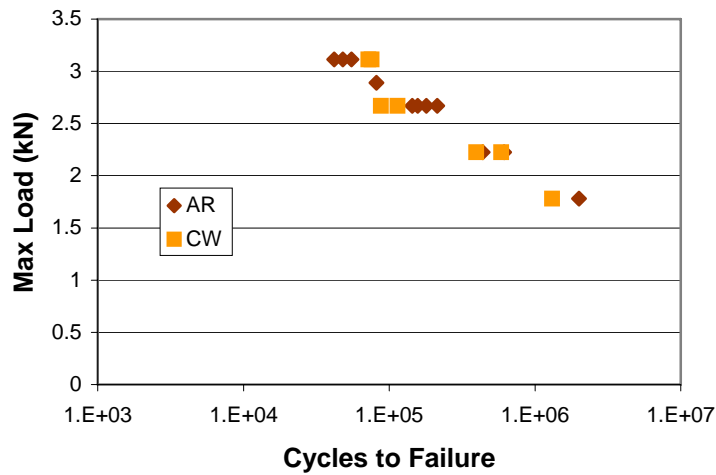


FIGURE 5.35. FATIGUE OF SPR FOR SHEET THICKNESS 1.6 MM.

5.3.2.4 METALLOGRAPHY

Crack initiation during fatigue is revealed in Figure 5.36. The cracks shown are on the pierced sheet at location A from Figure 2.10 are a result of fretting. The scuffed area in the figure shows fretting, all cold worked and non-cold worked samples showed fretting scars.

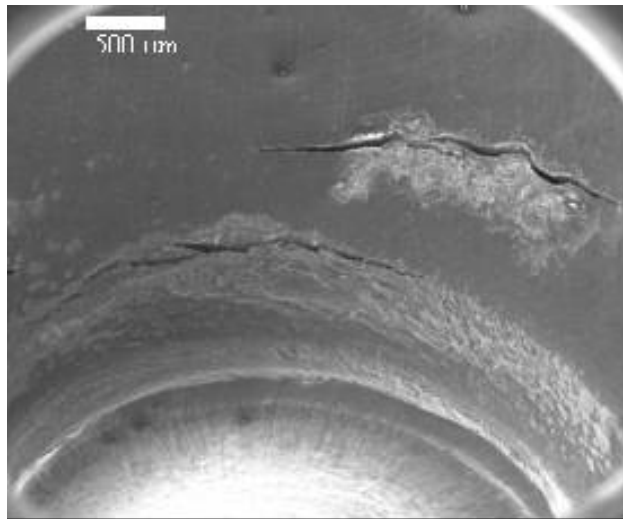


FIGURE 5.36. CRACK INITIATION (SEM).

After crack initiation the crack propagated through the sheet metal during fatigue testing and eventually resulted in failure shown in Figure 5.37. As shown in the figure there are two distinct fretting locations the bright area near the crack is two body fretting while three body fretting is the black region to the left and right of two body fretting. Another reason cold working has no affect on the fatigue life of SPR is the macrostresses from cold working may have no influence on the microstresses created from two and three body fretting. Published research on the relationship between microstress and macrostress is limited.

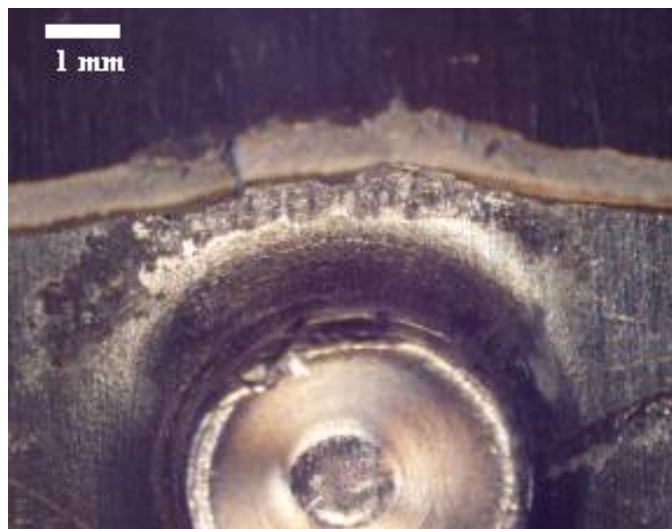


FIGURE 5.37. SPR FAILURE FROM FRETTING.

CHAPTER 6:

CONCLUSION

Presented in this research was the effect of cold working on mechanical properties for two different sheet metal joining techniques used in automotive applications. For both RSW and SPR similar cold working processes were performed on the sheet metal by driving an indenter in to the material. The results that have been shown complement each other to give superb conclusions.

6.1 RSW

Post-weld cold working was performed on RSWs after the RSW process. Mechanical properties checked in RSWs were microhardness, tensile strength and fatigue strength. X-Ray diffraction was used on steel RSW for determining the residual stress contours; also FEA was performed for both material types.

6.1.1 STEEL

The effect of weld quality on cold worked steel RSWs and was a main focus for this study. The following are conclusion made for steel

1. Fatigue life of RSWs increases with increasing nugget diameter.
2. There was little to no improvement in fatigue life for post weld cold worked samples with poor weld quality (nugget diameter $< 4t$), whereas adequately sized spot-welds can have fatigue life increased by up to 10 times.

3. Three different types of fatigue failure modes were observed with the undersized post-weld cold working processed RSW samples: type A where crack propagated through the nugget, type B crack propagated through nugget with cracks seen in the HAZ, and type C cracks propagated through the HAZ. For undersized welds that were post-weld cold worked the fatigue failure occurred often at the nugget (type A or B).
4. All adequately sized spot-welds had failure Type C (failure in the HAZ) which promises a higher cycles to failure than does either failure type A or failure type B.
5. The residual stresses determined by X-Ray Diffraction correlated well to those produced by FEA.
6. Through FEA, undersized nuggets have tensile residual stress after cold working at the notch region, which is detrimental in fatigue life. Whereas for adequate sized nuggets there is a compressive residual stress imparted from cold working at the notch region, resulting in a delay of crack initiation and propagation.

6.1.2 ALUMINUM

The ultimate cold working process parameters was the main focus for Al RSW.

1. The post-weld cold working process increased the fatigue lives of Al spot welds when compared with the as-welded specimens. At a maximum load of 686 N (which is 40%

of max tensile-shear load), a fatigue life improvement for the 7.1 mm IS and 300 MPa IP was approximately 80 times, and an improvement for the 4.6 mm IS, 450 MPa IP parameter was approximately 70 times.

2. For both indenters, the optimum indenting pressure was found based on the fatigue properties of the Al RSWs. The optimum parameters of the cold working process with respect to fatigue life of the Al RSW are 450 MPa IP with 4.6 mm IS and 300MPa IP with 7.1mm IS. When the indenting pressure is too low the effects on the residual stress distribution is insignificant having little impact on the mechanical properties and too high indenting pressure causes gross deformation of the faying surfaces making the weld unstable.
3. The main reason of the improved fatigue strength on the post-weld cold worked Al RSW is compressive residual stresses induced during the cold working process. This correlates with the finite element analysis, decent amount of compressive residual stresses were induced around the nugget and heat affected zone on the Al RSWs.
4. FEM help support the results of the fatigue testing. For both IS, FEA showed the models with the highest compressive residual stresses at the faying surface also had the highest fatigue life. The average value of the compressive stresses at the faying surface for the two optimum cold working parameters (4.6 mm IS with 450 MPa IP and 7.1 mm IS with 300 MPa IP) is 150 MPa whereas the average of the other four parameters is 110 MPa.

6.2 SPR

The cold working process was done before the joint was made, the purpose for cold working was to simulate stamped sheet metal. The SPR process force, tensile strength and fatigue strength were all analyzed for both cold worked and non-cold worked specimens. Following are several conclusions made from this research.

1. For the provided rivet the optimum material type for performing cold working on was Al 5052 with sheet thicknesses of 1.27 mm and 1.6 mm.
2. The RSF for sheet thickness 1.27 mm increased by 57% in region I and 36% in region II as a result of cold working. For sheet thickness 1.6 mm the RSF increased by 45% in region I and 23% in region II as a result of cold working. This requires different machine settings for stamped parts in a automotive industry where SPR is being performed
3. Cold working had no effect on tensile-shear properties of SPR, with the theory being the stress distribution field created during riveting negated the residual stresses induced by cold working.
4. Fatigue properties were not affected by cold working prior to SPR. The first reason is because of the stress negation noted in conclusion #3, the second is that the main failure mechanism of SPR is fretting fatigue. In fretting fatigue failure, the surface residual stress is maybe relaxed as the number of fretting fatigue cycles increased. Therefore, the residual stresses on SPR did not effect SPR fatigue lives.

5. All samples showed fretting scars and failed in the base material during fatigue testing.

CHAPTER 7:

FUTURE RESEARCH

Research on the post-weld cold working can be taken one step further. A FEM of the RSW process used in this research could be developed which would be beneficiary in knowing the residual stress distribution. This FEM could then be implemented into the post-weld cold working FEA to give more exact notch stress readings.

Future research on SPR can be directed in several paths, which are as follows:

1. Study effects of different cold working parameters on process force and mechanical properties.
2. Study the microhardness of cold worked SPR.
3. Develop FEM of the SPR process with cold worked sheet metal to show the stress distribution field.
4. Determine the effects of cold working on mechanical properties for different rivet/die combinations.

BIBLIOGRAPHY

ASTM E915-90, "STANDARD TEST METHOD FOR VERIFYING THE ALIGNMENT OF X-RAY DIFFRACTION INSTRUMENTATION FOR RESIDUAL STRESS MEASUREMENT," ANNUAL BOOK OF ASTM STANDARDS, AMERICAN SOCIETY FOR TESTING AND MATERIALS, PHILADELPHIA, PA, SEC. 3, 03.01, PP. 776-778, 1992.

ATZENI, E., IPPOLITO, R. AND SETTINERI, L., "EXPERIMENTAL AND NUMERICAL INVESTIGATION ON SELF-PIERCING RIVETS," NAMRI/SME, VOL. 33, PP. 477-484, 2005.

CALLISTER, WILLIAM D. JR., "MATERIAL SCIENCE AND ENGINEERING AND INTRODUCTION," 7TH ED, JOHN WILEY & SONS, INC., PP. 113, 228 AND 231, 2007.

CAI, W., WANG, P.C. AND YANG, W. "ASSEMBLY DIMENSIONAL PREDICTION FOR SELF-PIERCING RIVETED ALUMINUM PANELS," *INTERNATIONAL JOURNAL OF MACHINE TOOLS & MANUFACTURE*, 45, PP. 695-704, 2005

CHAKHERLOU, T.N., AND VOGWELL, J., "THE EFFECT OF COLD EXPANSION ON IMPROVING THE FATIGUE LIFE OF FASTENER HOLES," *ENGINEERING FAILURE ANALYSIS*, VOL. 10, PP. 13-24, 2003.

CHAO, YUH J., "ULTIMATE STRENGTH AND FAILURE MECHANISM OF RESISTANCE SPOT WELD SUBJECTED TO TENSILE, SHEAR, OR COMBINED TENSILE/SHEAR LOADS," *JOURNAL OF ENGINEERING MATERIALS AND TECHNOLOGY*, VOL. 125, PP. 125-132, APRIL 2003.

CHEN, Y.K., HAN, L., CHRYSANTHOU, A. AND O'SULLIVAN, J.M., "FRETTING WEAR IN SELF-PIERCING RIVETED ALUMINIUM ALLOY SHEET," *WEAR*, VOL. 255, PP. 1463-1470, 2003.

CHO, Y., HU, S. J. AND LI, W., "RESISTANCE SPOT WELDING OF ALUMINUM AND STEEL: A COMPARATIVE EXPERIMENTAL STUDY," *PROC. INSTN MECH. ENGRS.*, VOL. 217, PART B., 2003.

CHO, Y., AND RHEE, S., "EXPERIMENTAL STUDY OF NUGGET FORMATION ON RESISTANCE SPOT WELDING," *WELDING JOURNAL*, PP. 195-201, 2003.

DARWISH, S.M. AND AL-DEKHIAL, S.D., "STATISTICAL MODELS FOR SPOT WELDING OF COMMERCIAL ALUMINUM SHEETS," *INTERNATIONAL JOURNAL OF MACHINE TOOLS & MANUFACTURE DESIGN, RESEARCH AND APPLICATIONS*, VOL. 39, PP. 1589-1610, 1999.

EASTERBROOK, E.T., FLINN, B.D., MEYER, C.A. AND JUHLIN, N., "THE STRESSWAVE FATIGUE LIFE ENHANCEMENT PROCESS," SAE TECHNICAL PAPER SERIES 2001-01-2578, 2001.

EL-SAYED, M.E.M., STAWIARSKI, T., AND FRUTIGER, R., "FATIGUE ANALYSIS OF SPOT-WELDED JOINTS UNDER VARIABLE AMPLITUDE LOAD HISTORY," ENGINEERING FRACTURE MECHANICS, VOL. 55, NO. 3, PP. 363-369, 1996.

FLINN, B., SPITSEN, R., KIM, D., NAM, T. AND EASTERBROOK, E.T., "FATIGUE STRENGTH IMPROVEMENT OF LOW CARBON STEEL RESISTANCE SPOT WELDS BY THE STRESSWAVE™ PROCESS," SAE TECHNICAL PAPER 2005-01-0903

FU, MAOFENG AND MALLICK, P.K., "FATIGUE OF SELF-PIERCING RIVETED JOINTS IN ALUMINUM ALLOY 6111," INTERNATIONAL JOURNAL OF FATIGUE, VOL. 25, ISSUE 3, PP. 183-189, MARCH 2003.

GEAN, A., WESTGATE, S.A., KUCZA, J.C., AND EHRSTROM, J.C., "STATIC AND FATIGUE BEHAVIOR OF SPOT-WELDED 5182-0 ALUMINUM ALLOY SHEET," WELDING RESEARCH SUPPLEMENT, PP. 80-86, MARCH 1999.

GENTILCORE, M., "AN ASSESSMENT OF THE FATIGUE PERFORMANCE OF AUTOMOTIVE SHEET STEELS," SAE INTERNATIONAL, 2004.

HAGGAG, F.M., AND BELL, G.E.C., "MEASUREMENT OF YIELD STRENGTH AND FLOW PROPERTIES IN SPOT WELDS AND THEIR HAZS AT VARIOUS STRAIN RATES," PROCEEDINGS OF THE ASM 3RD INTERNATIONAL CONFERENCE ON TRENDS IN WELDING RESEARCH, GATLINBURG, TENN., JUNE 1-5, 1992.

HAN, L., CHRYSANTHOU, A. AND O'SULLIVAN, J.M., "FRETTING BEHAVIOUR OF SELF-PIERCING RIVETED ALUMINIUM ALLOY JOINTS UNDER DIFFERENT INTERFACIAL CONDITIONS," MATERIALS & DESIGN, 2004

HAN, Z., INDACOCHEA, J.E., CHEN, C. H., AND BHAT, S., "WELD NUGGET DEVELOPMENT AND INTEGRITY IN RESISTANCE SPOT WELDING OF HIGH-STRENGTH COLD-ROLLED SHEET STEELS," PROCEEDINGS OF 71ST AWS ANNUAL CONVENTION, APRIL 22-27, 1990, ANAHEIM, CALIF.

HENRYSSON, H.F., ABKULWAHAB, F., JOSEFSON, B.L., AND FERMER, M., "RESIDUAL STRESSES IN RESISTANCE SPOT WELDS: FINITE ELEMENT SIMULATIONS, X-RAY MEASUREMENTS AND INFLUENCE ON FATIGUE BEHAVIOUR," WELDING IN THE WORLD, VOL. 43, 1999.

IYER, K., HU, S.J., BRITTMAN, F.L., WANG, P.C., HAYDEN, D.B. AND MARIN, S.P., "FATIGUE OF SINGLE- AND DOUBLE-RIVET SELF-PIERCING RIVETED LAP JOINTS," FATIGUE FRACT. ENGNMATER STRUCT., VOL. 28, PP. 997-1007, 2005.

KANG, H., BARKEY, M.E. AND LEE, Y., "EVALUATION OF MULTIAXIAL SPOT WELD FATIGUE PARAMETERS FOR PROPORTIONAL LOADING," INTERNATIONAL JOURNAL OF FATIGUE, VOL. 22, PP. 691-702, 2000.

KHANNA, S. K., HE, C. AND AGRAWAL, H. N., "RESIDUAL STRESS MEASUREMENT IN SPOT WELDS AND THE EFFECT OF FATIGUE LOADING ON REDISTRIBUTION OF STRESSES USING HIGH SENSITIVITY MOIRE INTERFEROMETRY," JOURNAL OF ENGINEERING MATERIALS AND TECHNOLOGY, VOL. 123, PP. 132-138, 2001.

KIM, D., XU, J., LI, W. AND BLAKE, D., "FORCE CHARACTERISTICS OF SELF-PIERCING RIVETING," NAMRI 2006.

KIM D., SPITSEN, R., KHOSLA, T., LI, W., RYU, S. AND LIM, B.: THE FEASIBILITY STUDY OF POST-WELD COLD WORKING PROCESSES TO IMPROVE THE FATIGUE STRENGTH OF ALUMINUM RESISTANCE SPOT WELDS TRANSACTIONS OF NAMRI/SME, VOL. 33, PP.251-258, 2005.

LEE, H., KIM, N. AND LEE T., "OVERLOAD FAILURE CURVE AND FATIGUE BEHAVIOR OF SPOT-WELDED SPECIMENS," ENGINEERING FRACTURE MECHANICS, VOL. 72, PP. 1203-1221, 2005.

LEE, Y., WEHNER, T.J., LU, M., MORRISSETT, T.W. AND PAKALNINS, E., "ULTIMATE STRENGTH OF RESISTANCE SPOT WELDS SUBJECTED TO COMBINED TENSION AND SHEAR," AMERICAN SOCIETY FOR TESTING AND MATERIALS, 1998.

LEON, A., "BENEFITS OF SPLIT MANDREL COLDWORKING," INTERNATIONAL JOURNAL OF FATIGUE, VOL. 20, NO. 1 PP. 1-8, 1998.

LI, B., AND FATEMI, A., "AN EXPERIMENTAL INVESTIGATION OF DEFORMATION AND FATIGUE BEHAVIOR OF COACH PEEL RIVETED JOINTS," INTERNATIONAL JOURNAL OF FATIGUE, VOL. 28, ISSUE 1, PP. 9-18, JAN. 2006.

LI, WEI, CHENG, S., HU, J. AND SHRIVER, J., "STATISTICAL INVESTIGATION ON RESISTANCE SPOT WELDING QUALITY USING A TWO-STATE, SLIDING -LEVEL EXPERIMENT," JOURNAL OF MANUFACTURING SCIENCE AND ENGINEERING, VOL. 123, PP. 513-520, AUGUST 2001.

LONG, X., AND KHANNA, S.K., "NUMERICAL SIMULATION OF RESIDUAL STRESSES IN A SPOT WELDED JOINT," JOURNAL OF ENGINEERING MATERIALS AND TECHNOLOGY, VOL. 125, PP. 222-226, APRIL 2003.

LORENZO, G. DI. AND LANDOLFO, R., "SHEAR EXPERIMENTAL RESPONSE OF NEW CONNECTING SYSTEMS FOR COLD-FORMED STRUCTURES," JOURNAL OF CONSTRUCTIONAL STEEL RESEARCH, VOL. 60, PP. 561-579, 2004

OZDEMIR, A.T., AND HERMANN, R., "EFFECT OF EXPANSION TECHNIQUE AND PLATE THICKNESS ON NEAR-HOLE RESIDUAL STRESSES AND FATIGUE LIFE OF COLD EXPANDED HOLES," JOURNAL OF MATERIALS SCIENCE, VOL. 34, ISSUE 6, PP. 1243-1252, MARCH 15, 1999.

PAN, N. AND SHEPPARD, S.D., "STRESS INTENSITY FACTORS IN SPOT WELDS," ENGINEERING FRACTURE MECHANICS, VOL. 70, PP. 671-684, 2003.

PORCARO, R., HANSEN, A.G., AALBERG, A. AND LANGSETH, M., "JOINING OF ALUMINIUM USING SELF-PIERCING RIVETING: TESTING, MODELLING AND ANALYSIS," IJ CRASH, VOL. 9, NO. 2, PP. 141-154, 2004.

RADAJ, D., "DESIGN AND ANALYSIS OF FATIGUE RESISTANT WELDED STRUCTURES," HALSTED PRESS, NEW YORK, 1990.

RADAJ, D., "STRESS SINGULARITY, NOTCH STRESS AND STRUCTURAL STRESS AT SPOT-WELDED JOINTS," ENGINEERING FRACTURE MECHANICS, VOL. 34, NO. 2, PP. 495-506, 1989.

RWMA, RESISTANCE SPOT WELDING MANUAL 1: 119-143, 1981.

RUPP, A., STORZEL K. AND GRUBISIC V., "COMPUTER AIDED DIMENSIONING OF SPOT WELDED AUTOMOTIVE STRUCTURES," SAE TECHNICAL REPORT NO. 950711, DETROIT, MICHIGAN, 1995.

SENKARA, J. AND ZHANG, H., "CRACKING IN SPOT WELDING ALUMINUM ALLOY AA5754," WELDING RESEARCH SUPPLEMENT, PP.194-201, JULY 2000.

SENKARA, J., ZHANG, H., AND HU, J., "EXPULSION PREDICTION IN RESISTANCE SPOT WELDING," WELDING JOURNAL, PP. 123-132, APRIL 2004

SHEPPARD, S.D. AND STRANGE, M., "FATIGUE LIFE ESTIMATION IN RESISTANCE SPOT WELDS: INITIATION AND EARLY GROWTH PHASE," FATIGUE FRACTURE MATERIAL STRUCTURE, VOL. 15, NO. 6, PP. 531-549, 1992.

SPITSEN, R., "THE EFFECT OF POST-WELD COLD WORKING ON THE FATIGUE STRENGTH AND MECHANICAL PROPERTIES OF LOW CARBON STEEL AND ALUMINUM RESISTANCE SPOT WELDS," MS THESIS, WASHINGTON STATE UNIVERSITY VANCOUVER, VANCOUVER, WA, MAY 2005.

SPITSEN R., KIM, D., FLINN, B., RAMULU, M. AND EASTERBROOK, E. T., "THE EFFECTS OF POST-WELD COLD WORKING PROCESSES ON THE FATIGUE STRENGTH OF LOW CARBON STEEL RESISTANCE SPOT WELDS," PROCEEDINGS OF 2004 ASME INTERNATIONAL MECHANICAL ENGINEERING CONGRESS & EXPOSITION, ANAHEIM, CALIFORNIA, ANAHEIM HILTON, NOVEMBER 13-19, 2004.

STEVENSON, R., WANG, P.-C., "FRICTION STIR RIVETING – IMPACT OF PROCESS PARAMETERS ON JOINT PERFORMANCE," PROCEEDINGS OF 2005 ASME INTERNATIONAL MECHANICAL ENGINEERING CONGRESS & EXPOSITION, NOVEMBER 5-11, 2005, ORLANDO, FLORIDA.

STRESSWAVE, INC., 6644 SOUTH 196TH STREET, SUITE T-106, KENT, WA 98032

SUN, X. AND DONG, P., "ANALYSIS OF ALUMINUM RESISTANCE SPOT WELDING PROCESSES USING COUPLED FINITE ELEMENT PROCEDURES," PP. 215-221, AUG 2000.

SUN, X., STEPHENS, E.V. AND KHALEEL, M.A., "FATIGUE BEHAVIORS OF SELF-PIERCING RIVETS JOINING SIMILAR AND DISSIMILAR SHEET METALS," INTERNATIONAL JOURNAL OF FATIGUE, VOL. 29, PP. 370-386, 2007.

THORNTON, P.H., KRAUSE, A.R., AND DAVIES, R.G., "THE ALUMINUM SPOT WELD FATIGUE STRENGTH IS DEPENDENT ON NUGGET DIAMETER RATHER THAN THE ABSENCE OF POROSITY AND EXPULSION," WELDING RESEARCH SUPPLEMENT, PP. 101-108, MARCH 1996.

TSAI, C. L., JAMMAL, O. A, PAPRITAN, J. C. AND DICKINSON, D.W., "MODELING OF RESISTANCE SPOT WELD NUGGET GROWTH," WELDING JOURNAL, VOL. 71, PP. S47-S54, 1992.

URBAN, M.R., "ANALYSIS OF THE FATIGUE LIFE OF RIVETED SHEET METAL HELICOPTER AIRFRAME JOINTS," INTERNATIONAL JOURNAL OF FATIGUE, VOL. 25, PP. 1013-1026, 2003.

WANG, BIN, HAO, C., ZHANG, J. AND ZHANG, H., "A NEW SELF-PIERCING RIVETING PROCESS AND STRENGTH EVALUATION," JOURNAL OF MANUFACTURING SCIENCE AND ENGINEERING, VOL. 128, PP. 580-587, MAY 2006.

WEBSTER, G.A., AND EZEILO, A.N., "RESIDUAL STRESS DISTRIBUTIONS AND THEIR INFLUENCE ON FATIGUE LIFETIMES," INTERNATIONAL JOURNAL OF FATIGUE, VOL. 23, PP. 375-383, 2001.

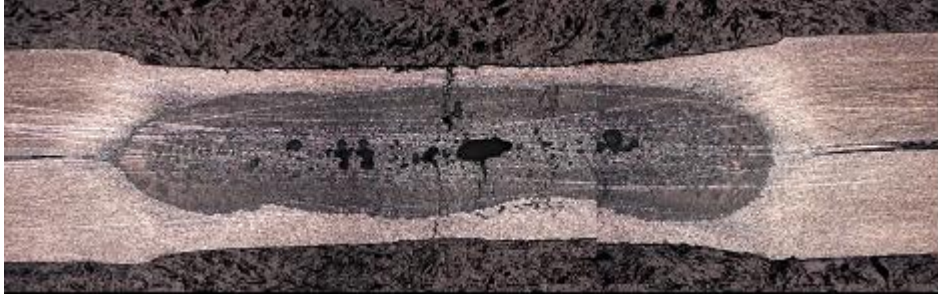
YANG Y.S. AND LEE S.H., "A STUDY ON THE JOINING STRENGTH OF LASER SPOT WELDING FOR AUTOMOTIVE APPLICATIONS," JOURNAL OF MATERIALS PROCESSING TECHNOLOGY, VOLUME 94, PP. 151-156, SEPTEMBER 29, 1999.

ZHANG, H., "EXPULSION AND ITS INFLUENCE ON WELD QUALITY," WELDING RESEARCH SUPPLEMENT, PP. 363-380, NOV. 1999

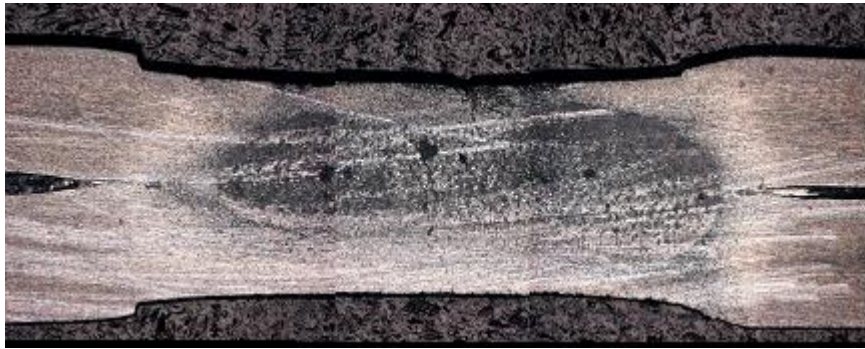
ZHANG, Y. AND TAYLOR, D., "SHEET THICKNESS EFFECT OF SPOT WELDS BASED ON CRACK PROPAGATION," ENGINEERING FRACTURE MECHANICS, VOL. 67, PP. 55-63, 2000.

ZHOU, M., ZHANG, H. AND HU, S. J., "RELATIONSHIPS BETWEEN QUALITY AND ATTRIBUTES OF SPOT WELDS," WELDING JOURNAL, VOL. 82, PP. 72S-77S, 2003.

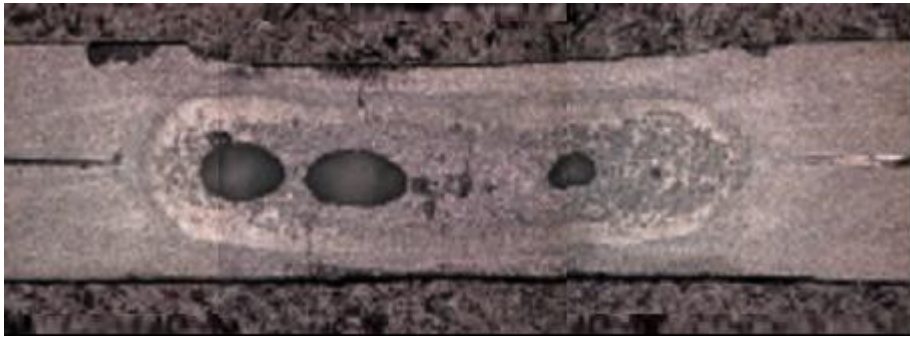
APPENDIX



Microstructure of Al 5052 RSW with cold working parameters of IS 4.6 mm and IP 300 MPa



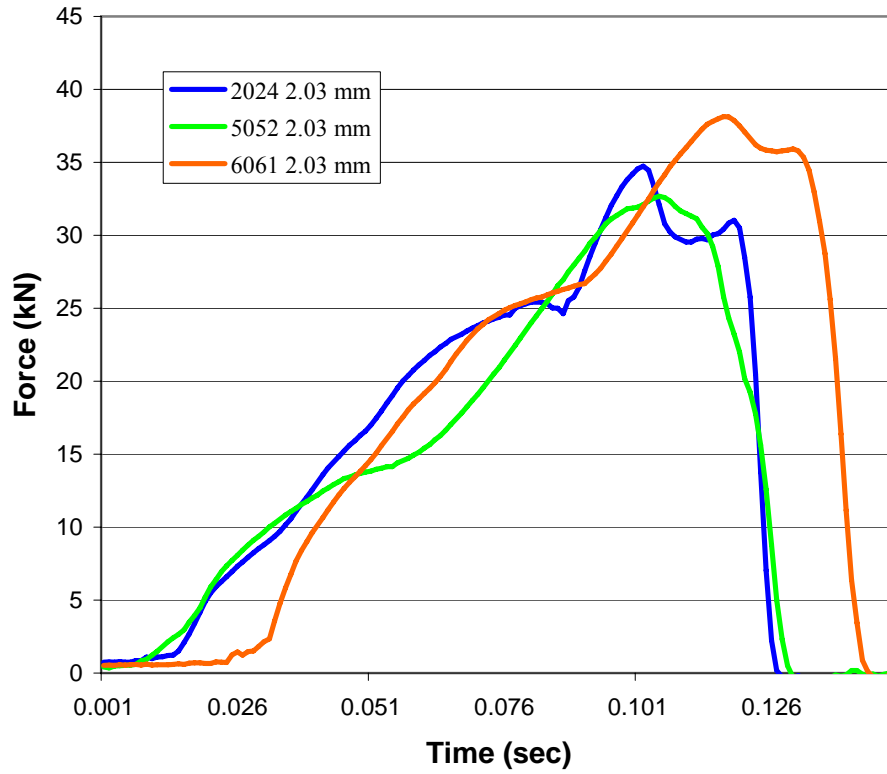
Microstructure of Al 5052 RSW with cold working parameters of IS 4.6 mm and IP 600 MPa



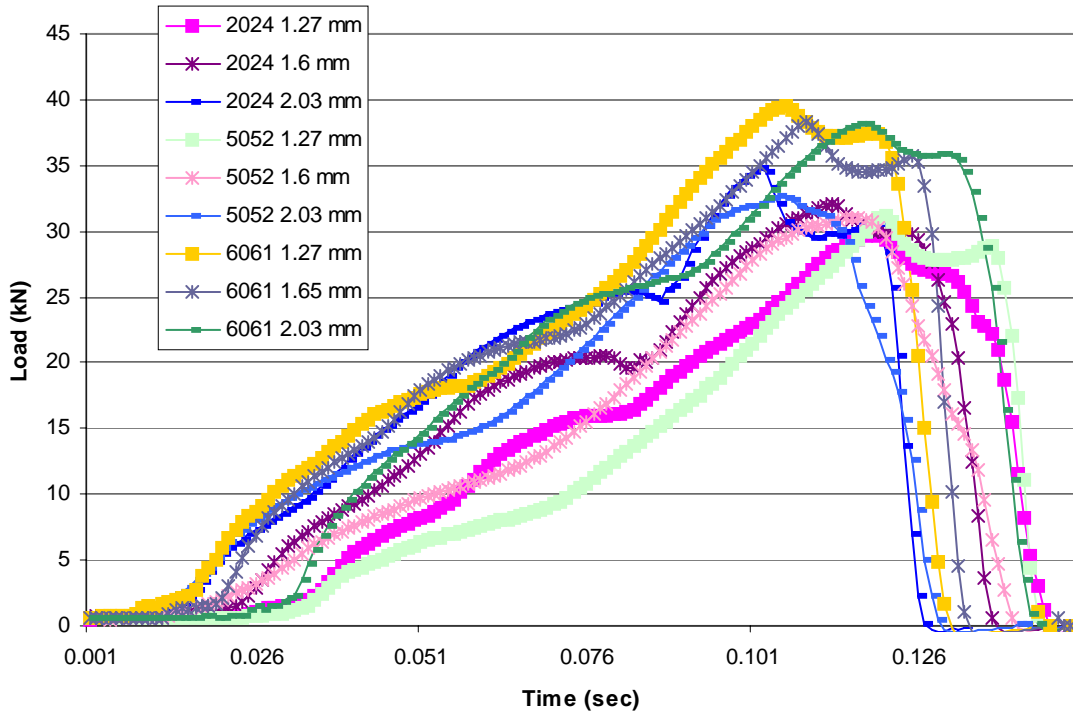
Microstructure of Al 5052 RSW with cold working parameters of IS 7.1 mm and IP 450 MPa



Microstructure of Al 5052 RSW with cold working parameters of IS 7.1 mm and IP 450 MPa



Process force for Al SPR with material thickness of 2.03 mm



Process force for all Al SPR specimens

Average SPR process forces and respective standard deviations for Al material types

	2024 1.27 mm		2024 1.6 mm		2024 2.03 mm	
	Region I	Region II	Region I	Region II	Region I	Region II
Average	15.93	29.80	20.50	32.05	25.43	31.03
STDV	0.05	0.19	0.04	0.13	0.03	0.02

	5052 1.27 mm		5052 1.6 mm		5052 2.07 mm	
	Region I	Region II	Region I	Region II	Region I	Region II
Average	7.79	31.14	10.21	31.04	13.84	32.67
STDV	0.01	0.05	0.01	0.14	0.06	0.17

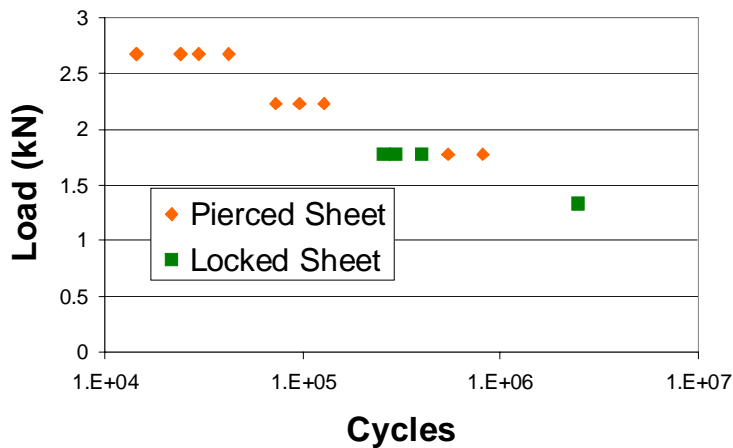
	6063 1.27 mm		6063 1.65 mm		6063 2.03 mm	
	Region I	Region II	Region I	Region II	Region I	Region II
Average	18.12	39.46	21.83	38.27	26.05	38.14
STDV	0.03	0.05	0.03	0.03	0.02	0.10

Data from SPR fatigue for Al 5052 1.27 mm sheet thickness.

As Received				
Sample #	Load (kN)	Time (min)	Cycles	Failure Location
13	1.78	245	294000	Back
18	1.33	2066	2479200	Back
12	2.22	80	96000	Front
14	2.67	35	42000	Front
16	2.67	12	14400	Front
17	1.78	677	812400	Front
38	2.67	12	14400	Front
39	2.67	20	24000	Front

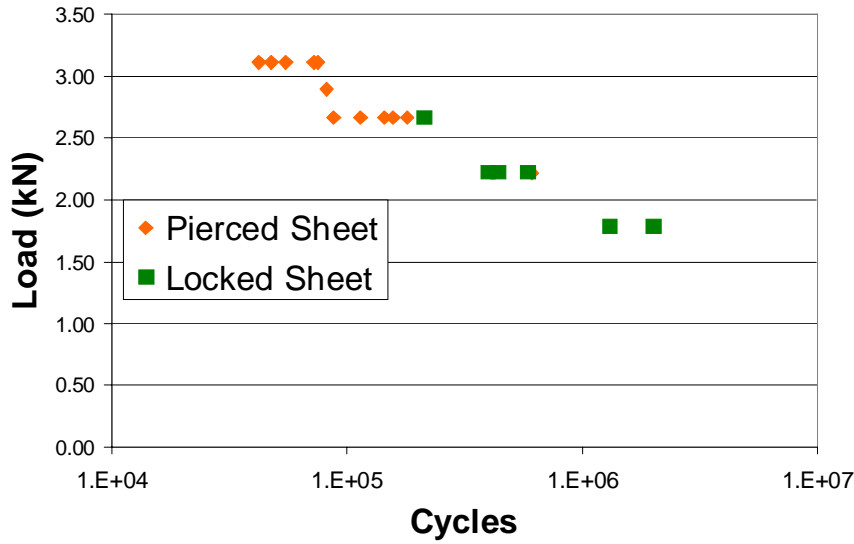
As Received				
Sample #	Load (kN)	Time (min)	Cycles	Failure Location
23	2.22	107	128400	Front
24	1.78	450	540000	Front
25	1.78	214	256800	Back
26	2.22	61	73200	Front
27	1.78	334	400800	Back
33	1.33	3650	4380000	No Failure
34	2.67	25	30000	Front
35	2.67	20	24000	Front

1.27 mm Failure Locations



Al 5052 1.27 mm sheet thickness SPR Fatigue

1.6 mm Failure Locations



Al 5052 1.6 mm sheet thickness SPR Fatigue

Data from SPR fatigue for Al 5052 1.6 mm sheet thickness.

As Received				
Sample #	Load (kN)	Time (min)	Cycles	Failure Location
7	2.67	178	213600	Back
9	2.22	365.25	438300	Back
41	1.78	1670	2004000	Back
2	3.11	35	42000	Front
3	3.11	46	55200	Front
4	2.67	120	144000	Front
8	2.67	150	180000	Front
11	3.11	40	48000	Front
19	2.22	512	614400	Front
22	2.89	68	81600	Front
15	2.67	131	157200	Front

Cold Worked				
Sample #	Load (kN)	Time (min)	Cycles	Failure Location
29	1.78	1093	1311600	Back
30	2.22	490	588000	Back
32	2.22	330	396000	Back
31	2.67	95	114000	Front
36	3.11	60	72000	Front
37	3.11	63	75600	Front
40	2.67	73	87600	Front